CHARLES UNIVERSITY

Faculty of Science

Study programme: Chemistry

Branch of study: Inorganic chemistry

Bc. Soňa Kohúteková

Molecular crystals for NLO applications - compounds of 1*H*-pyrazole-carboxamidine

Molekulové krystaly pro NLO aplikace - sloučeniny 1*H*-pyrazol-karboxamidinu

Diploma thesis

Supervisor: prof. RNDr. Ivan Němec, Ph.D.

Consultant: RNDr. Irena Matulková, Ph.D.

Prague, 2018

Prohlášení

Prohlašuji, že jsem tuto závěrečnou práci zpracovala samostatně a že jsem uvedla všechny použité informační zdroje a literaturu. Tato práce ani její podstatná část nebyla předložena k získání jiného nebo stejného akademického titulu.

V Praze, 15. 05. 2018 .....

Bc. Soňa Kohúteková

Acknowledgement

First and foremost, I would like to thank to my supervisor, prof. RNDr. Ivan Němec, Ph.D. for the patient guidance during the whole work on this thesis. I would also like to thank my consultant RNDr. Irena Matulková, Ph.D. for her valuable advices and introduction to the operating of Raman and infrared instruments. Besides, I would like to express my gratitude to RNDr. Ivana Císařová, CSc. for determination of single crystal structures, Doc. RNDr. Róbert Gyepes, Dr for his professional help with quantum-chemical calculations, Martina Malíková for measuring powder X-ray diffraction data and prof. RNDr. Petr Němec, Ph.D. for SHG measurements.

Last but not least, I am grateful to my family and friends - especially to Táňa and Láďa, for their encouragement and support.

Title: Molecular crystals for NLO applications – compounds of 1*H*-pyrazole-carboxamidine

Author: Bc. Soňa Kohúteková

Department: Department of Inorganic Chemistry

Supervisor: prof. RNDr. Ivan Němec, Ph.D.

Abstract: The aim of this diploma thesis is preparation and characterisation of novel compounds of 1*H*-pyrazole-carboxamidine in consideration of their potential application in the field of nonlinear optics. This thesis is focused on preparation of crystalline salts or adducts combining 1*H*-pyrazole-carboxamidine with selected inorganic and organic acids. Prepared materials were characterised mainly by the means of vibrational spectroscopy and X-ray diffraction analysis. Quantum-chemical calculations were used for a prediction of nonlinear optical properties as well as for interpretation of measured vibrational spectra. Four different approaches of calculations were used for an optimisation of computing time together with accuracy of the fit of calculated and measured spectra. Finally, measurements of second harmonic generation efficiency of two powder samples with non-centrosymmetric crystal structures were performed.

Key words: NLO, vibrational spectroscopy, crystal structure, quantum-chemical calculations

Název práce: Molekulové krystaly pro NLO aplikace – sloučeniny 1*H*-pyrazol-karboxamidinu
Autor: Bc. Soňa Kohúteková
Katedra: Katedra anorganické chemie
Vedoucí diplomové práce: prof. RNDr. Ivan Němec, Ph.D.

Abstrakt: Předkládaná diplomová práce je zaměřena na přípravu a studium nových sloučenin báze 1*H*-pyrazol-karboxamidinu s ohledem na jejich využití v nelineární optice. Primárním cílem bylo připravit a charakterizovat krystalické soli nebo adukty s vybranými anorganickými a organickými kyselinami. Připravené sloučeniny byly studovány především pomocí metod vibrační spektroskopie a rentgenové difrakce. Pro interpretaci vibračních spekter a predikci nelineárních optických vlastností molekul byly využity kvantově-chemické výpočty. Pro optimalizaci výpočetního času s ohledem na soulad mezi vypočtenými a naměřenými spektry byly použity čtyři různé přístupy k výpočtům. U necentrosymetrických materiálů byla na práškových vzorcích měřena účinnost generování druhé harmonické frekvence.

Klíčová slova: NLO, vibrační spektroskopie, krystalová struktura, kvantově-chemické výpočty

Contents

1 Introduction

The field of nonlinear optics is currently one of the most attractive fields of research because of its applications in various areas. Huge development in this field has begun after the construction of the first laser in 1960[1]. This highly energetic and coherent source of light enabled discovery of wide range of effects impossible to observe with common light sources. One of the discovered effects was second harmonic generation (SHG) caused by a nonlinear response of materials to light. The principle of this effect is based on annihilation of two photons of the same frequency which leads to production of one photon with double frequency. Shortly, SHG allows generation of new wavelengths of light but, unfortunately, it is possible to observe only in molecules with particular properties. The most important is that material has no centre of symmetry what is rare in nature. Therefore, preparation of suitable materials demands selection and design of promising molecules which is the main interest of nonlinear optics and crystal engineering.

1.1 Nonlinear optics (NLO)

Nonlinear optics is a branch of optics that studies interaction of light with matter where response of this system to the applied electromagnetic field is nonlinear in the amplitude of this field. For observation of nonlinear effects high light intensities provided by laser are required to modify the optical properties of material. Although, some of the nonlinear effects where discovered before the invention of laser.[2]

The examples of these phenomena might be Pockels and Kerr electro-optics effects known since the 19th century[3]. Both effects describe change in the refractive index of a material induced by applied electric field. In linear, Pockels, effect the response is proportional to the electric field while in Kerr effect the change in refractive index is proportional to the square of the electric field. The Pockels effect occurs only in materials without a centre of symmetry such as $LiNbO_3$, $LiTaO_3$ or GaAs.[4]

After the first laser was built rich diversity of nonlinear-optical effects was described including sum frequency generation (SFG) or difference frequency generation (DFG). They are both based on annihilation of two incident photons while, simultaneously, one photon is generated. Its frequency is a sum (SFG) or a difference (DFG) of frequencies

of initial photons. Special case of sum frequency generation is second harmonic generation in which two incident photons have same frequencies.[4]

1.1.1 Physical principles

Oscillating electric field $\vec{E}$ of the light that passes through molecules deforms their electron cloud. This displacement of electron density causes oscillation of dipole moment. For low light intensities (daylight ~10^2 V/cm) is response of dipole moment $\vec{\mu}$ linear with respect to the electric field $\vec{E}$ and can be express by equation (1):

$$\vec{\mu} = \alpha\vec{E}, \tag{1}$$

where α is linear polarization coefficient. In this case dipoles in molecules oscillate with the same frequency ω as frequency of incident light.[5]

If the electric field intensity is comparable to the atomic fields (~10^8 V/cm) response of molecules is no longer linear and the equation of nonlinear molecular polarization $\vec{p}$ is given by Taylor series expansion:

$$\vec{p} = \alpha\vec{E} + \beta\vec{E}^2 + \gamma\vec{E}^3 ..., \tag{2}$$

where β is the second order and γ the third order hyperpolarizability. Typically, only laser light is sufficiently intense to generate nonlinear-optics phenomena.[6]

An assembly of these dipoles forms a macroscopic polarization $\vec{P}$ that is given by the expression (3) analogous to equation (2):

$$\vec{P}(t) = \varepsilon_0(\chi^{(1)}\vec{E}(t) + \chi^{(2)}\vec{E}(t)^2 + \chi^{(3)}\vec{E}(t)^3 + \cdots), \tag{3}$$

where ε_0 is vacuum permittivity, $\chi^{(i)}$ are the susceptibility coefficients of the *i*-th order. Susceptibility is a proportional constant that not only represents degree of polarization of a dielectric material but also provides information about a symmetry of material. If the value of material $\chi^{(2)}$ (β of molecules) is 0 it means that the material is centrosymmetric and does not generates NLO phenomena. Therefore, absence of centre

of symmetry and high value of β is crucial for nonlinear-optical properties and both can be used as a primary guess of the suitability of a molecule for NLO.[3]

1.1.2 Second harmonic generation

Second harmonic generation, also called frequency doubling, is nonlinear optical phenomenon in which two photons of the same frequency ω_1 annihilates to produce one photon with double frequency ω_2. It is a special example of sum frequency generation. SHG was first demonstrated in 1961 by Peter Franken *et al.*[7] shortly after the construction of first laser in 1960 by Theodore Harold Maiman[1]. This ruby-laser radiation with wavelength 694.3 nm was used to generate SHG (~347.2 nm) in a quartz crystal[7].

Previously mentioned condition of quadratic nonlinearity of material is not the only one for SHG. For generation of SHG is also required law of conservation of energy (4) as well as the phase-matching condition (5) which allow that constructive interference and therefore a high-intensity response will occur.

$$\omega_2 = 2\omega_1 \tag{4}$$

$$\overrightarrow{k_2} = 2\overrightarrow{k_1}, \tag{5}$$

where $\overrightarrow{k_i}$ is the wave-vector of the *i*-th wave. Besides that, SHG efficiency also depends on quality and orientation of used crystal.

There are many examples of technical applications of SHG, such as optical modulation, optical switching or optical data storage[8]. Commercially is SHG used to generate visible wavelengths from infrared (IR) source. As an example used by industry is a production of a green laser pointers with a wavelength 532 nm from the Nd:YVO_4 laser radiation (λ = 1064 nm) which passes through a KTP (potassium titanyl phosphate) crystal[9]. Lately is SHG imaging intensively studied as a disease diagnostics tool[10-11]. Biological SHG was first reported in 1986 when Isaac Freund investigated the polarity of collagen fibres in rat tail tendon[12]. Breakthrough for SHG imaging microscopy happened in 2002 when Paul J. Campagnola reported practical implementation of tissue imaging at high resolution and rapid data acquisition using laser scanning[10-11]. All of these applications point out the great importance of SHG phenomena.

1.2 Materials for SHG

Despite many requirements for NLO materials providing SHG phenomena, suitable materials can be divided into three main groups.

First group contains inorganic salts and oxides. The preparation of these materials is quick and easy from water solutions and their main advantage is hardness, high melting points values and optical transparency in visible and UV region. Unfortunately, these crystals usually have low values of nonlinear coefficients, restricted birefringence, suffers from degradative photo effects and their optical transparency in infrared region is lower than in case of second group (organic molecules).[13] First commercially used materials for SHG were $NH_4H_2PO_4$ (ADP) and KH_2PO_4 (KDP). KDP is nowadays used as one of the standards for SHG quantification. By now, there exists much more inorganic examples like β-BaB_2O_4 (BBO) with six times higher SHG efficiency then KDP, $Ba_2NaNb_5O_{15}$, NH_4HSeO_4 or TeO_2. Another example is water insoluble $LiNbO_3$ with two times higher SHG efficiency than KDP and optical transparency in region 400 nm to 5 μm.[4]

Second large group of suitable materials for SHG are organic molecules. The main advantages of these molecules are high values of hyperpolarizability β, high resistance against photochemical degradation and possibility of modification of their physical and optical properties by chemical derivatization. Even though, all of these physical properties are promising for NLO applications, utilization of these molecules is limited. Usually, high values of hyperpolarizability are accompanied by high dipole moments which, unfortunately, leads to formation of unwanted centrosymmetric pairs. Despite of these complications, according to the similar structural elements it is possible to predict the potential of selected organic molecules.[4] Firstly, there are derivatives of aromatic molecules with highly delocalised π-electron systems caused by electron donor and electron acceptor functional groups. Another way of increasing delocalization of π-electron system is connection of aromatic rings together by fragment with conjugated double bonds or using 5- or 6-membered heterocyclic aromatic rings. Secondly, simple organic molecules like urea or guanidine are suitable too, see Figure 1. Urea crystal is one of the SHG standards and its nonlinear origin is in the conjugated system of bonds O⇐C←N−H.[4, 14]

Third large group of crystals providing SHG phenomenon is combining advantages of both previously mentioned molecules. Combination of organic cations that are

responsible for high hyperpolarizability with inorganic anions which improves thermal and optical properties of final product leads to crystals or cocrystals with promising NLO properties. Moreover, these systems are stabilised with wide range of weak intermolecular interactions (*e.g.* ion-induced dipole forces, ion-dipole forces, van der Waals forces), and, the most important, hydrogen bonds. This direct combination of particular molecules is a part of crystal engineering that leads to formation of hydrogen-bonded salts with expected optical properties.

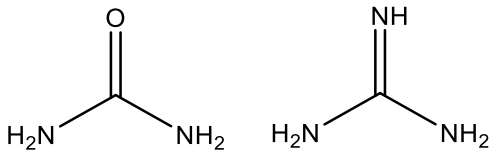

Urea Guanidine

Figure 1: Examples of organic molecules used for SHG.

1.3 1*H*-Pyrazole carboxamidine (pcam)

Target molecule **pcam**, shown in Figure 2, is a water-soluble derivative of pyrazole which is heterocyclic 5-membered ring of three carbon atoms and two adjacent nitrogen atoms. Base **pcam** contains both mentioned structural organic units responsible for NLO optical properties – the heterocyclic ring and the guanidine fragment. Nevertheless, utilization of this molecule as NLO material has not been studied yet.

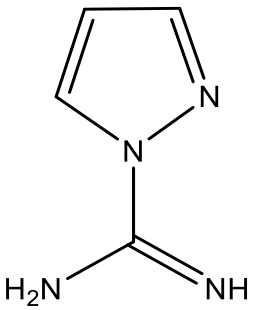

Figure 2: Structural formula of **pcam**.

According to The Cambridge Structural Database[15] (CSD) the X-ray structure of non-substituted **pcam** have not been described yet. This base is mostly used as a reactant in synthesis of wide range of molecules, for example, inhibitors[16], imaging

agents[17] or antibacterial molecules[18]. In synthesis usually represents electrophilic guanylating reagent which allows guanylation of amino group of primary amines. This reaction leads to guanylated product and 1*H*-pyrazole as a by-product and it is commonly used for a synthesis of arginine-containing peptides, see Figure 3.[19-21]

Recently there was a research concerning synthesis, characterisation and thermal properties of **pcam** dinitramide salt as a potential energetic salt. Prepared salt exhibited good resistance to thermal decomposition up to 433 K.[22] This might indicate promising thermal resistance of potential compounds of this base.

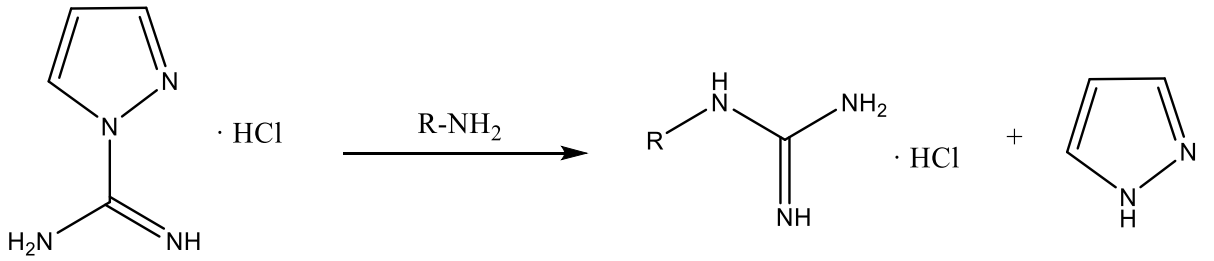

pcam·HCl Guanylated product 1*H*-pyrazole

Figure 3: Reaction of **pcam**·HCl with a primary amine.

2 Aim of thesis

The aim of this thesis is to study base 1*H*-pyrazole-carboxamidine in consideration of its potential application in the field of nonlinear optics. Nonlinear optical properties of chosen base will be predicted by quantum-chemical calculations. According to obtained results indicating promising NLO properties, the system of 1*H*-pyrazole-carboxamidine with selected organic and inorganic acids will be studied. Prepared crystalline salts or adducts will be characterised using vibrational spectroscopy and X-ray diffraction analysis. For interpretation of measured vibrational spectra quantum-chemical calculations will be used. Moreover, to optimise computing time and accuracy of the fit of calculated and measured spectra, four different approaches of quantum-chemical calculations will be tested. Finally, for compounds fulfilling symmetric condition, the second harmonic generation efficiency will be measured.

3 Experimental

3.1 Materials

All chemicals were obtained from commercial sources, see Table 1. Concentration of the used acidic solutions was 2 mol·dm^{-3} (HCl, $HClO_4$, HNO_3, H_3PO_4, H_2SO_4, H_2SeO_4, CH_3SO_3H, L-malic acid, L-tartaric acid); 1 mol·dm^{-3} (H_3PO_3, formic acid, oxalic acid); 0.5 mol·dm^{-3} (H_3BO_3, NH_2SO_3H, succinic acid) and 0.15 mol·dm^{-3} (adipic acid).

Table 1: List of the used chemicals.

1*H*-pyrazole-carboxamidine hydrochloride	99%, Sigma-Aldrich
adipic acid	purum, Fluka
boric acid	p.a., Lachema
ethanol	Merck, UVASOL
formic acid	85 - 87%, purum, Lachema
hydrochloric acid	35%, p. a., Lach-Ner
L-malic acid	97%, Sigma-Aldrich
methanesulfonic acid	98%, Alfa-Aesar
nitric acid	65%, p. a., Lach-Ner
oxalic acid dihydrate	p.a., Lachema
perchloric acid	70%, Merck
phosphoric acid	85%, purum, Lachema
phosphorous acid	97.5%, purum, Fluka
selenic acid	95%, Fluka
silver carbonate	99%, Sigma-Aldrich
succinic acid	p.a, Lachema
sulfamic acid	99.3%, Sigma-Aldrich
sulfuric acid	96%, p. a., Lach-Ner
L-tartaric acid	99.5%, Sigma-Aldrich

3.1.1 Preparation of 1*H*-pyrazole-carboxamidinium salts with acids

Crystals of new salts of **pcam** were prepared from a set of crystallisation solutions. The chosen molecule is commercially available in a form **pcam.HCl,** therefore Ag_2CO_3 was used to prepare starting **Hpcam**$^{1+}$ carbonate.

1*H*-pyrazole-carboxamidine hydrochloride (0.30 g; 2.05 mmol) was dissolved into the water (30 ml) and to this solution was added a stoichiometric amount of Ag_2CO_3 (0.29 g; 1.05 mmol). This suspension was stirred approximately thirty minutes at a room temperature until the dark precipitate of AgCl occurred. Insoluble AgCl was filtered on a glass frit S4. The colourless filtrate was spilled into the beaker and to this solution volume of the stock solution of particular acid was added according to the chosen molar

ratio. After approximately two weeks of crystallisation at room temperature the new salt was obtained.

Common inorganic and organic acids were used for crystallisation: adipic, boric, formic, hydrochloric, L-malic, methanesulfonic, nitric, oxalic, perchloric, phosphoric, phosphorous, selenic, succinic, sulfamic, sulfuric and L-tartaric acid. For every acid with **pcam** molar ratios (base : acid) 1:1; 1:2 and 2:1 were studied (see Table 4 (Chapter 4.2) and 21 (Chapter 4.3)).

3.2 Methods of characterisation

3.2.1 Quantum-chemical calculations

Quantum-chemical calculations for isolated molecules in vacuum of an uncharged base **pcam**, charged **Hpcam^{1+}** and **H$_2$pcam^{2+}** cations and neutral inorganic salts were performed using the Gaussian09W[23] software. Restricted closed-shell DFT method with B3LYP functional and 6-311++G(d,p) basis set, tight convergence criteria and an ultrafine grid was used for geometry optimisation. Calculations of geometry optimisation were followed by calculation of infrared and Raman vibrational frequencies, value of dipole moment and the first hyperpolarizability values. Visualisation of the calculated vibrational modes was performed using GaussView[24] program.

The quantum-chemical calculations for an isolated fragment selected from solved crystal structure (two cations and two nitrate anions) of salt **HpcamNO$_3$** were analogically performed as for previous ones but without tight convergence criteria and basis set 6-311G(d,p) was used.

Solid state DFT studies for inorganic crystalline salts of **pcam** were performed by the CRYSTAL14[25] (**HpcamCl·H$_2$O**, **HpcamH$_2$PO$_4$**) and CRYSTAL17[26] (**HpcamClO$_4$**, **HpcamNO$_3$ (I)** and **(II)**, **HpcamHSO$_4$**, **HpcamCH$_3$SO$_3$**, **HpcamNH$_2$SO$_3$**) software. Computations employed B3LYP functional, basis sets 6-31G(d,p) and 6-31+G(d,p) on oxygen atoms and an extra-extra-large integration grid consisting of 99 radial points and 1454 angular points in the region of chemical interest were used for geometry optimisation. The Pack-Monkhorst and the Gilat net for sampling the Brillouin zone consisted of 8 and 16 points. Derivatives needed for computing IR and Raman spectra were determined using the Coupled Perturbed Kohn-Sham[27] analytical

approach. Fractional coordinates of individual atoms were taken from the diffraction experiment and were optimised using tightened convergence criteria (keyword PREOPTGEOM) prior to computing spectral properties. The Raman spectrum was computed assuming the experimental wavelength 1064 nm and temperature 293 K.

Simulated vibrational spectra were compared to recorded ones. According to the variational principle computed energy with a trial wave function is always higher than the real energy (frequency of vibration) of a system. Therefore it is usually necessary to scale the theoretical frequencies. Scale factor is different for every method and basis set. For used B3LYP 6-311++G scale factor with value of 0.967 was recommended[28] and used for spectra shown below calculated by Gaussian program. All computed vibrations by CRYSTAL software[25-26] was scaled by the empirically determined factor 0.96.

3.2.2 Single crystal X-ray analysis

The single crystal X-ray diffraction data were collected on Bruker D8 VENTURE Kappa Duo PHOTON100 by IμS micro-focus sealed tube using Cu-Kα (λ = 1.54178 Å) or Mo-Kα (λ = 0.71073 Å). Computing programs SAINT[29] and PLATON[30] were used. The cooling was carried out by Cryosystem 800 Long Leg configuration (Oxford Cryosystems Ltd. UK). The phase problem was solved by direct methods (SIR-97[31] software) and the non-hydrogen atoms were refined anisotropically, using the full-matrix least-squares procedure (SHELX[32] software). For all the title structures, the difference electron density maps revealed all the hydrogen atoms.

The basic crystallographic data and information about measurement refinement parameters are listed in Supplement in Tables S5-S8 and are also included in CIF files which are available as Electronical Supplement files ES1 – ES14**.**

3.2.3 Powder X-ray diffraction

The powder diffraction data were collected on X`Pert PRO (PANalytical) diffractometer with $CuK_\alpha$ lamp ($\lambda$ = 1.54178 Å). The 2θ range was set from 5° to 60° with the step 0.013°. The data were processed by using X`Pert HighScore software[33].

Most of the powder samples were prepared by manual milling of the crystals in agate mortar. Ball mill was used for both nitrate phases because crystal shape caused the preferential orientation.

3.2.4 FTIR spectroscopy

The infrared spectra of prepared salts were recorded at the room temperature using DRIFTS (sample diluted in KBr) and nujol mulls (KBr windows) techniques on a Thermo Scientific Nicolet 6700 FTIR spectrometer with a 2 cm^{-1} resolution and Happ-Genzel apodization in the 400 - 4000 cm^{-1} region. All presented spectra were processed in OMNIC[34] software.

3.2.5 Raman spectroscopy

The Raman spectra of polycrystalline samples were recorded at the room temperature on a Thermo Scientific Nicolet 6700 FTIR spectrometer equipped with the Nicolet Nexus FT Raman module (2 cm^{-1} resolution, Happ-Genzel apodization, 1064 nm Nd:YVO_4 laser excitation, 500 mW power at the sample) in the 100 – 3700 cm^{-1} region. The uniformity of prepared crystals was also controlled on a Thermo Scientific DXR Raman Microscope interfaced to an Olympus microscope (objective 10x) in the 25 – 1800 cm^{-1} spectral region with approx. 3 cm^{-1} spectral resolution. The power of frequency-stabilised single mode diode laser (780 nm) impinging on the sample was 10 mW. All presented spectra were processed in OMNIC[34] software

3.2.6 SHG measurements

The SHG measurements were performed with 90 fs laser pulses generated at an 82 MHz repetition rate by a Ti:sapphire laser (Tsunami Spectra Physics) at 800 nm. For the quantitative determination of the SHG efficiency, the intensity of the back-scattered laser light at 400 nm generated in the samples was measured using a grating spectrograph with a diode array (InstaSpec II, Oriel), and the signal was compared with the one generated in KDP with 100 – 150 μm particle size. The measurements were performed using powdered samples with different particle size (100 – 125 μm, 125 – 150 μm, bigger than 150 μm) loaded into 5 mm glass cells with the aid of a vibrator. The measurements were repeated over different areas of the same sample (the results were then averaged). This experimental procedure minimises the signal fluctuations induced by the sample packing.

4 Results and discussion

4.1 Quantum-chemical calculations

The quantum-chemical calculations were primary used for a prediction of NLO properties of the target molecule by calculation of dipole moment, polarizability and hyperpolarizability values. Firstly, for considering which form of the base **pcam** is the most suitable for NLO, optimised geometries of an uncharged, monocationic and dicationic form of it were found (Table 2). All three optimised molecules belong to point group C_1.

Table 2: Optimised geometries of uncharged molecule (**pcam**), monocationic (**Hpcam^{1+}**) and dicationic (**H$_2$pcam^{2+}**) forms and their calculated values of total dipole moment μ and the total hyperpolarizability β_{tot} (B3LYP/6-311++G(d,p)).

	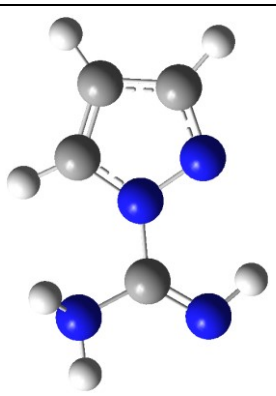 **pcam**	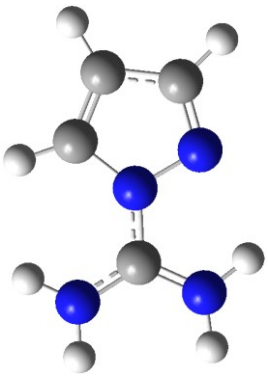 **Hpcam^{1+}**	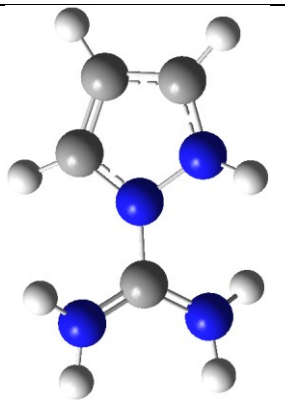 **H$_2$pcam^{2+}**
E (a.u)	-375.1256	-375.5054	-375.6911
μ (Debye)	3.6050	4.8961	3.3301
β_{tot} (esu)	$8.38 \cdot 10^{-31}$	$1.91 \cdot 10^{-30}$	$1.75 \cdot 10^{-30}$

Note: Calculated values of dipole moment, polarizability and the first hyperpolarizability components for all three forms are listed in Supplement in Tables S1-S3.

After the potential energy minima of all three forms were found, demanding physical values were calculated. Values of corresponding dipole moments, polarizabilities and hyperpolarizabilities are listed in Table 2. They indicate that the most promising form for application in nonlinear optics is monoprotonated form. The theoretical value of hyperpolarizability β_{tot} for monocation **Hpcam^{1+}** is almost 2.5 times higher than for the standard molecule of urea (B3LYP/6-311G; $\beta_{tot} = 7.80 \cdot 10^{-31}$ esu) that points out promising application in the field of nonlinear optics.

After geometry optimisation only vibrational spectra for this form were predicted and assigned considering that in measured crystal structures together with commercially available product the target molecule is monocation (**Hpcam**$^{1+}$). List of theoretical vibrational frequencies with expected intensities in infrared and Raman spectra and their assignment can be found in Table 3. Simulated infrared and Raman spectra of an isolated **Hpcam**$^{1+}$ cation in vacuum compared with real vibrational spectra of prepared **HpcamCl·H$_2$O** is compared in Figure 4. It is obvious, that calculated wavenumbers fit quite well to the measured bands and they are applicable for further interpretation of vibrational spectra of prepared salts.

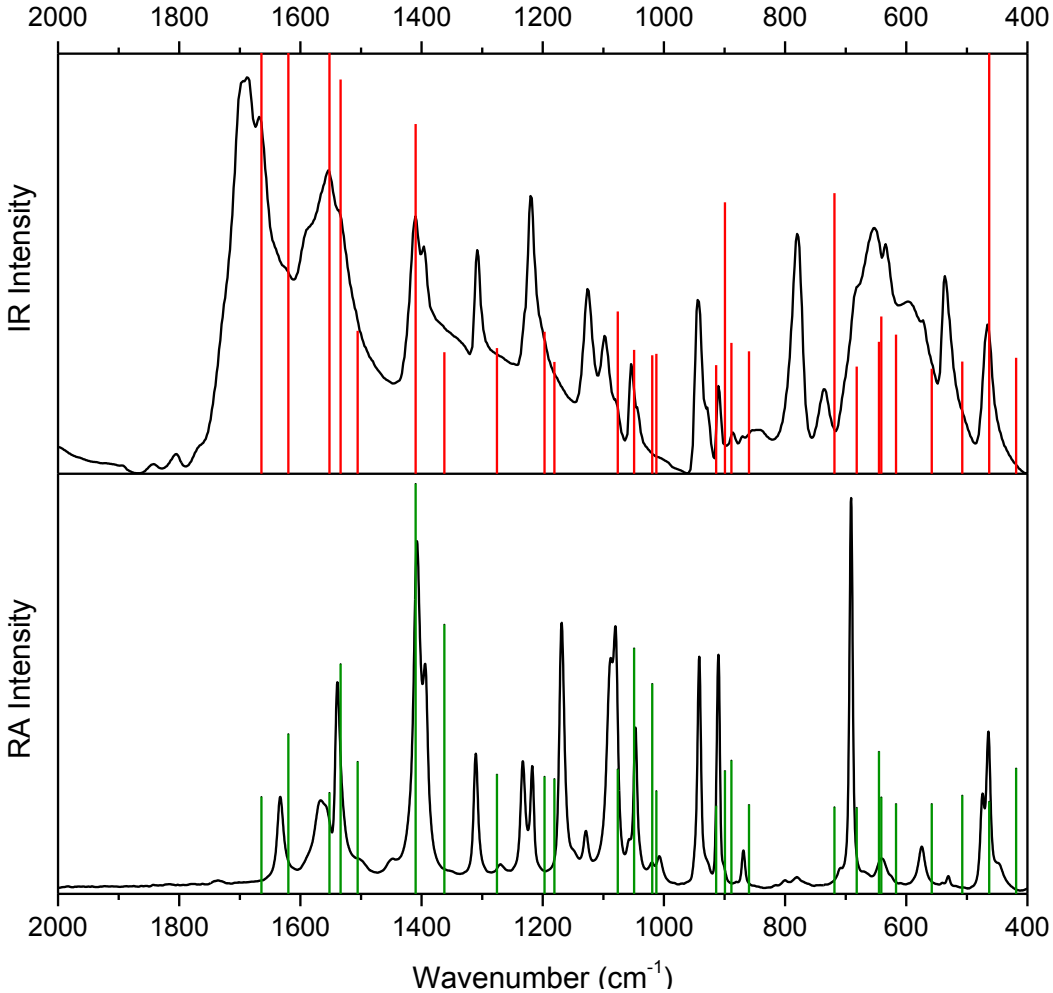

Figure 4: Simulated infrared (red lines, upper part) and Raman spectra (green lines, lower part) of an isolated **Hpcam**$^{1+}$ cation in vacuum compared with real vibrational spectra of prepared salt **HpcamHCl·H$_2$O**.

Table 3: Calculated vibrational frequencies for the **Hpcam**$^{1+}$ cation (B3LYP/6-311G++(d,p), unscaled).

$\tilde{\nu}$ (cm^{-1})	Relative Intensity IR/Ra (%)	Assignment	$\tilde{\nu}$ (cm^{-1})	Relative Intensity IR/Ra (%)	Assignment
34	0/0	τ rg-C$(NH_2)_2$	1085	2/15	ρ NH_2, δ CH
145	2/1	ω rg-C$(NH_2)_2$	1113	6/4	ν rg, ρ NH_2, δ CH
254	0/0	δ rg-C$(NH_2)_2$	1221	1/3	ν NN, δ rg, δ NCN, δ CH
333	30/0	ω NH_2	1238	4/3	ρ CH, ν rg, ω NH_2, ν CN
359	0/1	γ NH	1319	2/3	ν rg, ν CN_3, δ CN_3, δ CH
433	1/4	δ NCN	1409	2/17	ν rg, δ CH, δ CN_3
479	58/1	ω NH_2	1458	26/30	ν rg, δ rg, δ CH, ν C-rg
525	1/1	ρ rg-C$(NH_2)_2$	1557	4/4	δ NH_2
577	0/1	γ rg, γ CN_3	1586	30/13	ν NCN, ν rg, δ NH_2, δ CH
638	4/1	γ rg, γ CN_3	1605	46/2	ν NCN, ν rg, δ NH_2, δ CH
663	6/1	τ NH_2, γ NH	1675	97/7	δ NH_2, δ CN_3
667	3/5	δ NCN, ν C-rg, δ rg	1721	100/1	ν CN_3, δ NH_2, δ CN_3
705	0/0	γ CN_3, γ rg	3246	0/74	ν CH
743	19/0	γ CH	3258	1/30	ν CH
889	2/0	γ CH	3276	2/100	ν CH
919	3/5	δ rg, ω NH_2	3522	39/40	ν_s NH_2
930	18/4	δ rg, ν CN_3, ν CN, ν NN	3594	36/71	ν_s NH_2
945	0/0	γ CH	3674	41/42	ν_{as} NH_2
1047	2/2	ρ NH_2, δ CH	3706	27/25	ν_{as} NH_2
1054	1/11	ρ NH_2, ν CC, δ CH			

Note: Abbreviations and symbols: ν, stretching; δ, deformation or in-plane bending; γ, out-of-plane bending; ρ, rocking; ω, wagging; τ, torsion; $_s$, symmetric; $_{as}$, antisymmetric; rg, ring.

One of the goals of this thesis was to find the best way to interpret vibrational spectra of crystalline salts based on organic heteroaromatic cation and inorganic anion. The main aim was to reach the best match of theoretical results with the properties of real materials together with the shortest calculation time. Four different approaches were compared: model of an isolated **Hpcam**$^{1+}$ cation in vacuum, model of an isolated uncharged unit (**Hpcam**$^{1+}$ cation and acid anion) in vacuum, model of an isolated fragment selected from real crystal structure (consisting of two **Hpcam**$^{1+}$ cations and two acid anions) and solid state computations using CRYSTAL[25-26] software.

4.1.1 Initial calculations concerning 1*H*-pyrazole-carboxamidinium nitrate (HpcamNO$_3$ (I))

Quantum-chemical calculation using all four, previously mentioned, approaches were applied only for **HpcamNO$_3$ (I)**. Nitrate salt was chosen because of its simple planar inorganic anion with only four vibrational modes active in both infrared and Raman spectra. These modes are unlike vibrational modes of carboxylic acids easily to assign and they are clearly distinguishable from vibrational modes of the base. Comparison of all four approaches of theoretical and measured vibrational spectra is shown in Figures 5 - 8. All of the vibrational spectra are compared in the region 400 – 2000 cm^{-1} characteristic mainly for deformation vibrations of molecules*.

Simulated spectra of model based on an isolated monocation **Hpcam^{1+}** in vacuum (Figure 5) surprisingly achieved a very good match with measured vibrational spectra of the salt. Important advantage of this model together with good results (useful for assignment of vibrations) is a very short calculation time. The main differences of calculated and real IR spectra can be observed in 1500 - 1700 cm^{-1} region and they are probably associated with neglecting of H-bonding influencing δ NH$_2$ modes. Absence of anionic bands might be considered as a disadvantage but in case of simple inorganic anions they are easy to assign according to the literature[35].

* Region 2000 – 4000 cm^{-1} corresponds to manifestations of valence vibrations of N-H, O-H and C-H groups and there are broad bands in measured spectra caused by hydrogen bonds which are not considered in simulated spectra.

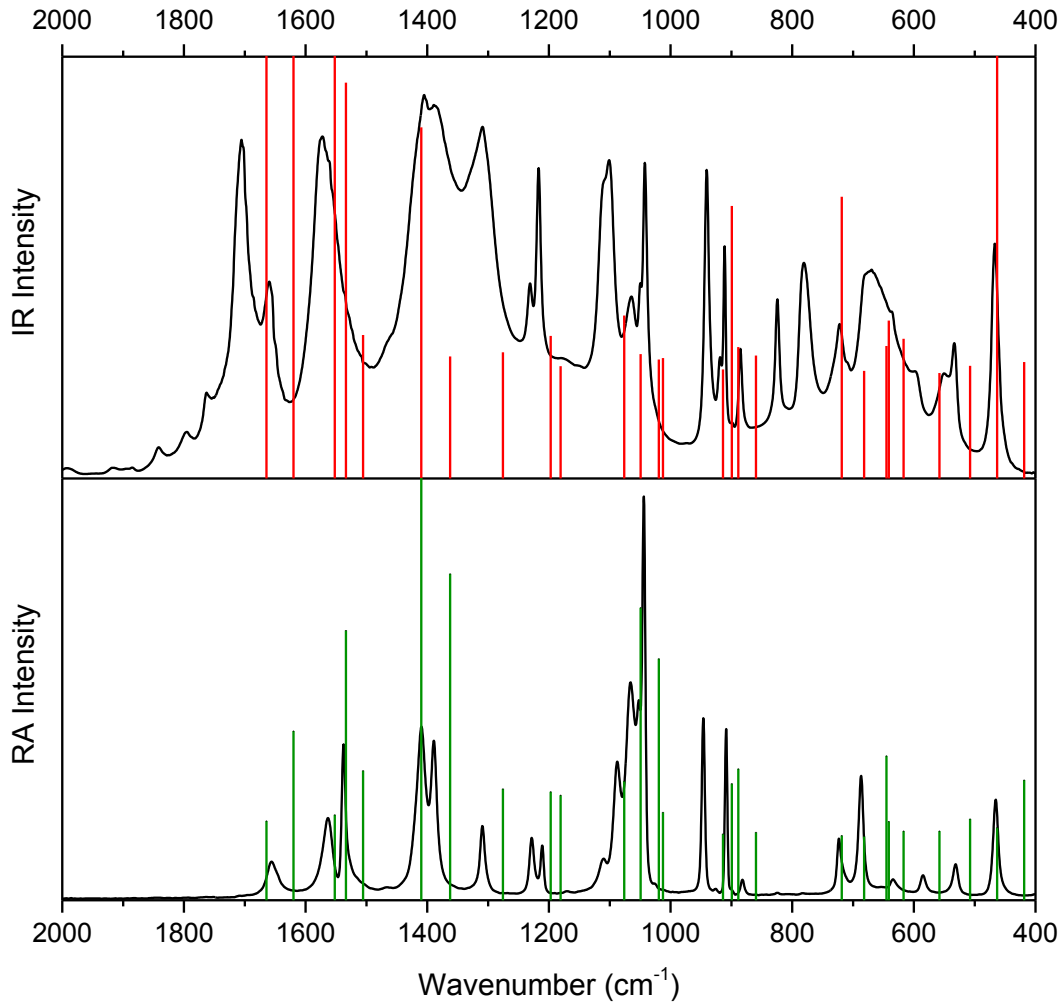

Figure 5: Simulated IR (red lines, upper part) and Raman spectra (green lines, lower part) of an isolated **Hpcam**$^{1+}$ cation in vacuum compared with real vibrational spectra of salt **HpcamNO$_3$ (I)**.

The utilisation of model based on an isolated cation and acid anion in vacuum (Figure 6) and model containing an isolated fragment of real crystal structure (Figure 7) slightly decreased differences in positions of recorded and calculated modes. On the other hand optimisation of the modes led to the arrangement of ions which is not consistent with the real structure. This fact could be observed in Figure 7 where the position of the calculated bands are more scattered than in Figure 6.

CPU time of these models is much longer than in the first approach.

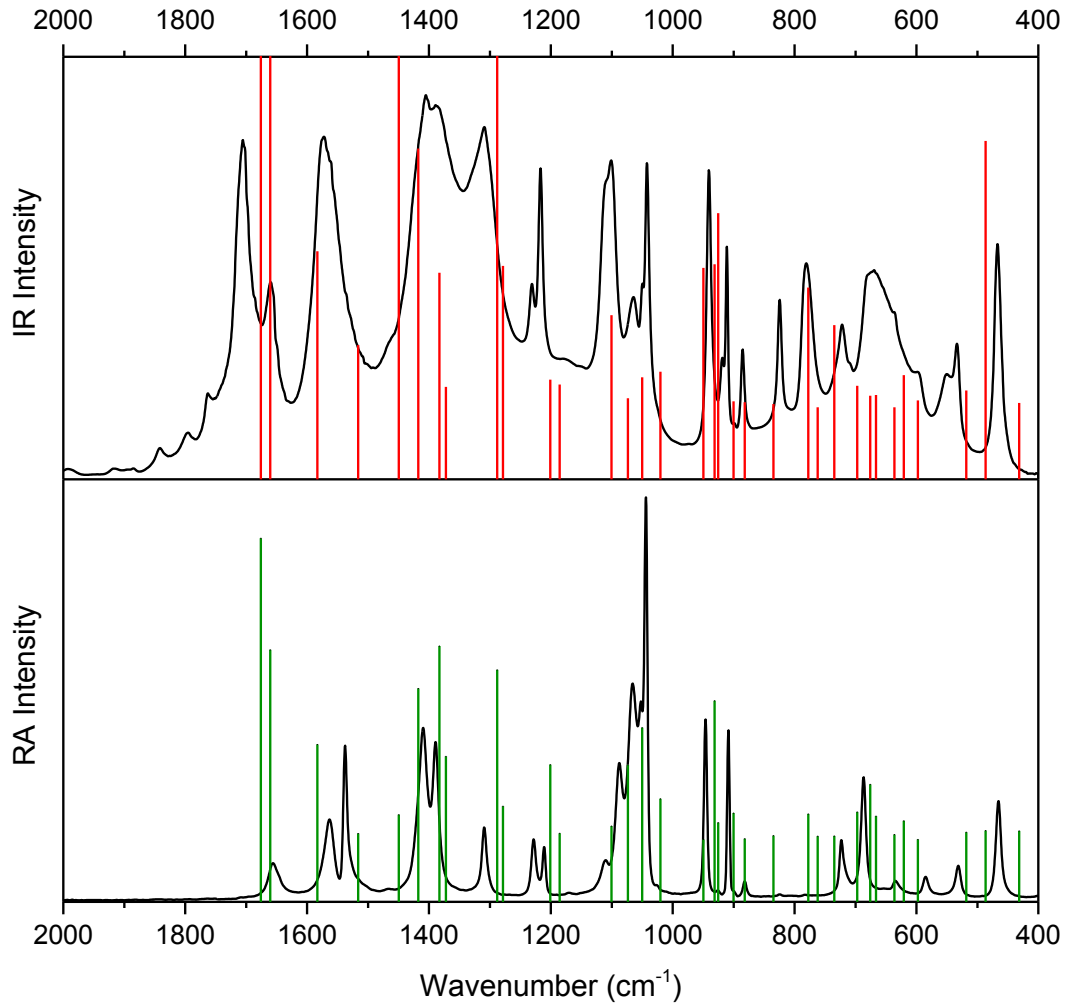

Figure 6: Simulated IR (red lines, upper part) and Raman spectra (green lines, lower part) of an isolated base cation and acid anion in vacuum compared with real vibrational spectra of salt **HpcamNO$_3$ (I)**.

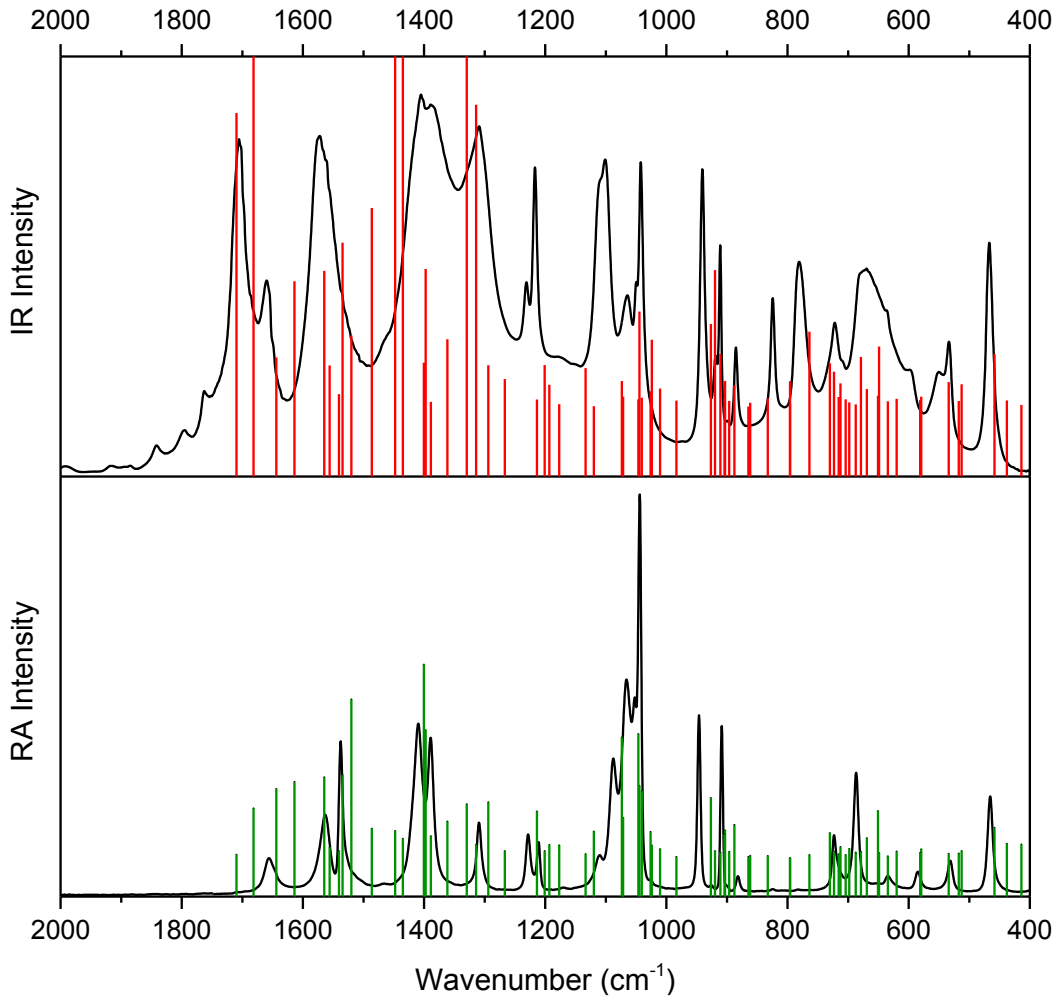

Figure 7: Simulated IR (red lines, upper part) and Raman spectra (green lines, lower part) of an isolated fragment of crystal structure (two molecules of base cation and two molecules of nitrate anion) of salt **HpcamNO$_3$ (I)** compared with its real vibrational spectra.

The best match of the calculated and recorded vibrational spectra of all four chosen models provide definitely solid state calculations (CRYSTAL17 software[26]) (Figure 8). Number of simulated modes and their positions fits very well with measured spectra as well as relative intensities of bands. Disadvantage of this approach is definitely computing time and computer requirements.

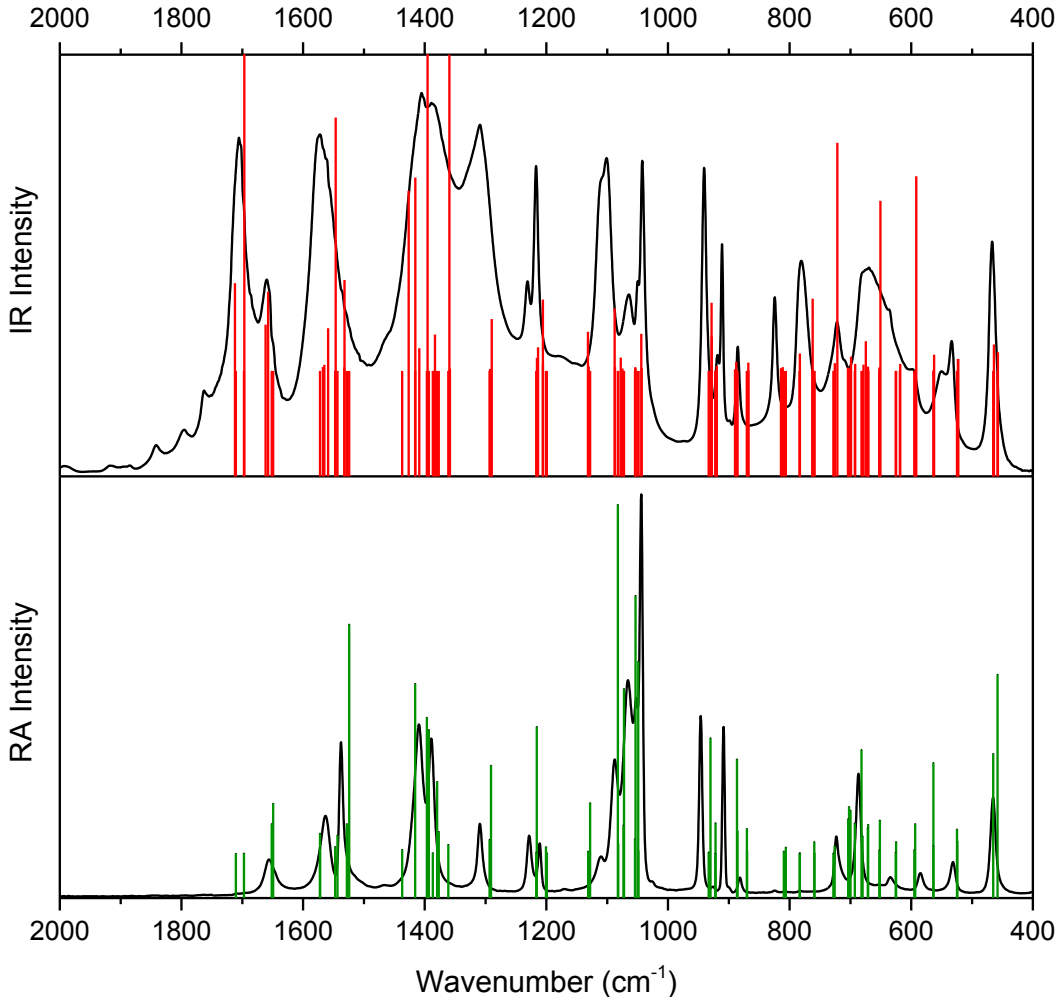

Figure 8: Solid state simulated IR (red lines, upper part) and Raman spectra (green lines, lower part) salt **HpcamNO$_3$ (I)** compared with real vibrational spectra.

4.1.2 Inorganic salts of pcam

For the rest of inorganic salts only first and last model were applied for simulation and interpretation of their spectra (model of an isolated monocation **Hpcam^{1+}** in vacuum and solid state calculations) according to the results of different approaches to quantum-chemical calculations for salt **HpcamNO$_3$ (I)**. Comparison of both approaches of theoretical and measured vibrational spectra for the rest of the inorganic salts is shown for each salt individually in Chapter 4.2.

4.2 Prepared salts of 1*H*-pyrazole-carboxamidine with inorganic acids

Inorganic salts of **pcam** crystallised very well. Except systems with boric, phosphorous and selenic acids which did not provide crystalline product, the rest of the used acids formed well developed crystals within two weeks. Used acids, ratios and prepared products are listed in Table 4. All of the used molar ratios of particular acid led to the same crystalline salt.

Table 4: Crystalline salts of 1*H*-pyrazole-carboxamidine with inorganic acids.

Acid	Ratio (B:A)		
	1:1	1:2	2:1
HCl	**HpcamCl·H_2O**		
$HClO_4$	**HpcamClO_4**		
HNO_3	**HpcamNO_3 (I) + (II)**		
H_3PO_4	**HpcamH_2PO_4**		
H_2SO_4	**HpcamHSO_4**		
CH_3SO_3H	**HpcamCH_3SO_3**		
NH_2SO_3H	**HpcamNH_2SO_3**		

Out of prepared crystals only **HpcamCl·H_2O** crystallise in triclinic space group *P*-1. The rest of these inorganic salts crystallise in monoclinic space groups - $P2_1/n$ (**HpcamNO_3 (I)**, **HpcamCH_3SO_3**) or space group $P2_1/c$ (rest). Base is monoprotonated in all of the prepared salts.

Crystal structures and vibrational spectra of all of the prepared crystals are described in this chapter individually. Basic crystallographic data and structure refinement details for all these inorganic salts are listed in tables in Supplement (Tables S5 and S6) and Electronic Supplement (ES1 – ES8). Vibrational modes of infrared and Raman spectra of these inorganic salts were assigned. Bands corresponding to the vibrations of cation were assigned using quantum-chemical calculations (see Table 3) and bands caused by vibrations of anions were assigned according to the literature[35].

The phase uniformity of prepared salts was verified by powder X-ray diffraction, results of which are listed in Tables S9 – S16 in Supplement for each salt individually. Measured diffraction patterns are consistent with calculated diffraction maxima (Diamond software[36]) from single crystal data.

4.2.1 1*H*-pyrazole-carboxamidinium chloride monohydrate (HpcamCl·H_2O)

Crystal structure

This product was obtained from water solution of **pcam** with hydrochloric acid in molar ratios 1:1, 1:2 and 2:1 (Table 4). The same product occurs by recrystallisation of commercial product **pcam·HCl**. It is the only triclinic structure out of all prepared inorganic crystal salts of **pcam**. Asymmetric unit is shown in Figure 9, crystal packing in Figure 10, hydrogen bonds details are listed in Table 5, diffraction maxima and d-spacing obtained by powder X-ray diffraction are listed in Table S9 in Supplement.

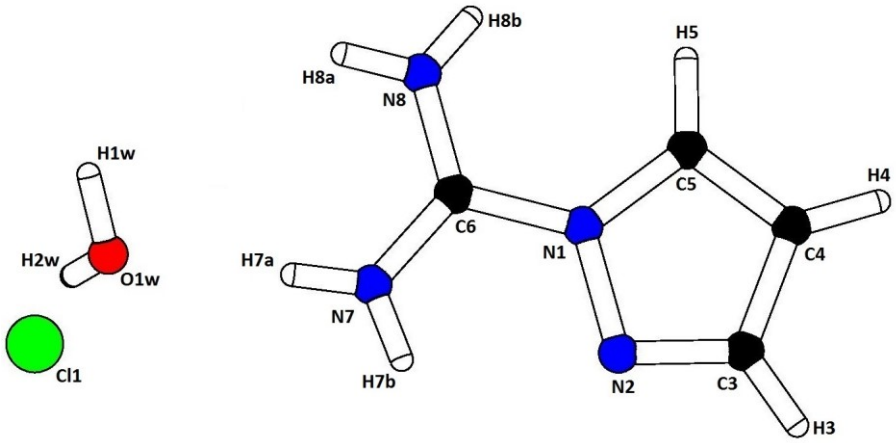

Figure 9: Asymmetric unit of **HpcamCl·H_2O**.

As is apparent from Figure 10 in this structure centrosymmetric pairs of cations are formed. They are connected by intermolecular N7-H7b...N2 hydrogen bonds. Conformation of the cations is also stabilised by intramolecular H-bond involving atom H7b as well.

These pairs of cations form chains bonded *via* hydrogen bonds formed by two chloride anions and two molecules of water between the pairs. This conformation of molecules lead to the formation of non-bonded layers, shown in Figure 10.

Distances *d*(D···A) of bonds connecting amino hydrogen atoms H8a and H8b with chloride anion differ only slightly (3.212(2) and 3.220(2) Å). They are expectable weaker than hydrogen bond formed *via* amino hydrogen atom H7a and water molecule with *d*(D···A) only 2.783(2) Å. The arrangement of molecules in layers is also stabilised by H-bonds between C3-H3...O1w and C5-H5...Cl1. These two distances *d*(D···A) are the longest out of all prepared salts (3.495(2) and 3.565(2) Å).

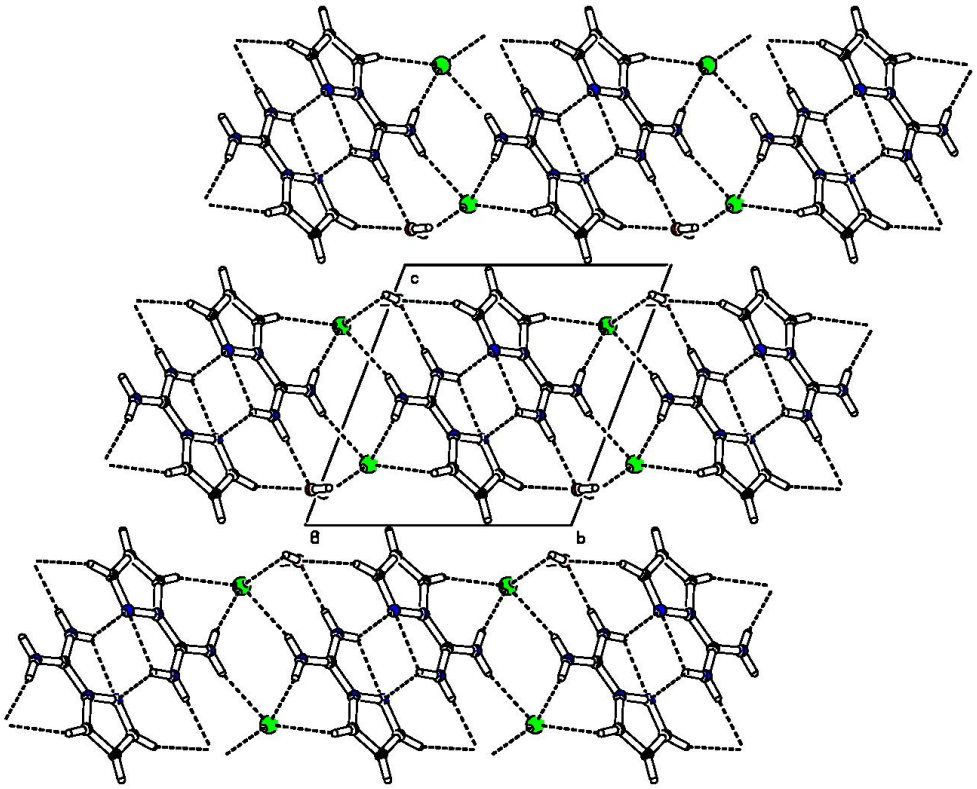

Figure 10: Crystal packing of **HpcamCl·H₂O** (projection to plane *bc*). Dashed lines indicate H-bonds.

Table 5: Hydrogen bonds geometry of **HpcamCl·H₂O**.

	d(D – H) (Å)	*d*(H···A) (Å)	*d*(D···A) (Å)	∢ D-H···A (°)
O1w-H1w...Cl1[a]	0.87	2.52	3.251(2)	142
O1w-H2w...Cl1	0.85	2.34	3.156(2)	163
N7-H7a...O1w	0.84	1.94	2.783(2)	178
N7-H7b...N2	0.85	2.28	2.667(2)	108
N7-H7b...N2[b]	0.85	2.26	2.993(2)	145
N8-H8a...Cl1[a]	0.85	2.38	3.212(2)	165
N8-H8b...Cl1[c]	0.81	2.42	3.220(2)	171
C3-H3...O1w[b]	0.95	2.59	3.495(2)	158
C5-H5...Cl1[c]	0.95	2.67	3.565(2)	158

Symmetry codes: a) -1+x, y, z; b) 2-x, 1-y, 1-z; c) 1-x, 2-y, 1-z

Vibrational spectra

FTIR and Raman spectra of salt **HpcamCl·H₂O** are depicted in Figure 11. The calculated spectra are in a good match with the measured ones (Figures 12 and 13) so these calculations (according to the Table 3) were used for vibrational modes assignment. The band assignment is listed in Table 6. The overall character of vibrational spectra is in agreement with crystal structure solution – i.e. crystal formed by **Hpcam**$^{1+}$ cations, Cl^- anions and water molecules connected by system of H-bonds.

Table 6: The band assignment of FTIR and Raman spectra of **HpcamCl·H_2O**.

FTIR (cm^{-1})	Raman (cm^{-1})	Assignment	FTIR (cm^{-1})	Raman (cm^{-1})	Assignment
	107 s	External modes	1045 sh	1047 m	ρ NH_2, δ CH
	126 vs		1055 w	1057 sh	ρ NH_2, ν CC, δ CH
	190 s		1080 sh	1080 s	ρ NH_2, δ CH
	242 s		1098 m	1088 sh	
	464 m	δ NCN	1127 m	1129 w	ν rg, ρ NH_2, δ CH
466 m	474 m	ω NH_2		1169 s	?
538 m	531 vw	ρ rg-$C(NH_2)_2$		1217 m	ν NN, δ rg, δ NCN, δ CH
573 sh	574 w	γ rg, γ CN_3	1221 s	1233 m	ρ CH, ν rg, ω NH_2, ν CN
598 sh				1270 vw	?
636 m	641 w	γ rg, γ CN_3	1309 m	1311 m	ν rg, ν CN_3, δ CN_3, δ CH
653 m		τ NH_2, γ NH	1397 m	1394 s	ν rg, δ CH, δ CN_3
682 sh	691 s	δ NCN, ν C-rg, δ rg	1411 m	1408 vs	ν rg, δ rg, δ CH, ν C-rg
	708 vw	γ CN_3, γ rg		1539 m	δ NH_2
736 w		γ CH	1555 sh	1566 m	ν NCN, ν rg, δ NH_2, δ CH
780 m	780 vw	?	1592 sh		?
848 vw		?	1668 vs	1633 m	δ NH_2, δ CN_3, δ H_2O
873 vw		?	1686 vs	1736 vw	ν CN_3, δ NH_2, δ CN_3
887 vw	869 w	γ CH		3064 vw	ν NH…X
911 w	910 s	δ rg, ω NH_2	3100 vs	3101w	ν CH
929 sh		γ CH	3128 s	3121 w	
946 m	942 s	δ rg, ν CN_3, ν CN, ν NN		3133 m	
			3320 vs	3339 wb	ν NH…X, ν OH…Cl
	1008 w	?	3378 s		ν NH…X
	1020 w	?			

Note: Symbol X – atom N, O or Cl.

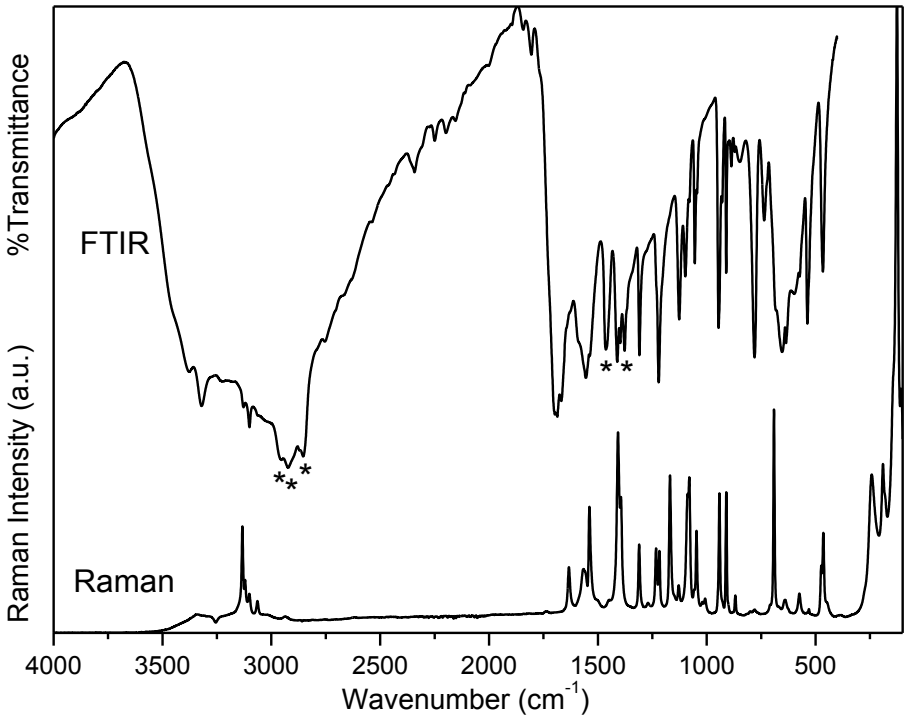

Figure 11: FTIR (nujol mull) and Raman spectra of **HpcamCl·H_2O**. Nujol bands are labelled by asterisk.

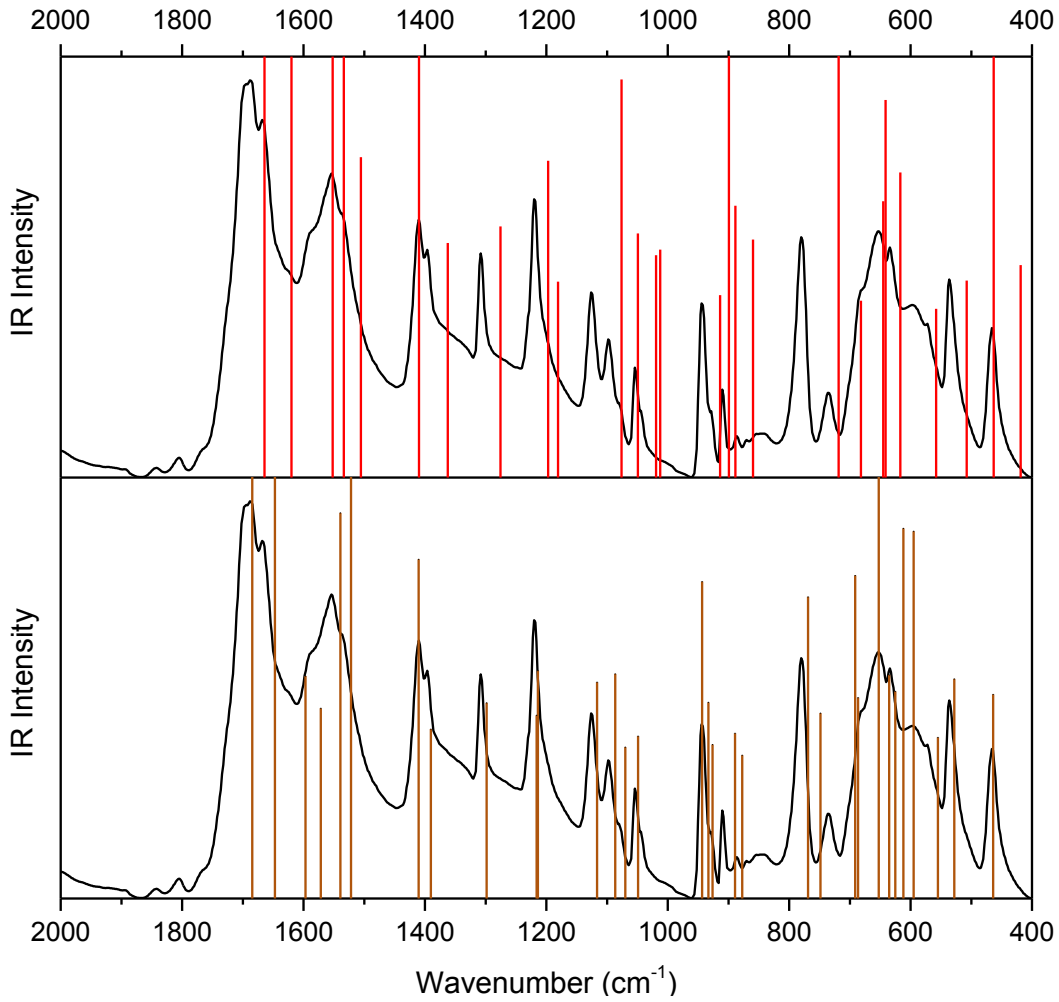

Figure 12: Recorded FTIR spectrum of salt **HpcamCl·H₂O** compared with simulated IR spectrum of an isolated **Hpcam**$^{1+}$ cation in vacuum (red lines, upper part) and with solid state simulated IR spectrum (brown lines, lower part).

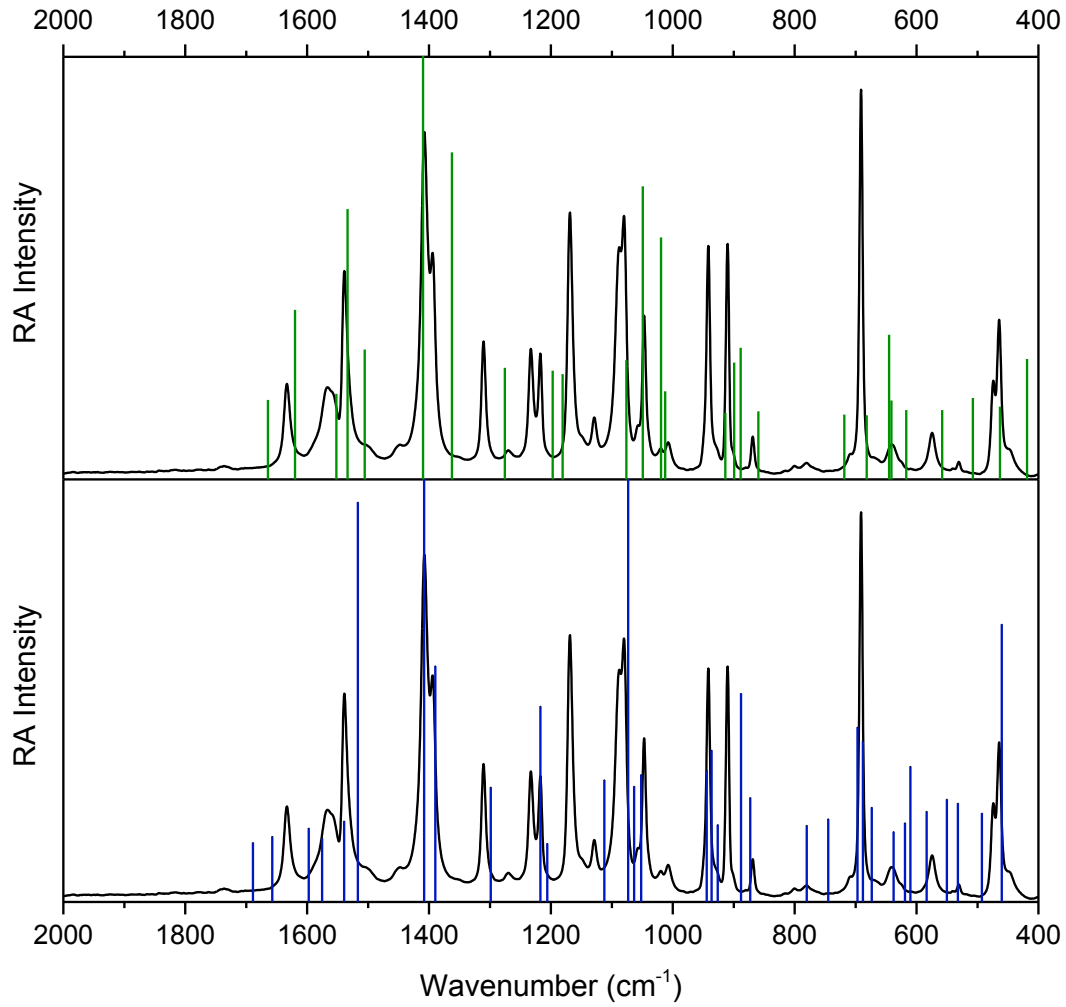

Figure 13: Recorded Raman spectrum of salt **HpcamCl·H₂O** compared with simulated Raman spectrum of an isolated **Hpcam**$^{1+}$ cation in vacuum (green lines, upper part) and with solid state simulated Raman spectrum (blue lines, lower part).

4.2.2 1*H*-pyrazole-carboxamidinium perchlorate (HpcamClO₄)

Crystal structure

This salt was obtained from water solution of **pcam** with perchloric acid in molar ratios 1:1, 1:2 and 2:1 (Table 4). Asymmetric unit is shown in Figure 14, crystal packing in Figure 15, hydrogen bonds details are listed in Table 7, diffraction maxima and d-spacing obtained by powder X-ray diffraction are listed in Table S10 in Supplement.

Crystal structure is hydrogen bonded and based on alternating cations and anions as is shown in packing in Figure 15. They does not form continual layers because only two oxygen atoms O2 and O4 of tetrahedral perchlorate anions are hydrogen bonded with amino hydrogen atoms H7a and H8a in the plane of cations. Distances *d*(D···A) of these two H-bonds slightly differ (2.939(3) and 2.980(4) Å). The rest two oxygen atoms

O1 and O3 are forming H-bonds with the rest two hydrogen atoms H7b and H8b of amino groups of cations below and above the in-plane pair of anion with cation. These two distances *d*(D···A) differ a lot (3.053(3) and 2.878(3) Å). The structure is also stabilised by intramolecular N7-H7b...N2 interaction as well as by weak H-bonds involving carbon atoms, see Table 7.

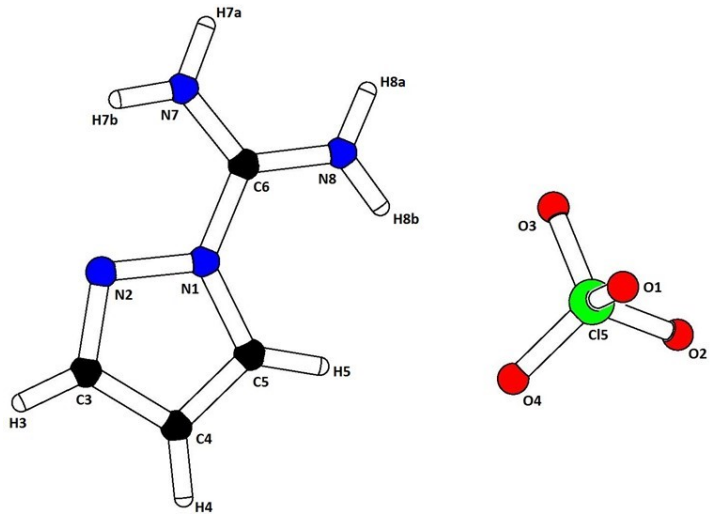

Figure 14: Assymetric unit of **HpcamClO$_4$**.

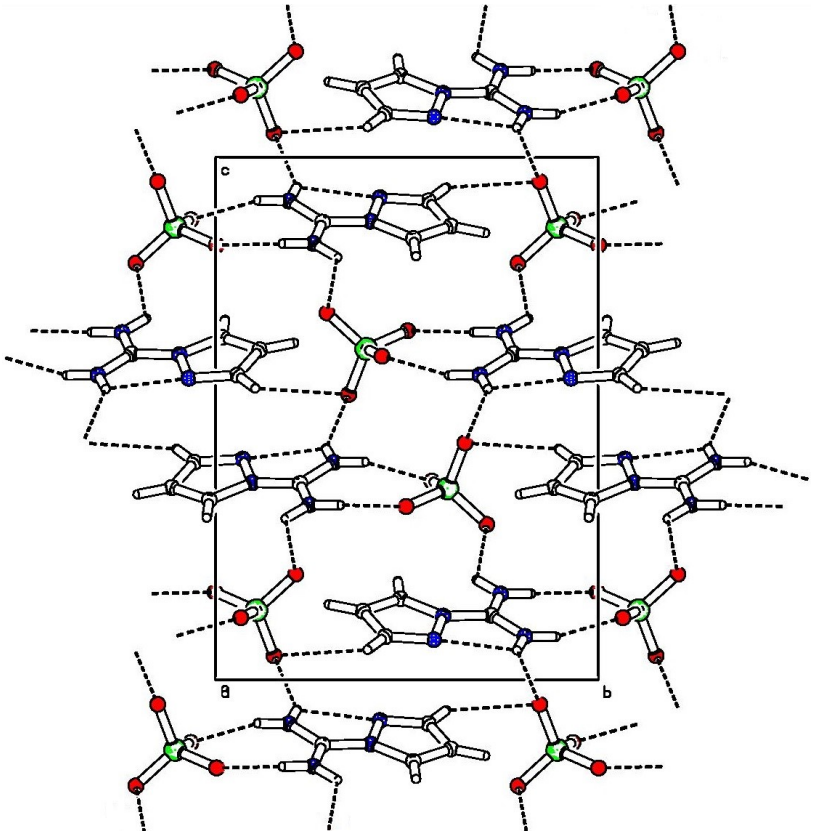

Figure 15: Crystal packing of **HpcamClO$_4$** (projection to plane *bc*). Dashed lines indicate hydrogen bonds.

Table 7: Hydrogen bonds geometry of **HpcamClO4**.

	d(D – H) (Å)	*d*(H···A) (Å)	*d*(D···A) (Å)	∢ D-H···A (°)
N7-H7a...O2[a]	0.88	2.09	2.939(3)	163
N7-H7b...N2	0.88	2.28	2.644(3)	105
N7-H7b...O1[b]	0.88	2.28	3.053(3)	146
N8-H8a...O4[a]	0.88	2.11	2.980(4)	169
N8-H8b...O3	0.88	2.28	2.878(3)	126
C3-H3...O1[c]	0.95	2.58	3.277(4)	130
C5-H5...O4	0.95	2.60	3.491(4)	157

Symmetry codes: a) 1-x, -1/2+y, 3/2-z; b) -1+x, 1/2-y, 1/2+z; c) –x, 1/2+y, 3/2-z

Vibrational spectra

FTIR and Raman spectra of salt **HpcamClO4** are depicted in Figure 16. Vibrational bands of perchlorate anion were assigned using the literature[35]. Vibrational manifestations of cation were assigned using quantum-chemical calculations. The comparison of the calculated spectra with the measured ones is shown in Figures 17 and 18. The band assignment is listed in Table 8.

The overall character of vibrational spectra is in agreement with crystal structure solution – i.e. crystal formed by **Hpcam**$^{1+}$ cations and ClO_4^- anions connected by system of H-bonds.

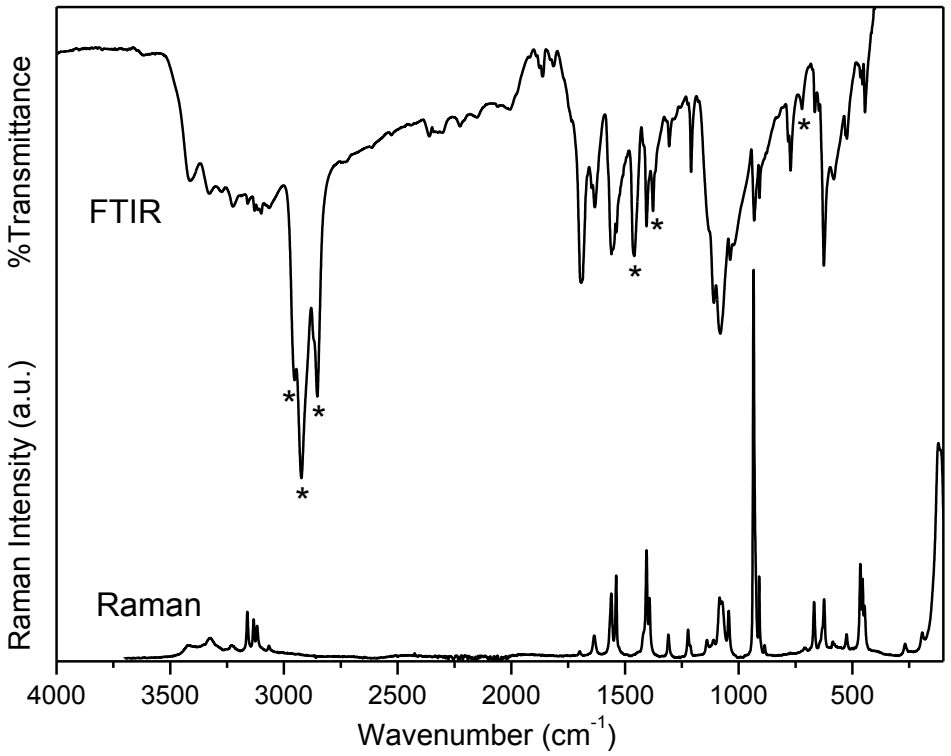

Figure 16: FTIR (nujol mull) and Raman spectra of **HpcamClO4**. Nujol bands are labelled by asterisk.

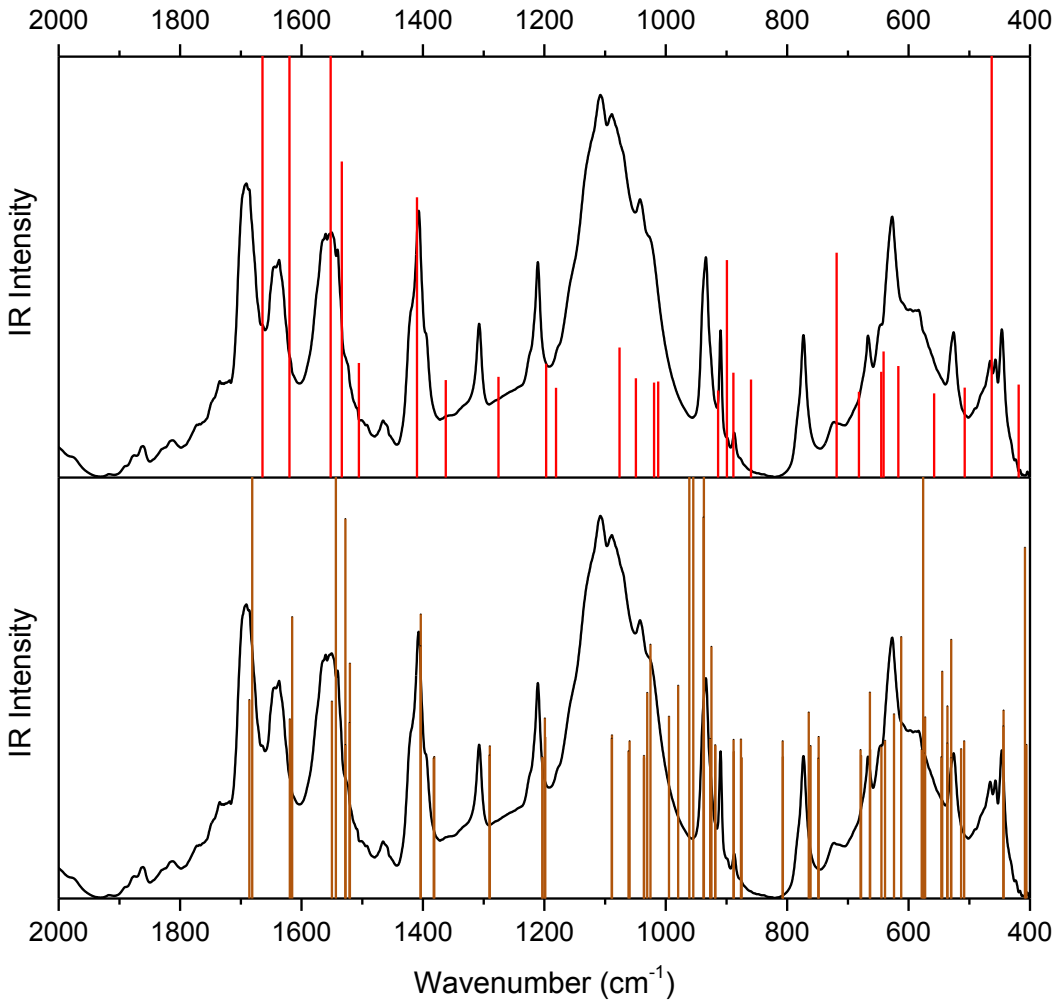

Figure 17: Recorded FTIR spectrum of salt **HpcamClO$_4$** compared with simulated IR spectrum of an isolated **Hpcam**$^{1+}$ cation in vacuum (red lines, upper part) and with solid state simulated IR spectrum (brown lines, lower part).

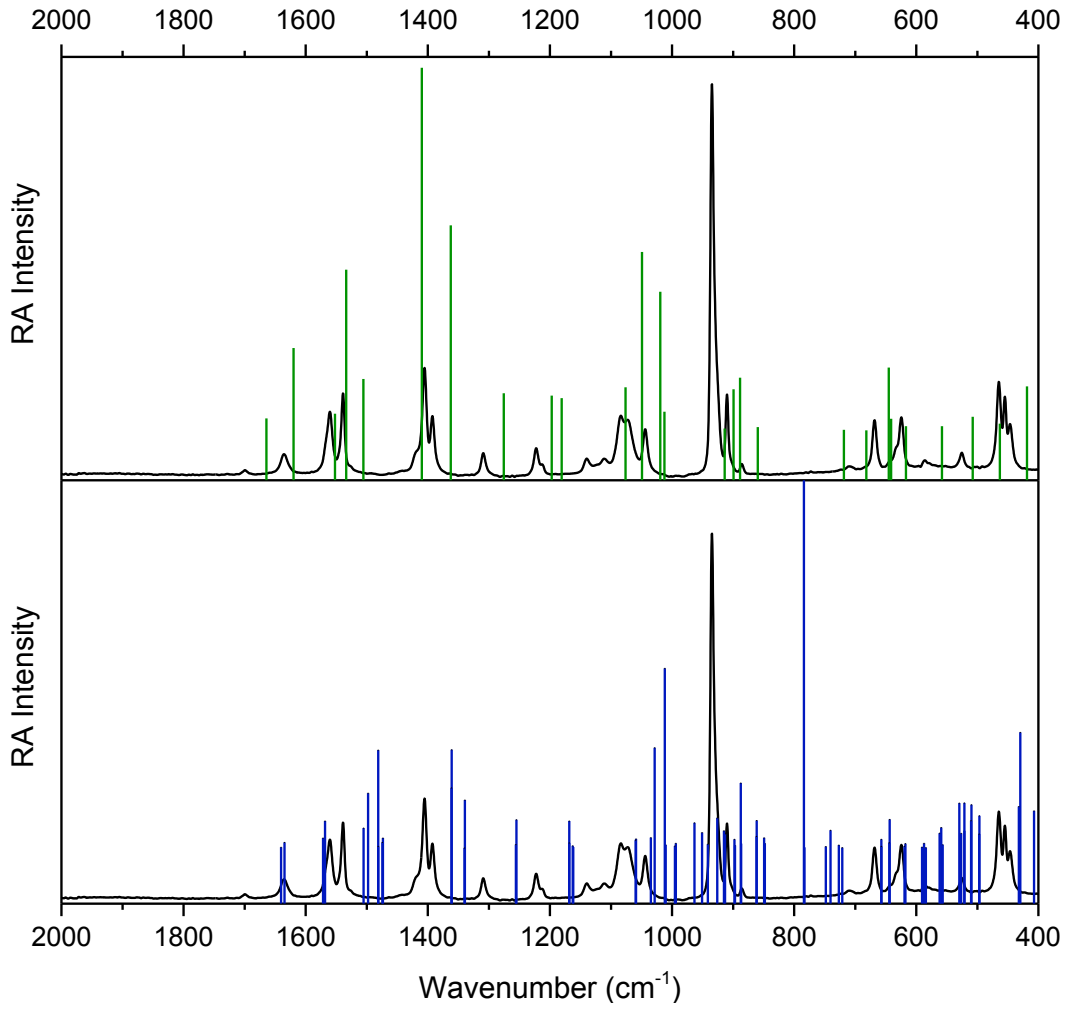

Figure 18: Recorded Raman spectrum of salt **HpcamClO$_4$** compared with simulated Raman spectrum of an isolated **Hpcam^{1+}** cation in vacuum (green lines, upper part) and with solid state simulated Raman spectrum (blue lines, lower part).

Table 8: The band assignment of FTIR and Raman spectra of **HpcamClO4**.

FTIR (cm^{-1})	Raman (cm^{-1})	Assignment	FTIR (cm^{-1})	Raman (cm^{-1})	Assignment
	122 s	External modes	1109 vs	1111 w	ν_3 ClO_4^-, ν rg, ρ NH_2,
	193 w				δ CH
	268 vw		1140 sh	1140 w	?
444 w	446 m	ν_2 ClO_4^-	1209 m	1213 w	ν NN, δ rg, δ NCN, δ CH
456 vw	455 m		1224 sh	1223 m	ρ CH, ν rg, ω NH_2, ν CN
464 vw	465 m	ω NH_2	1306 w	1309 m	ν rg, ν CN_3, δ CN_3, δ CH
524 w	525 w	ρ rg-$C(NH_2)_2$		1392 m	ν rg, δ CH, δ CN_3
582 m	586 vw	γ rg, γ CN_3	1405 m	1405 s	ν rg, δ rg, δ CH, ν C-rg
625 m	624 m	ν_4 ClO_4^-, γ rg, γ CN_3	1538 m	1539 m	δ NH_2
647 vw	643 vw	ν_4 ClO_4^-, τ NH_2, γ NH	1560 m	1560 m	ν NCN, ν rg, δ NH_2,
665 vw	668 m	ν_4 ClO_4^-, δ NCN,			δ CH
		ν C-rg, δ rg	1633 m	1635 w	δ NH_2, δ CN_3
772 w		?	1647 sh		?
782 w		?	1691 s	1699 vw	ν CN_3, δ NH_2, δ CN_3
	886 vw	γ CH	3065 mb	3066 vw	ν NH…O
908 m	910 m	δ rg, ω NH_2	3116 sh	3118 m	ν CH
932 m	935 vs	ν_1 ClO_4^-, δ rg, ν CN_3,	3129 m	3133 m	
		ν CN, ν NN	3159 mb	3161 m	
1038 m	1044 m	ν_3 ClO_4^-, ρ NH_2, ν CC,	3225 mb	3228 vw	ν NH…O
		δ CH	3276 mb		
	1073 m	?	3329 mb	3325 wb	
1081 vs	1084 m	ν_3 ClO_4^-, ρ NH_2, δ CH	3413 m	3417 wb	

4.2.3 1*H*-pyrazole-carboxamidinium nitrates (HpcamNO3 (I) and HpcamNO3 (II))

Crystal structure

From the water solution of base **pcam** with nitric acid in molar ratios 1:1, 1:2 and 2:1 (Table 4) two different modifications of nitrate salt were obtained in all of the prepared ratios. After crystallisation at room temperature fraction of modification **HpcamNO3 (I)** was dominant. Otherwise, crystallisation at lower temperature (6 °C) caused increase of **HpcamNO3 (II)** modification content.

Asymmetric units of both of these salts consist of one base cation and one nitrate anion arranged in a different way, see Figure 19. Prismatic **HpcamNO3 (I)** crystallise in $P2_1/n$ space group. Product **HpcamNO3 (II)** have the shape of a bar and crystallise in $P2_1/c$ space group. Despite small differences in lattice parameters their unit cell volumes are quite similar (Supplement Table S6). Crystal packing for each modification is shown in Figures 20 and 21, hydrogen bonds geometry is listed in Tables 9 and 10, diffraction maxima and d-spacing obtained by powder X-ray diffraction are listed in Tables S11 and S12 in Supplement.

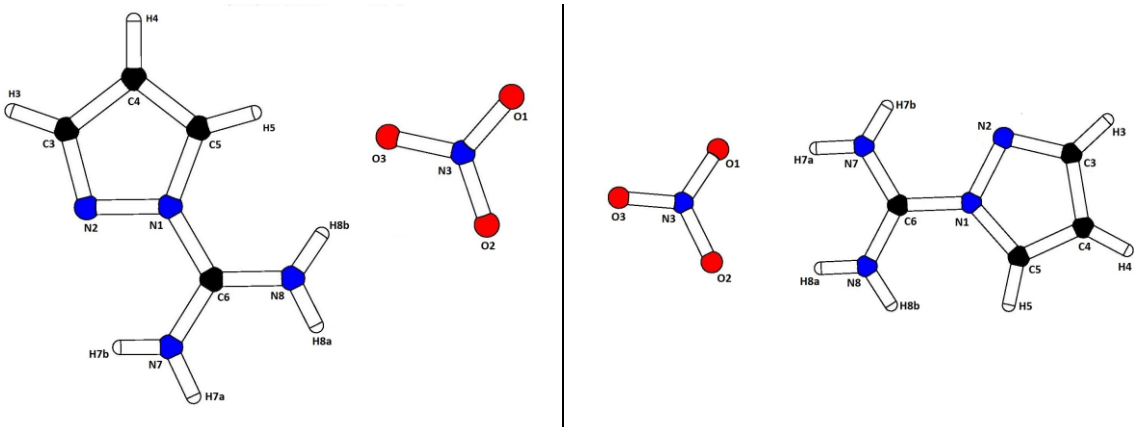

HpcamNO$_3$ (I) **HpcamNO$_3$ (II)**

Figure 19: Asymmetric units of both nitrate phases.

Alternating cations and anions form H-bonded layers connected only by weak van der Waals interactions in both of the modifications, see Figures 20 and 21. Centrosymmetric pairs of cations in both of these nitrate phases are formed. Two cations are connected by intermolecular N7-H7b...N2 H-bonds. Same hydrogen atom H7b is also involved in intramolecular interaction. Distances *d*(D···A) of both bonds N7-H7b...N2 for each modification are similar, see Tables 9 and 10. The main difference between both structures are different H-bonding patterns between cation and nitrate anion.

Nitrate anions connect three cations in layers of **HpcamNO$_3$ (I)** structure. Two oxygen atoms O1 and O2 form bonds with hydrogen atoms H8a and H7a of same cation with similar distances *d*(D···A) (2.855(2) and 2.848(2) Å). The last oxygen atom O3 of nitrate is shared between two molecules by amino group in H-bond N8-H8b...O3 with similar distance *d*(D···A) (2.832(2) Å) like in previous two bonds and by H-bond C4-H4...O3 with much longer *d*(D···A) (3.381(2) Å).

In layers of **HpcamNO$_3$ (II)** structure nitrate anions also connect three **Hpcam^{1+}** cations Oxygen atom O3 form only one hydrogen bond - N8-H8b...O3; with *d*(D···A) = 2.798(2) Å. This hydrogen atom is also shared in a hydrogen bond N8-H8b...O2 with much longer distance *d*(D···A) (3.266(2) Å). Oxygen atom O2 is also involved in another two bonds – bond C5-H5...O2 with the same molecule of cation and bond N8-H8a...O2 with another **Hpcam^{1+}** cation. The last oxygen atom O1 of nitrate forms two H-bonds. Distance *d*(D···A) of N7-H7a...O1 with the same cation as O2 bonds is the shortest with the length 2.769(2) Å. Last type of hydrogen bond involving nitrate is C4-H4...O1 that connects third molecule of cation.

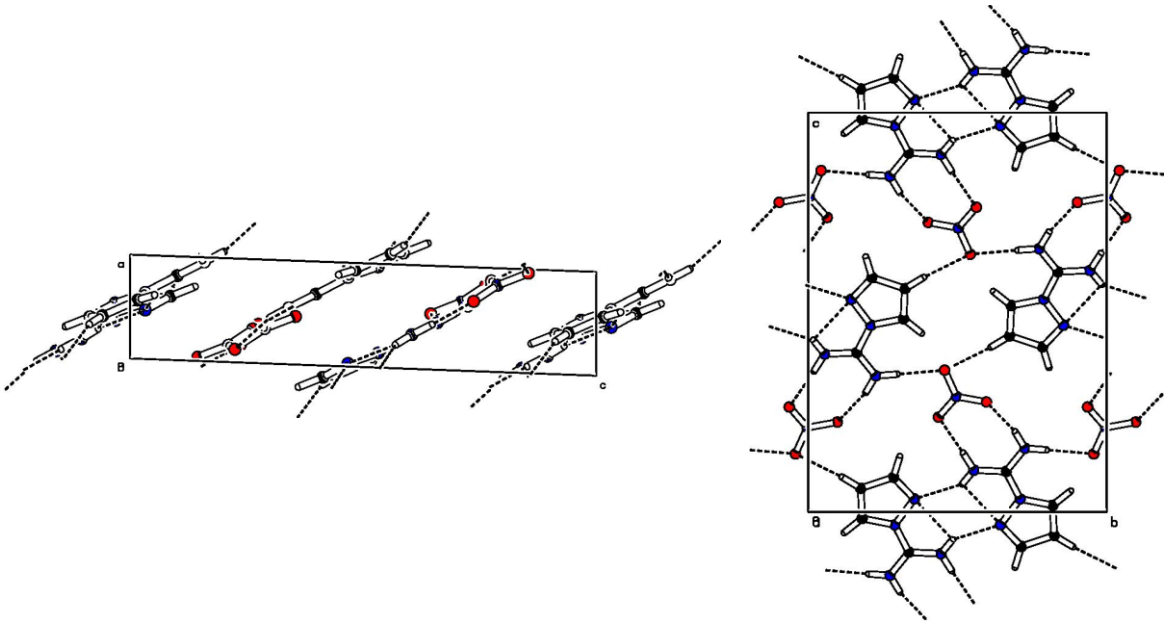

Figure 20: Crystal packings of **HpcamNO$_3$ (I)** (projection to plane *ac* - left, projection to plane *bc* - right). Dashed lines indicate hydrogen bonds.

Table 9: Hydrogen bonds geometry of **HpcamNO$_3$ (I)**.

	d(D – H) (Å)	*d*(H···A) (Å)	*d*(D···A) (Å)	∢ D-H···A (°)
N7-H7a...O2[a]	0.90(2)	1.95(2)	2.848(2)	178(2)
N7-H7b...N2	0.83(2)	2.37(2)	2.677(2)	103(2)
N7-H7b...N2[b]	0.83(2)	2.24(2)	2.983(2)	150(2)
N8-H8a...O1[a]	0.87(2)	2.00(2)	2.855(2)	166(2)
N8-H8b...O3	0.87(2)	1.96(2)	2.832(2)	177(2)
C4-H4...O3[c]	0.95	2.45	3.381(2)	167
C5-H5...O3	0.95	2.31	3.140(2)	146

Symmetry codes: a) 1/2-x, -1/2+y, 1/2-z; b) 2–x, -y, 1-z; c) 2–x, 1-y, 1-z

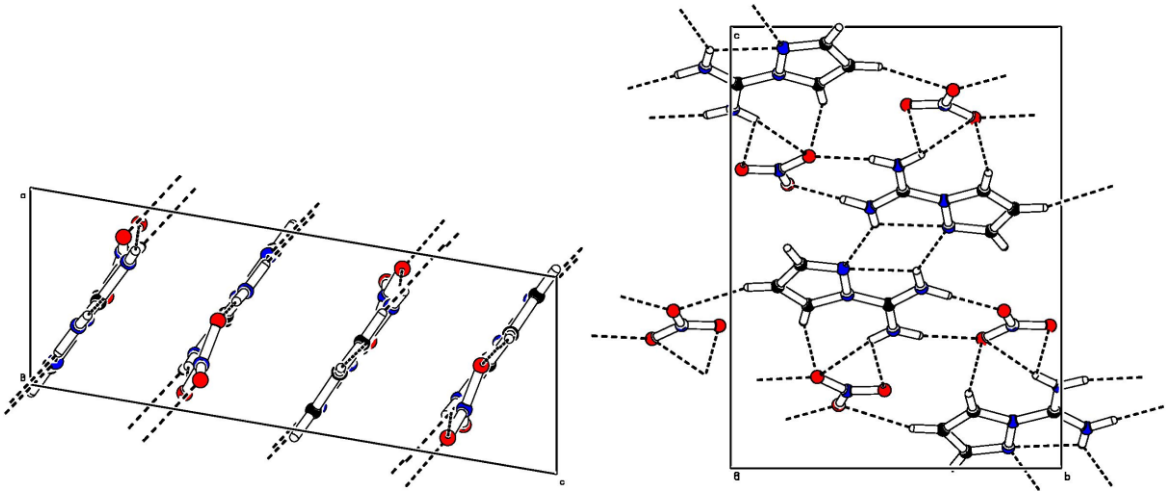

Figure 21: Crystal packings of **HpcamNO$_3$ (II)** (projection to plane *ac* - left, projection to plane *bc* - right). Dashed lines indicate hydrogen bonds.

Table 10: Hydrogen bonds geometry of **HpcamNO$_3$ (II)**.

	d(D – H) (Å)	d(H···A) (Å)	d(D···A) (Å)	∢ D-H···A (°)
N7-H7a...O1	0.90	1.87	2.769(2)	178
N7-H7b...N2	0.87	2.30	2.671(2)	105
N7-H7b...N2[a]	0.87	2.23	2.977(2)	143
N8-H8a...O2	0.87	2.09	2.953(2)	170
N8-H8b...O2[b]	0.87	2.40	3.266(2)	170
N8-H8b...O3[b]	0.87	2.31	2.798(2)	116
C4-H4...O1[c]	0.94	2.51	3.423(2)	163
C5-H5...O2[b]	0.94	2.58	3.479(2)	160

Symmetry codes: a) 2-x, 1-y, 1-z; b) -x, -1/2+y, 1/2-z; c) x, -1+y, z

Vibrational spectra

FTIR and Raman spectra of both phases **HpcamNO$_3$ (I)** and **HpcamNO$_3$ (II)** are shown below (Figures 22 and 23). Vibrational bands of nitrate anion were assigned using the literature[35]. The vibrational manifestations of cation were assigned using quantum-chemical calculations. The band assignments of both phases are listed separately in Tables 11 and 12.

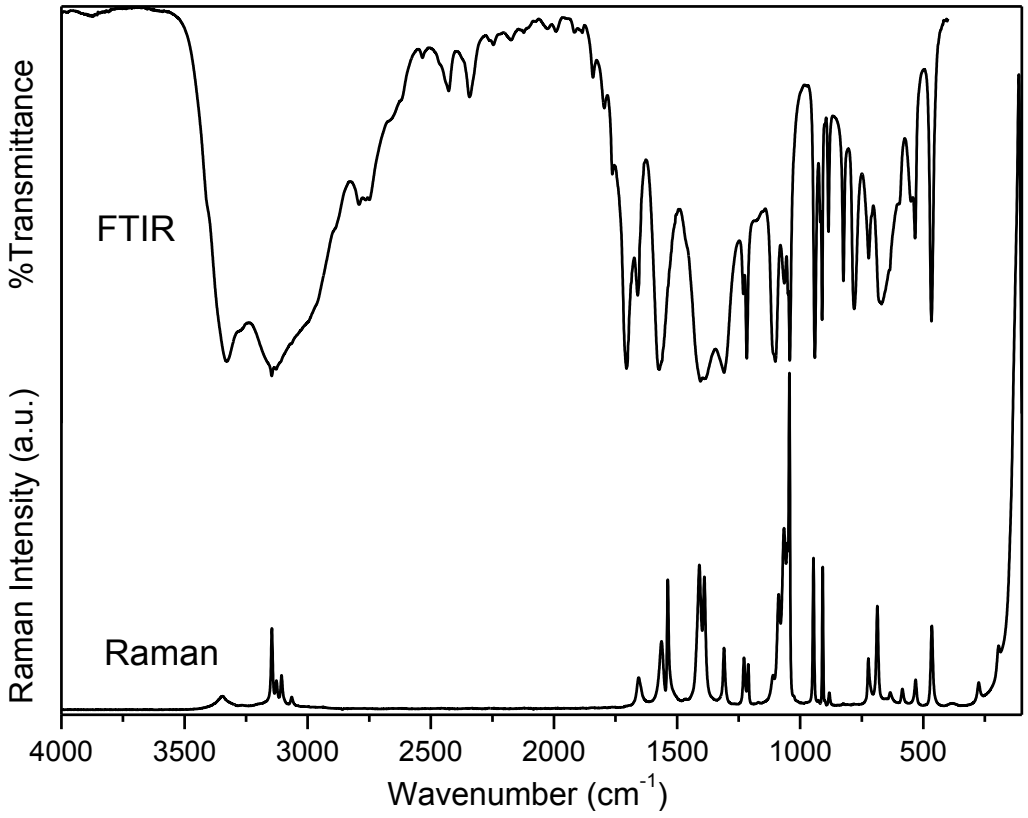

Figure 22: FTIR and Raman spectra of **HpcamNO$_3$ (I)**.

Table 11: The band assignment of FTIR and Raman spectra of **HpcamNO$_3$ (I)**.

FTIR (cm^{-1})	Raman (cm^{-1})	Assignment	FTIR (cm^{-1})	Raman (cm^{-1})	Assignment
	112 vs	External modes	1062 w	1066 m	?
	194 m		1098 m	1087 m	ρ NH_2, δ CH
	275 w		1110 sh	1110 w	ν rg, ρ NH_2, δ CH
465 m	465 m	ω NH_2	1216 m	1211 w	ν NN, δ rg, δ NCN, δ CH
533 w	531 w	ρ rg-$C(NH_2)_2$	1231 w	1228 w	ρ CH, ν rg, ω NH_2, ν CN
547 sh		γ rg, γ CN_3	1306 vs	1309 m	ν rg, ν CN_3, δ CN_3, δ CH
597 wb	585 w		1387 vs	1389 m	ν_3 NO_3^-, ν rg, δ CH, δ CN_3
	634 vw		1408 m	1409 m	ν rg, δ rg, δ CH, ν C-rg
675 w	687 m	δ NCN, ν C-rg, δ rg		1537 m	δ NH_2
	723 m	ν_4 NO_3^-, γ CH	1574 s	1563 m	ν NCN, ν rg, δ NH_2, δ CH
783 m		?	1659 m	1656 w	δ NH_2, δ CN_3
825 m		ν_2 NO_3^-	1708 vs		ν CN_3, δ NH_2, δ CN_3
886 w	882 vw	γ CH		3065 vw	ν NH…X
910 m	909 m	δ rg, ω NH_2		3106 w	ν CH
919 w			3125 m	3126 w	
940 m	946 m	δ rg, ν CN_3, ν CN, ν NN	3144 s	3145 m	
1041 m	1044 s	ν_1 NO_3^-, ρ NH_2, δ CH	3328 s	3345 wb	ν NH…X
1049 w	1052 s	ρ NH_2, ν CC, δ CH			

Note: Symbol X – atom N or O.

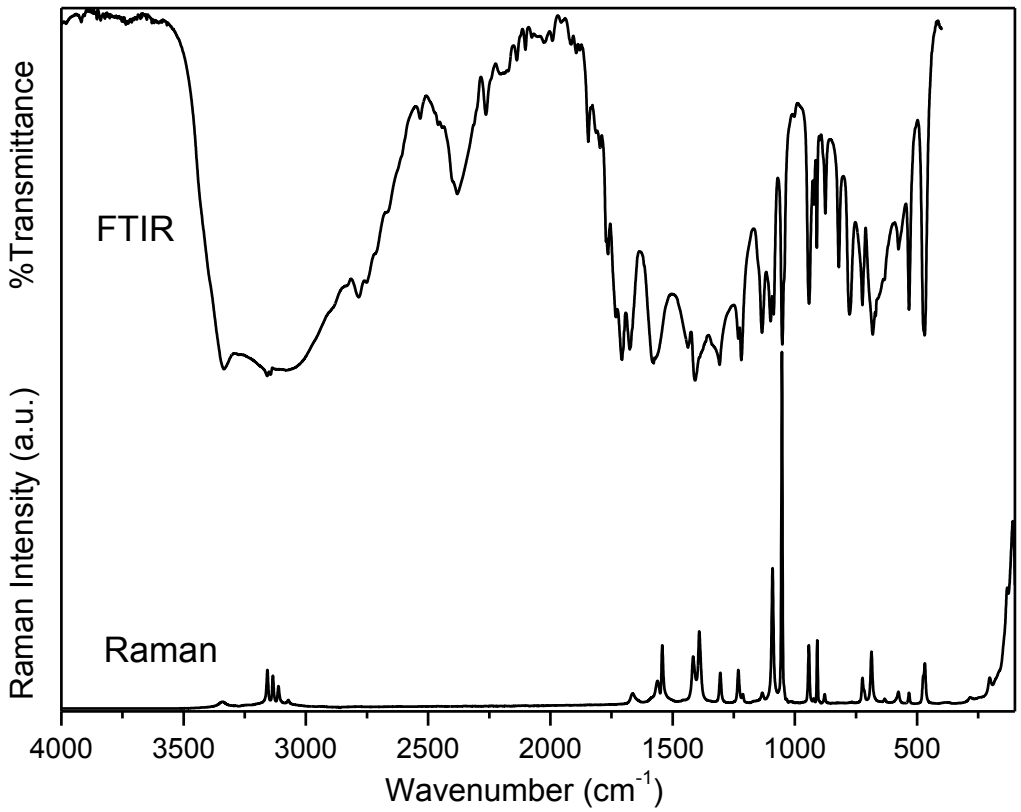

Figure 23: FTIR and Raman spectra of **HpcamNO$_3$ (II)**.

Table 12: The band assignment of FTIR and Raman spectra of **HpcamNO$_3$ (II)**.

FTIR (cm^{-1})	Raman (cm^{-1})	Assignment	FTIR (cm^{-1})	Raman (cm^{-1})	Assignment
	108 s	External modes	1231 m	1231 m	ρ CH, ν rg, ω NH_2,
	132 s				ν CN
	203 m		1308 m	1305 m	ν rg, ν CN_3, δ CN_3,
	282 wb				δ CH
469 vs	468 m	ω NH_2	1380 sh	1391 m	ν_3 NO_3^-, ν rg, δ CH,
533 s	533 w	ρ rg-$C(NH_2)_2$			δ CN_3
576 m	577 w	γ rg, γ CN_3	1408 s	1416 m	ν rg, δ rg, δ CH, ν C-rg
634 sh	633 vw		1437 m		?
669 s			1542 sh	1542 m	δ NH_2
682 vs	687 m	δ NCN, ν C-rg, δ rg	1560 m	1562 m	ν NCN, ν rg, δ NH_2,
	717 sh	γ CH			δ CH
	723 m	ν_4 NO_3^-, γ CH	1571 m		
776 s		?	1578 mb		
820 m		ν_2 NO_3^-	1649 vw	1664 wb	δ NH_2, δ CN_3
875 m	878 w	γ CH	1675 m		
910 m	908 m	δ rg, ω NH_2	1707 m		ν CN_3, δ NH_2, δ CN_3
922 w	923 vw	δ rg, ν CN_3, ν CN, ν NN	1732 w		?
942 s	943 m	δ rg, ν CN_3, ν CN, ν NN	3080	3072 vw	ν NH…X
1052 m	1053 vs	ν_1 NO_3^-, ρ NH_2, ν CC,	3144	3112 w	ν CH
		δ CH		3135 m	
1087 m		ρ NH_2, δ CH	3158	3157 m	
1099 m	1091 s	ρ NH_2, δ CH	3335	3342 wb	ν NH...X
1134 m	1133 w	?			
1219 m	1213 vw	ν NN, δ rg, δ NCN,			
		δ CH			

Note: Symbol, X – atom N or O.

The comparison of calculated spectra of **HpcamNO$_3$ (I)** is discussed in Chapter 4.1.1 and for **HpcamNO$_3$ (II)** is shown in Figure 24. Solid state calculations by CRYSTAL17 software for second modification of nitrate **HpcamNO$_3$ (II)** have not reached convergence and therefore these results are not presented. Potential energy minimum of this modification is the most likely very close to the first one and that might be a reason why these calculations have not found optimised structure which corresponds to the real one.

Both nitrate modifications are easy to distinguish by vibrational spectroscopy because of different characteristic bands near ν_1 NO_3^- vibration. The difference is easier to see in Raman spectra in which in the region 1038 – 1094 cm^{-1} there are three intensive bands for **HpcamNO$_3$ (I)** and only two for **HpcamNO$_3$ (II)** (Figures 22 and 23). In FTIR spectra the difference is not that obvious but in closer look region 1040 – 1150 cm^{-1} can be used for distinguishing of the phases, see Figures 22 and 23.

The overall character of both nitrate vibrational spectra is in agreement with crystal structure solution – i.e. crystals are formed by **Hpcam**$^{1+}$ cations and NO_3^- anions connected by system of H-bonds.

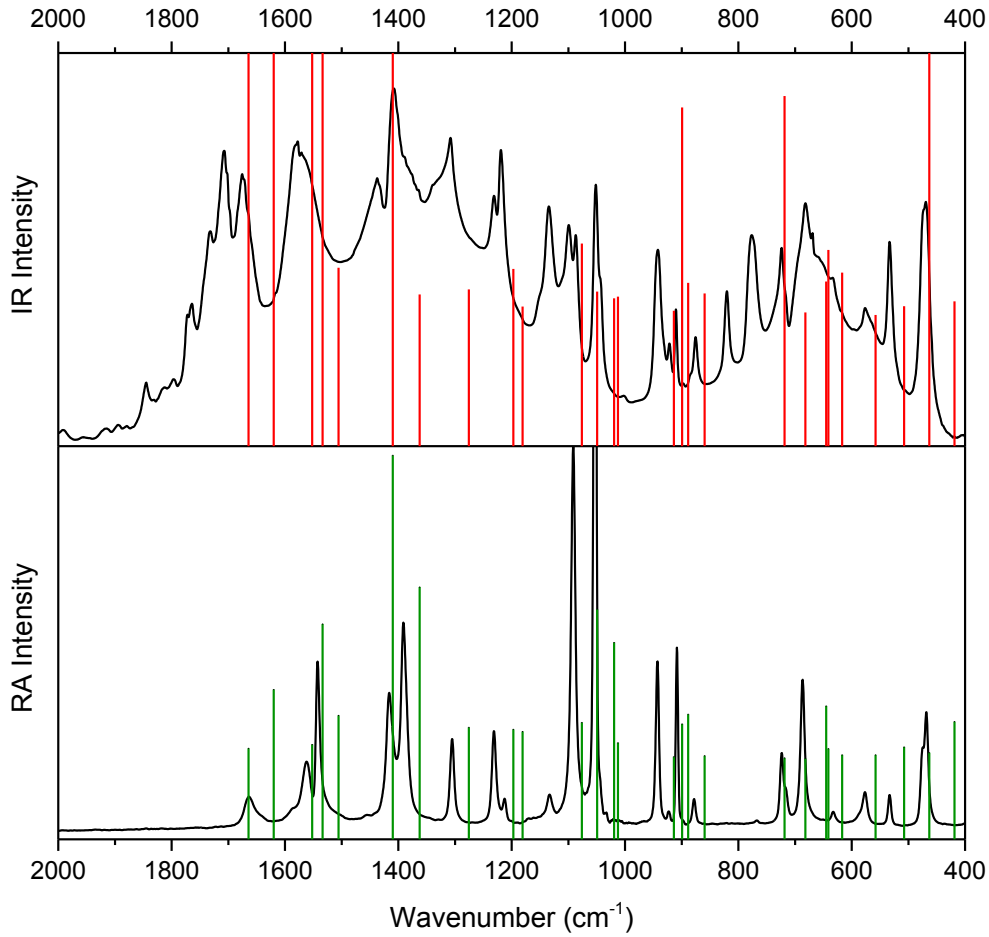

Figure 24: Simulated IR (red lines, upper part) and Raman spectra (green lines, lower part) of an isolated **Hpcam**$^{1+}$ cation in vacuum compared with real vibrational spectra of prepared salt **HpcamNO$_3$ (II)**.

4.2.4 1*H*-pyrazole-carboxamidinium dihydrogen phosphate (HpcamH$_2$PO$_4$)

Crystal structure

This salt was obtained from water solution of **pcam** with phosphoric acid in molar ratios 1:1, 1:2 and 2:1 (Table 4). Asymmetric unit is shown in Figure 25, crystal packing in Figure 26, hydrogen bonds geometry is listed in Table 13, diffraction maxima and d-spacing obtained by powder X-ray diffraction are listed in Table S13 in Supplement.

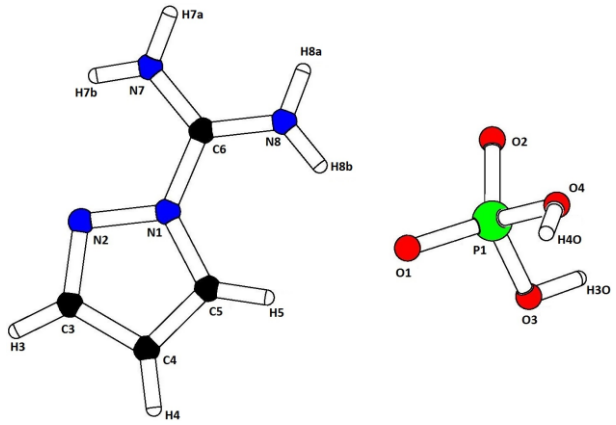

Figure 25: Asymmetric unit of **HpcamH$_2$PO$_4$**.

Dihydrogen phosphate anion is the only double-protonated anion in prepared inorganic crystals. These two protons enable much more possibilities of hydrogen bonds which can be seen in complicated, hydrogen-bonded crystal structure. Dihydrogen phosphate anions form layers by two hydrogen-bonded parallel chains in which base cations are embed.

These layers are formed by strong O3-H3O...O1 and O4-H4O...O2 interactions with *d*(D···A) that slightly differ (2.595(2) and 2.580(2 Å). **Hpcam^{1+}** cations are not arranged in layers. In this structure there are again present intramolecular interactions N7-H7b...N2. All four amino hydrogen atoms (H7a, H7b, H8a, H8b) as well as H5 are bonded to the oxygen atoms of anions (see Table 13).

Table 13: Hydrogen bonds geometry of **HpcamH$_2$PO$_4$**.

	d(D – H) (Å)	*d*(H···A) (Å)	*d*(D···A) (Å)	∢ D-H···A (°)
O3-H3O...O1[a]	0.96	1.64	2.595(2)	178
O4-H4O...O2[b]	0.86	1.72	2.580(2)	174
N7-H7a...O2[c]	0.91(2)	1.96(2)	2.852(2)	166(2)
N7-H7b...N2	0.86(2)	2.31(2)	2.664(2)	105(2)
N7-H7b...O2[d]	0.86(2)	2.20(2)	2.858(2)	134(2)
N8-H8a...O4[c]	0.85(2)	2.05(2)	2.894(2)	174(2)
N8-H8b...O1	0.89(2)	1.91(2)	2.799(2)	173(2)
C5-H5...O1	0.95	2.35	3.220(2)	152

Symmetry codes: a) x, 3/2-y, -1/2+z; b) x, 3/2-y, 1/2+z; c) -x, -1/2+y, 1/2-z; d) x, 1/2-y, 1/2+z

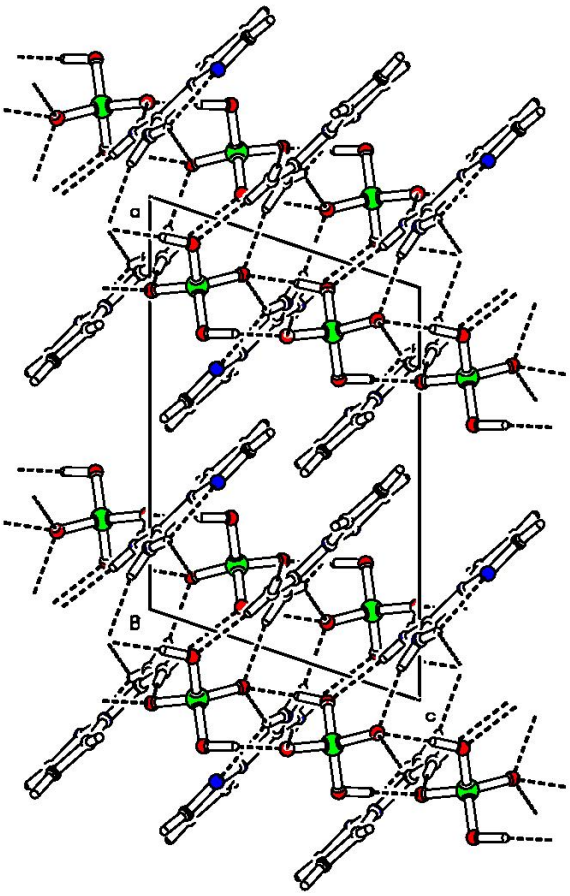

Figure 26: Crystal packing of **HpcamH$_2$PO$_4$** (projection to plane *ac*). Dashed lines indicate hydrogen bonds.

Vibrational spectra

FTIR and Raman spectra of salt **HpcamH$_2$PO$_4$** are depicted in Figure 27. Vibrational modes of dihydrogen phosphate anion were assigned using the literature[35, 37]. The rest of the vibrational bands were assigned using quantum-chemical calculations. The comparison of the calculated spectra with the measured ones is shown below, see Figures 28 and 29. The band assignment is listed in Table 14.

The overall character of vibrational spectra is in agreement with crystal structure solution – i.e. crystal formed by **Hpcam^{1+}** cations and $H_2PO_4^-$ anions connected by H-bonds.

Table 14: The band assignment of FTIR and Raman spectra of **HpcamH$_2$PO$_4$**.

FTIR (cm^{-1})	Raman (cm^{-1})	Assignment	FTIR (cm^{-1})	Raman (cm^{-1})	Assignment
	129 s	External modes		1019 s	ρ NH_2, δ CH
	149 m		1041 w	1040 s	ρ NH_2, ν CC, δ CH
	189 m		1074 w		?
	225 wb			1081 vs	ρ NH_2, δ CH
	285 w		1101 mb		ν_3 PO_4, ρ NH_2, δ CH
	368 m	ν_2 PO_4	1123 m		ν rg, ρ NH_2, δ CH
	393 m		1143 mb	1137 w	?
409 sh		?	1205 w		ν NN, δ rg, δ NCN, δ CH
464 sh	463 s	δ NCN	1218 w	1226 m	ν_3 PO_4, ν NN, δ rg,
472 w		ω NH_2			δ NCN, δ CH
489 wb	482 m	?	1247 wb		δ POH, ρ CH, ν rg,
514 w	515 m	ν_4 PO_4, ρ rg-$C(NH_2)_2$			ω NH_2, ν CN
528 w	534 m	ν_4 PO_4	1309 vw	1304 m	ν rg, ν CN_3, δ CN_3, δ CH
548 w	553 vw		1412 w	1409 w	ν rg, δ CH, δ CN_3
	576 w	γ rg, γ CN_3		1542 s	δ NH_2
590 w			1573 sh	1570 m	ν NCN, ν rg, δ NH_2, δ CH
632 w	636 vw		1580 m		
682 vw	685 m	δ NCN, ν C-rg, δ rg	1640 w		?
775 m		?	1687 m	1674 w	δ NH_2, δ CN_3
868 w	873 w	γ CH	1709 m	1701 wb	ν CN_3, δ NH_2, δ CN_3
	893 m	δ POH		3071 w	ν NH…O
910 w	909 m	δ rg, ω NH_2	3065 vs	3124 m	ν CH
	926 vs	ν_1 PO_4, δ rg, ν CN_3,	3103 vs	3139 w	
		ν CN, ν NN	3138 vs		
941 m		δ rg, ν CN_3, ν CN,	3157 s	3156 m	
		ν NN	3331 vs		ν NH…O
957 mb	950 m	ν_3 PO_4			

Note: The notation derived from the ideally tetrahedral PO_4 moiety is used for the description of the $H_2PO_4^-$ modes.

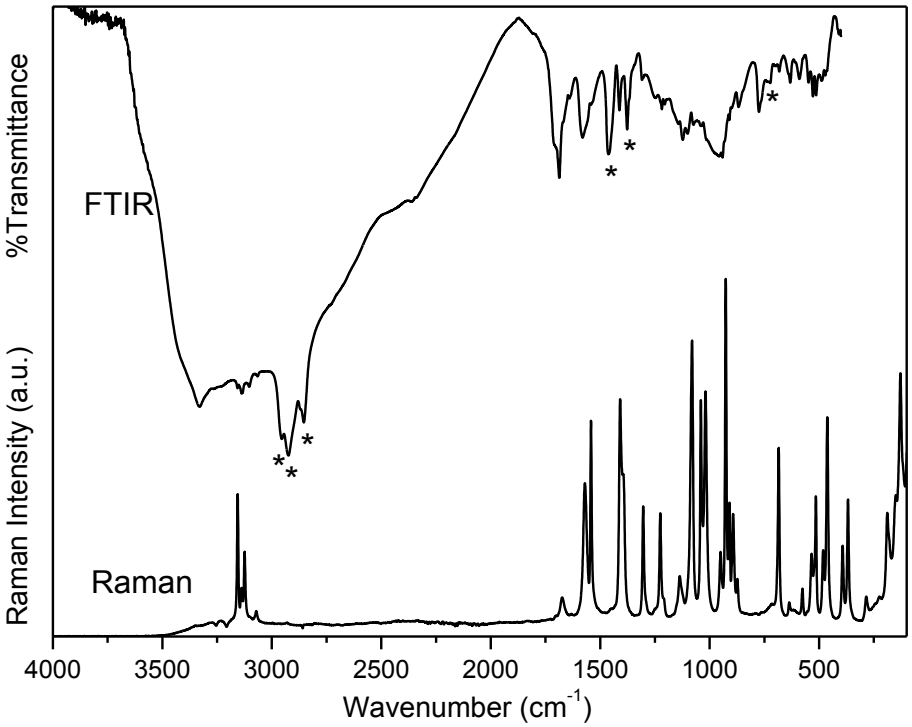

Figure 27: FTIR (nujol mull) and Raman spectra of **$HpcamH_2PO_4$**. Nujol bands are labelled by asterisk.

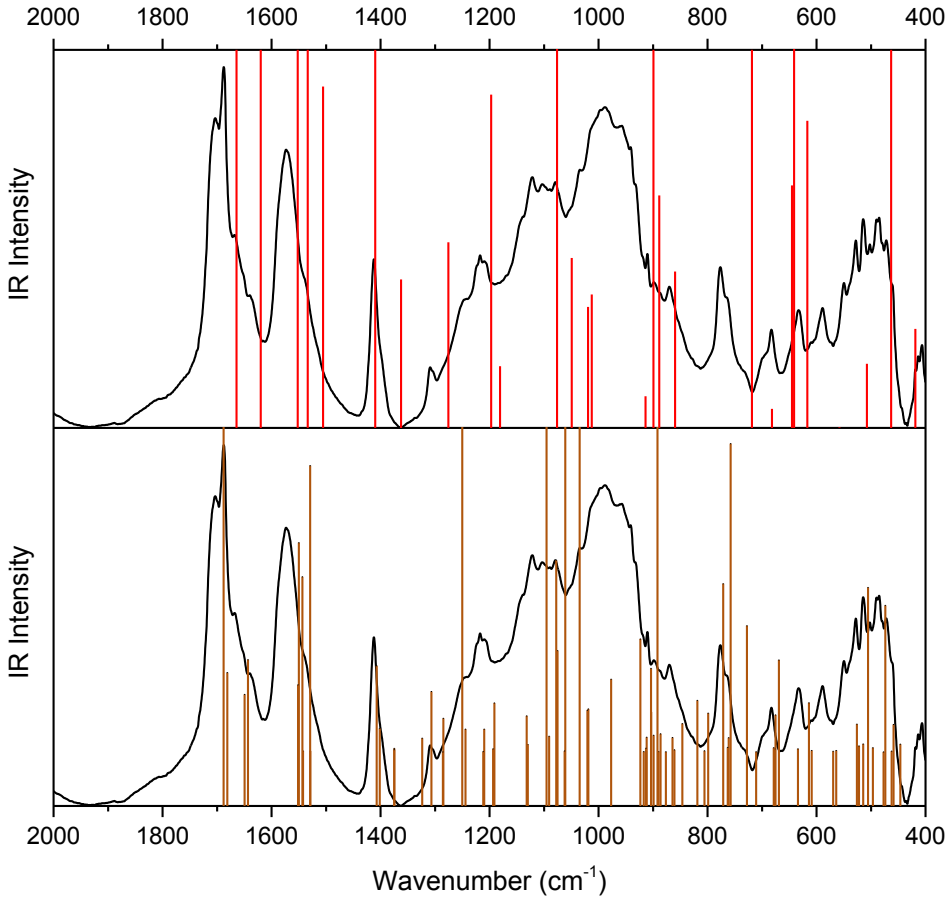

Figure 28: Recorded FTIR spectrum of salt **$HpcamH_2PO_4$** compared with simulated IR spectrum of an isolated **$Hpcam^{1+}$** cation in vacuum (red lines, upper part) and with solid state simulated IR spectrum (brown lines, lower part).

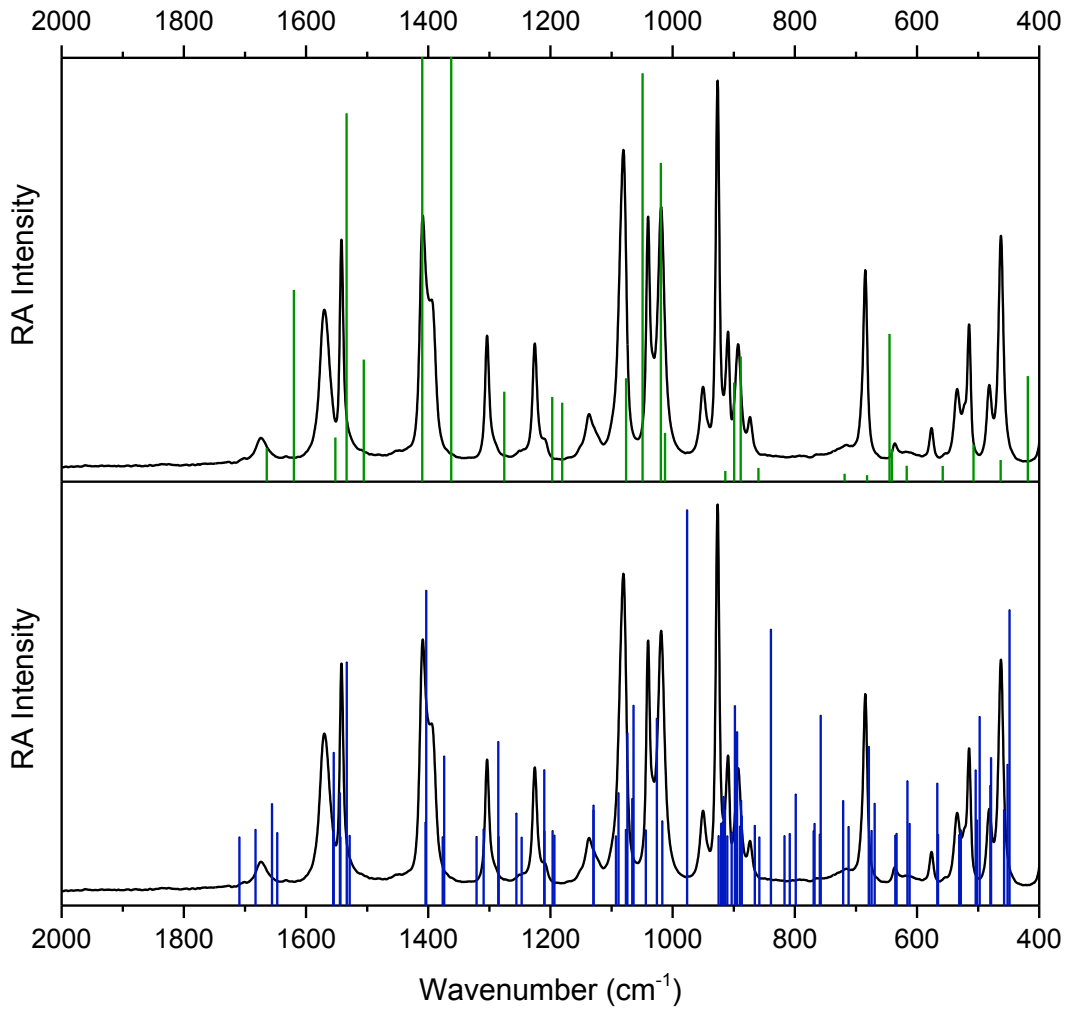

Figure 29: Recorded Raman spectrum of salt **HpcamH$_2$PO$_4$** compared with simulated Raman spectrum of an isolated **Hpcam**$^{1+}$ cation in vacuum (green lines, upper part) and with solid state simulated Raman spectrum (blue lines, lower part).

4.2.5 1*H*-pyrazole-carboxamidinium hydrogen sulfate (HpcamHSO$_4$)

Crystal structure

This salt was obtained from water solution of **pcam** with sulfuric acid in molar ratios 1:1, 1:2 and 2:1 (Table 4). Asymmetric unit is shown in Figure 30, crystal packing in Figure 31, hydrogen bonds geometry is listed in Table 15, diffraction maxima and d-spacing obtained by powder X-ray diffraction are listed in Table S14 in Supplement.

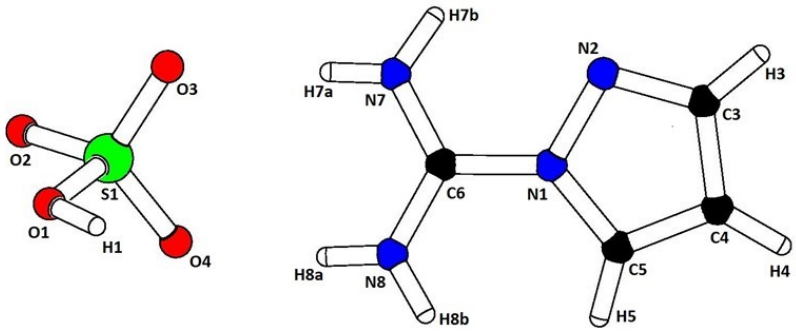

Figure 30: Asymmetric unit of **HpcamHSO4**.

As it is apparent from Figure 31 there are no centrosymmetric pairs of cations formed in this structure. Paralel vertical layers of non-bonded cations are embed in the horizontal hydrogen-bonded chains of anions. These chains are connected by strong hydrogen bonds O1-H1...O2 with $d(D\cdots A) = 2.586(2)$ Å. Rest two oxygen atoms O3 and O4 of anions form bonds with three hydrogen atoms H7a, H8a and H8b of amino groups of base. The last hydrogen atom H7b is involved in the H-bond with O2 as well as in intramolecular interaction N7-H7b...N2. Distances $d(D\cdots A)$ of all these N-H…O interactions varies, see Table 15.

Table 15: Hydrogen bonds geometry of **HpcamHSO4**.

	d(D – H) (Å)	d(H···A) (Å)	d(D···A) (Å)	∢ D-H···A (°)
O1-H1...O2[a]	0.90	1.69	2.586(2)	176
N7-H7a...O3	0.83	2.07	2.902(2)	176
N7-H7b...N2	0.90	2.34	2.698(2)	104
N7-H7b...O2[b]	0.90	2.14	2.914(2)	144
N8-H8a...O4	0.84	2.06	2.876(2)	163
N8-H8b...O3[c]	0.88	2.50	3.097(2)	126
N8-H8b...O4[d]	0.88	2.13	2.912(2)	148
C3-H3...O1[e]	0.95	2.51	3.365(2)	149

Symmetry codes: (a) x, 1/2-y, 1/2+z; b) 1-x, -y, 1-z; c) 1-x, 1/2+y, 1/2-z; d) 1-x, 1-y, 1-z; e) 1+x, 1/2-y, -1/2+z

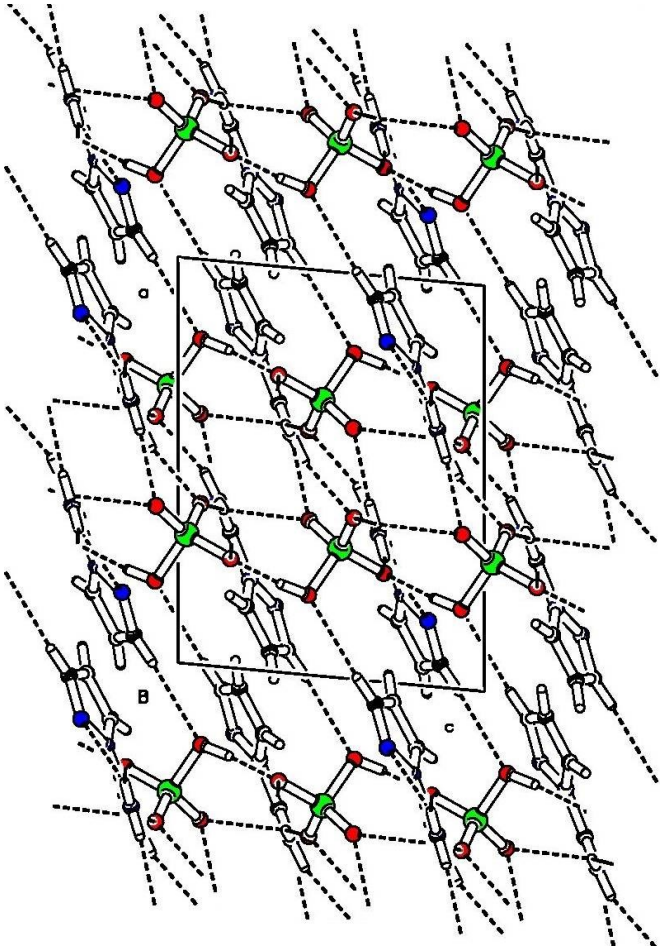

Figure 31: Crystal packing of **HpcamHSO4** (projection to plane *ac*). Dashed lines indicate hydrogen bonds.

Vibrational spectra

FTIR and Raman spectra of salt **HpcamHSO4** are depicted in Figure 32. Vibrational bands of hydrogen sulfate anion were assigned using the literature[35, 38]. The rest of the vibrational bands were assigned using quantum-chemical calculations. The comparison of the calculated spectra with the measured ones is shown below, see Figures 33 and 34. The band assignment is listed in Table 16.

The overall character of vibrational spectra is in agreement with crystal structure solution – i.e. crystal formed by **Hpcam**$^{1+}$ cations and HSO_4^- anions connected by H-bonds.

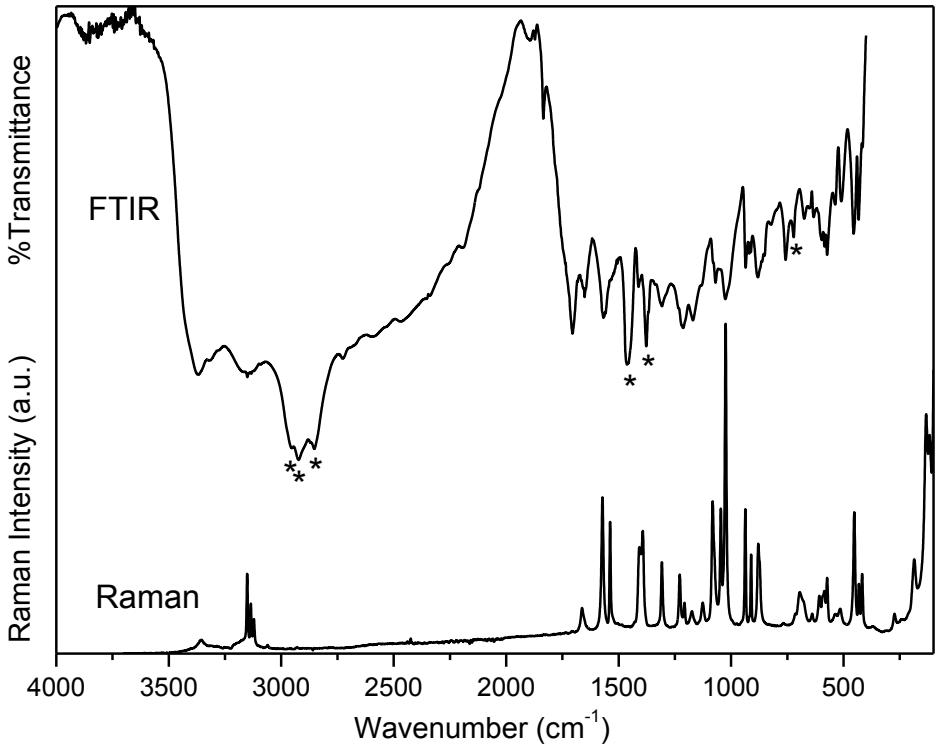

Figure 32: FTIR (nujol mull) and Raman spectra of **HpcamHSO4**. Nujol bands are labelled by asterisk.

Table 16: The band assignment of FTIR and Raman spectra of **HpcamHSO4**.

FTIR (cm^{-1})	Raman (cm^{-1})	Assignment	FTIR (cm^{-1})	Raman (cm^{-1})	Assignment
	118 s	External modes	912 m	911 m	δ rg, ω NH_2
	133 s		919 m		
	186 m		935 m	937 s	γ CH
	274 w		1025 s	1024 vs	ν_1 SO_4
416 vw	417 m	ν_2 SO_4		1046 m	ρ NH_2, ν CC
433 m	432 m		1069 s	1082 s	ν_3 SO_4, ρ NH_2, δ CH
455 s	452 s	ω NH_2		1126 w	ν rg, ρ NH_2, δ CH, ν_3 SO_4
510 w	515 wb	ν_4 SO_4	1169 vs	1174 w	ν_3 SO_4
537 w	536 vw	ρ rg-$C(NH_2)_2$	1213 vs	1207 w	ν NN, δ rg, δ NCN, δ CH,
573 s	573 m	γ rg, γ CN_3			ν_3 SO_4
585 m	585 m	ν_4 SO_4		1228 m	ρ CH, ν rg, ω NH_2, ν CN
597 m	594 mb		1307 m	1308 m	ν rg, ν CN_3, δ CN_3, δ CH
	608 m			1393 m	ν rg, δ CH, δ CN_3
633 w	640 vw	γ rg, γ CN_3	1411 w	1408 m	ν rg, δ rg, δ CH, ν C-rg
652 vw		τ NH_2, γ NH		1538 m	δ NH_2
675 w	695 m	δ NCN, ν C-rg, δ rg	1568 m	1572 s	ν NCN, ν rg, δ NH_2, δ CH
758 m		γ CH	1652 w	1663 w	δ NH_2, δ CN_3
	767 vw	?	1705 s	1708 vw	ν CN_3, δ NH_2, δ CN_3
				3061 vw	ν NH…O
823 vw		?		3121 w	ν CH
851 sh		?		3135 w	
880 m	879 m	ν S-O(H)	3151 m	3151 m	
			3369 m	3355 wb	ν NH…O

Note: The notation derived from the ideally tetrahedral SO_4 moiety is used for the description of the HSO_4^- modes.

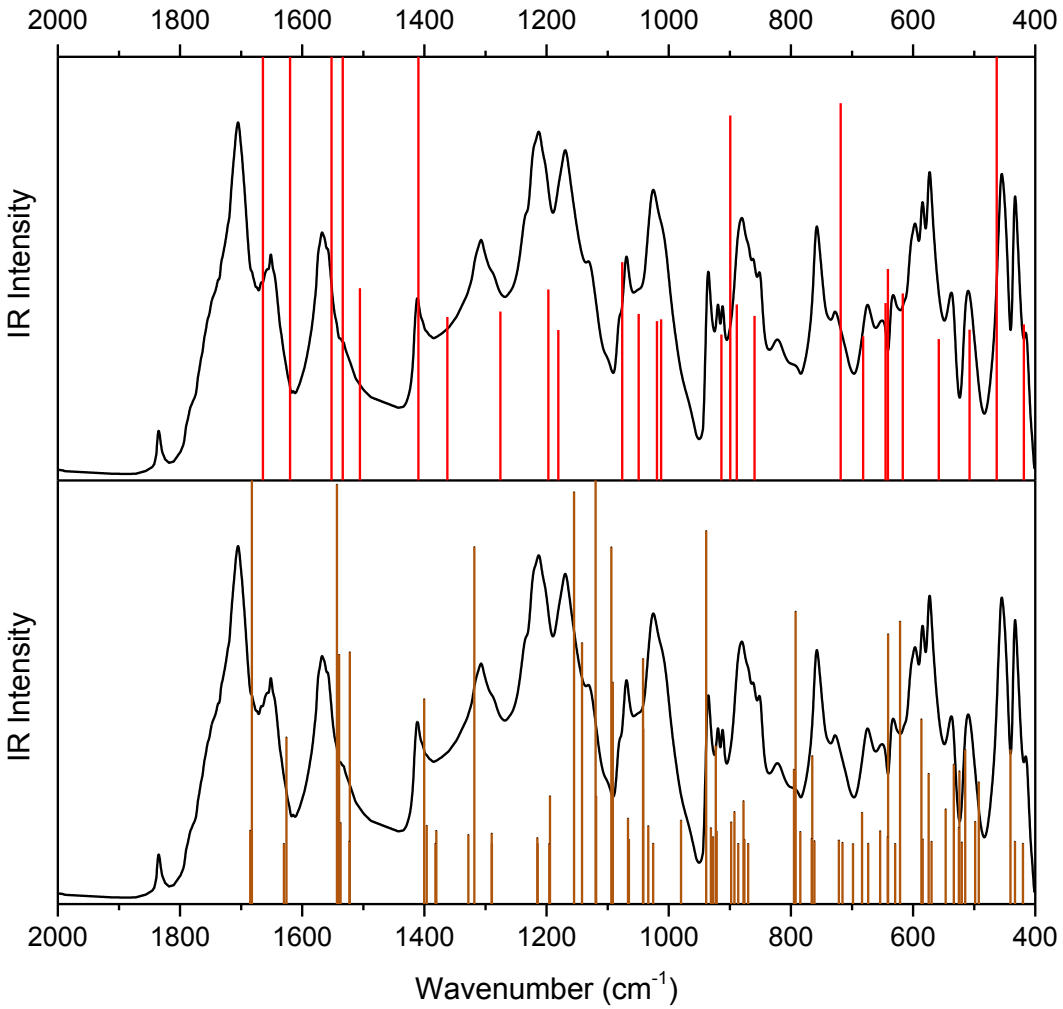

Figure 33: Recorded FTIR spectrum of salt **HpcamHSO$_4$** compared with simulated IR spectrum of an isolated **Hpcam**$^{1+}$ cation in vacuum (red lines, upper part) and with solid state simulated IR spectrum (brown lines, lower part).

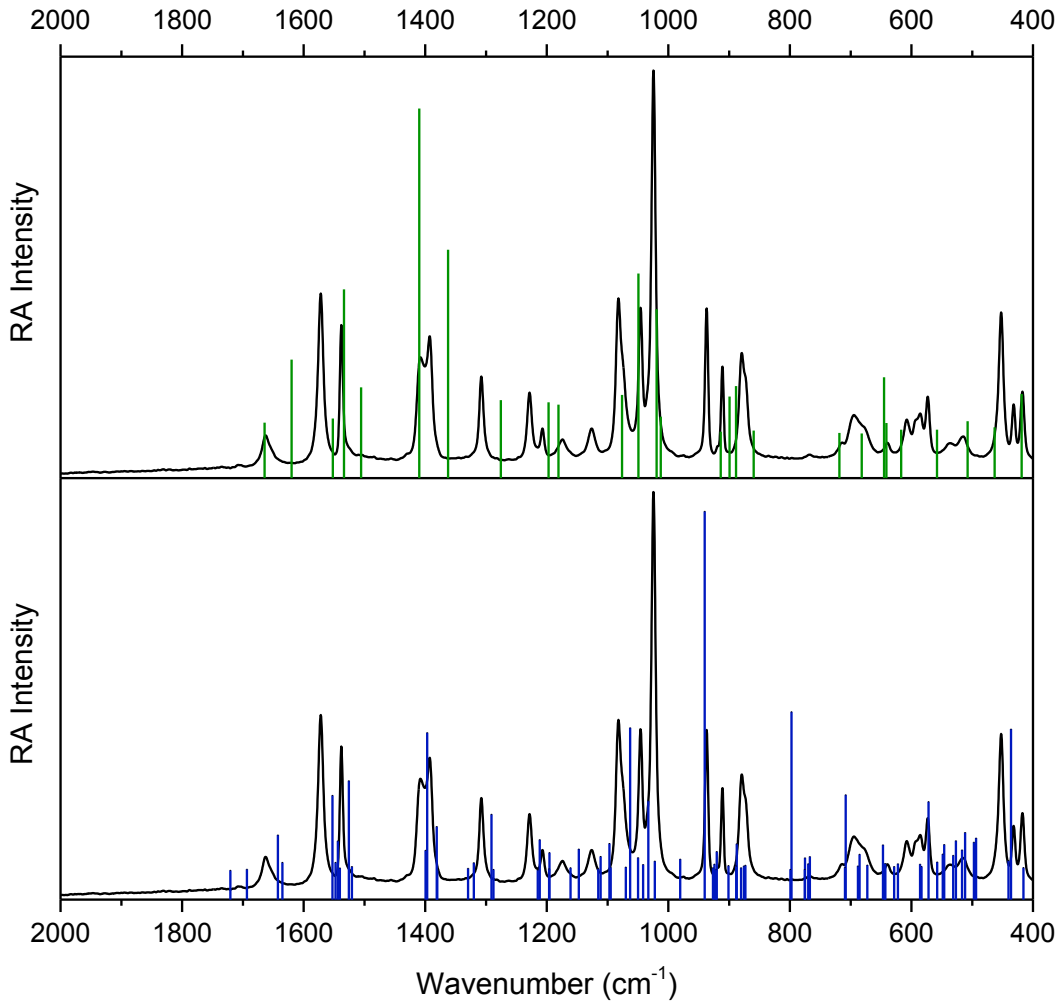

Figure 34: Recorded Raman spectrum of salt **HpcamHSO$_4$** compared with simulated Raman spectrum of an isolated **Hpcam^{1+}** cation in vacuum (green lines, upper part) and with solid state simulated Raman spectrum (blue lines, lower part).

4.2.6 1*H*-pyrazole-carboxamidinium methanesulfonate (HpcamCH$_3$SO$_3$)

Crystal structure

This salt was obtained from water solution of **pcam** with methanesulfonic acid in molar ratios 1:1, 1:2 and 2:1 (Table 4). Asymmetric unit is shown in Figure 35, crystal packing in Figures 36, hydrogen bonds geometry is listed in Table 17, diffraction maxima and d-spacing obtained by powder X-ray diffraction are listed in Table S15 in Supplement.

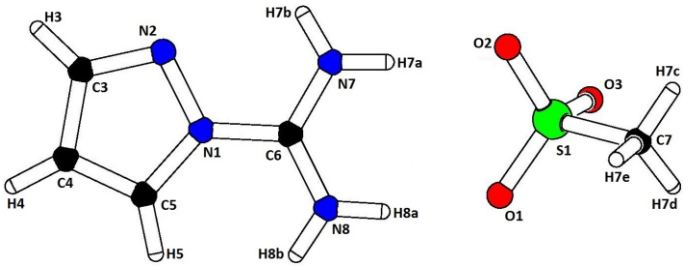

Figure 35: Asymmetric unit of **HpcamCH$_3$SO$_3$**.

Crystal packing in Figure 36 indicates formation of centrosymmetric pairs of cations which are again stabilised by intramolecular and intermolecular N7-H7b...N2 hydrogen bonds. These pairs are connected by centrosymmetric pairs of methanesulfonate anions and all together form hydrogen-bonded layers. Distances *d*(D···A) of N-H...O hydrogen bond involving atoms H7a, H8a and H8b are comparable to each other (2.801(2), 2.821(2) and 2.889(2) Å).

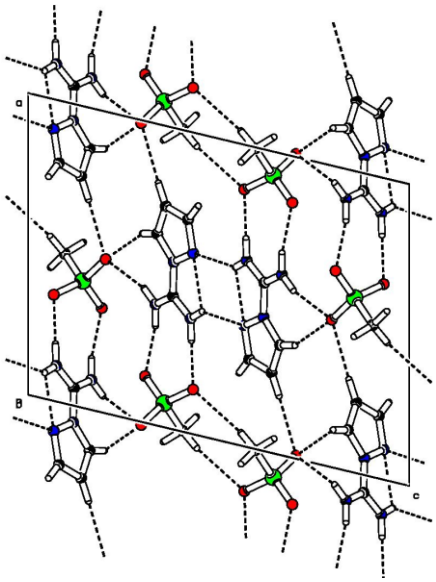

Figure 36: Crystal packing of **HpcamCH$_3$SO$_3$** (projection to plane *ac*). Dashed lines indicate hydrogen bonds.

Table 17: Hydrogen bonds geometry of **HpcamCH$_3$SO$_3$**.

	d(D – H) (Å)	*d*(H···A) (Å)	*d*(D···A) (Å)	∢ D-H···A (°)
N7-H7a...O2	0.88	1.93	2.801(2)	172
N7-H7b...N2	0.88	2.30	2.661(2)	105
N7-H7b...N2^a	0.88	2.23	2.990(2)	144
N8-H8a...O1	0.88	2.00	2.821(2)	156
N8-H8b...O3^b	0.88	2.03	2.889(2)	164
C4-H4...O3^c	0.95	2.43	3.384(2)	178
C5-H5...O3^b	0.95	2.26	3.136(2)	152
C7-H7c...O2^d	0.98	2.53	3.474(2)	162

Symmetry codes: a) 1-x, -y, 1-z; b) 3/2-x, 1/2+y, 3/2-z; c) -1+x, y, z; d) 2-x, 1-y, 1-z

Vibrational spectra

FTIR and Raman spectra of salt **HpcamCH$_3$SO$_3$** are depicted in Figure 37. Vibrational bands of methanesulfonate anion were assigned using the literature[39]. The rest of the vibrational bands were assigned using quantum-chemical calculations. The comparison of the calculated spectra with the measured ones is shown below, see Figures 38 and 39. The band assignment is listed in Table 18. The overall character of vibrational spectra is in agreement with crystal structure solution – i.e. crystal formed by **Hpcam^{1+}** cations and $CH_3SO_3^-$ anions connected by H-bonds.

Table 18: The band assignment of FTIR and Raman spectra of **HpcamCH$_3$SO$_3$**.

FTIR (cm^{-1})	Raman (cm^{-1})	Assignment	FTIR (cm^{-1})	Raman (cm^{-1})	Assignment
	117 s	External modes		1053 m	ρ NH_2, ν CC, δ CH
	132 vs		1088 m		ρ NH_2, δ CH
	155 m		1103 sh	1093 s	ν rg, ρ NH_2, δ CH
	197 m		1145 s	1145 w	?
	286 vw		1189 vs	1195 m	ν SO_3
	348 m		1229 s	1222 w	ν SO_3, ν NN, δ rg,
	358 m				δ NCN, δ CH
476 m	471 m	ω NH_2		1235 m	ρ CH, ν rg, ω NH_2, ν CN
520 sh	520 m	?	1315 m	1315 m	ν rg, ν CN_3, δ CN_3, δ CH
	529 m	ρ rg-$C(NH_2)_2$	1324 sh		δ CH_3
533 m	536 w	δ SO_3	1338 w		δ CH_3
545 m	545 w		1403 m	1403 s	ν rg, δ CH, δ CN_3
556 m	558 m		1412 s	1411 s	ν rg, δ rg, δ CH, ν C-rg
613 sh	590 w	?		1431 m	δ CH_3
	639 vw	γ rg, γ CN_3		1539 m	δ NH_2
666 s	689 m	δ NCN, ν C-rg, δ rg	1557 m	1555 m	ν NCN, ν rg, δ NH_2, δ CH
720 w	719 vw	γ CH		1633 vw	δ NH_2, δ CN_3
778 s	780 s	ν C-S		1669 w	?
793 vs		?	1679 m		δ NH_2, δ CN_3
	869 vw	?	1717 vs		ν CN_3, δ NH_2, δ CN_3
891 w	892 vw	γ CH	2957 m	2944 m	ν_s CH_3
912 m	910 m	δ rg, ω NH_2		3020 w	ν_a CH_3
927 w	925 vw	γ CH		3029 w	
948 m	942 sh	δ rg, ν CN_3, ν CN, ν NN		3065 vw	ν NH…X
	952 m	?	3114 m	3112 m	ν CH
959 m	961 sh	?	3137 m	3137 m	
972 sh	969 sh	ρ CH_3	3339 m	3356 wb	ν NH…X
1042 vs	1044 vs	ν SO_3, ρ NH_2, δ CH			

Note: Symbol X – atom N or O.

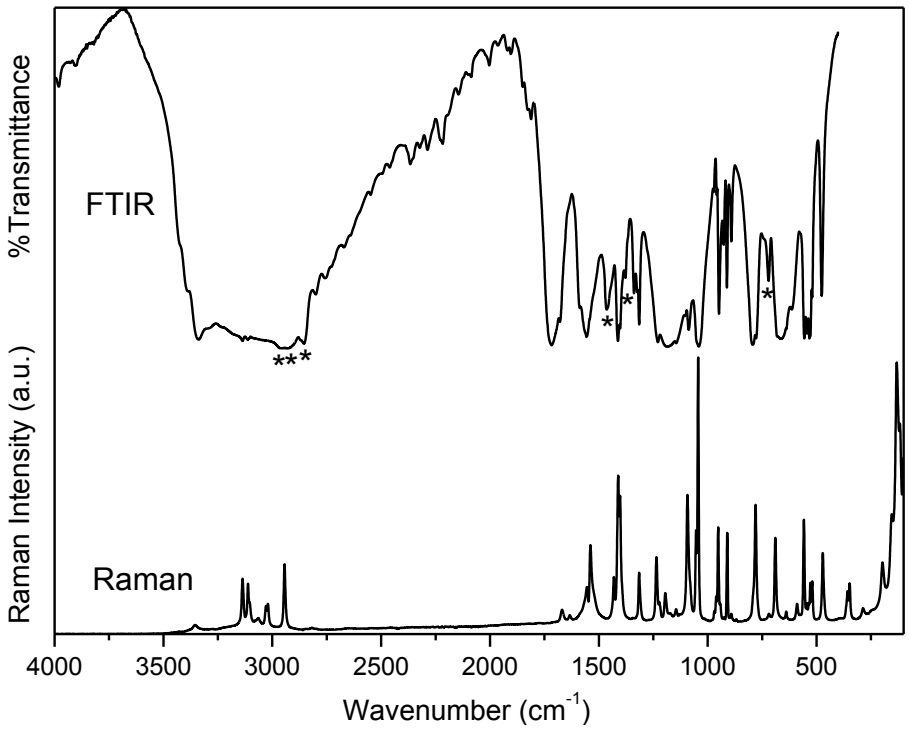

Figure 37: FTIR (nujol mull) and Raman spectra of **HpcamCH$_3$SO$_3$**. Nujol bands are labelled by asterisk.

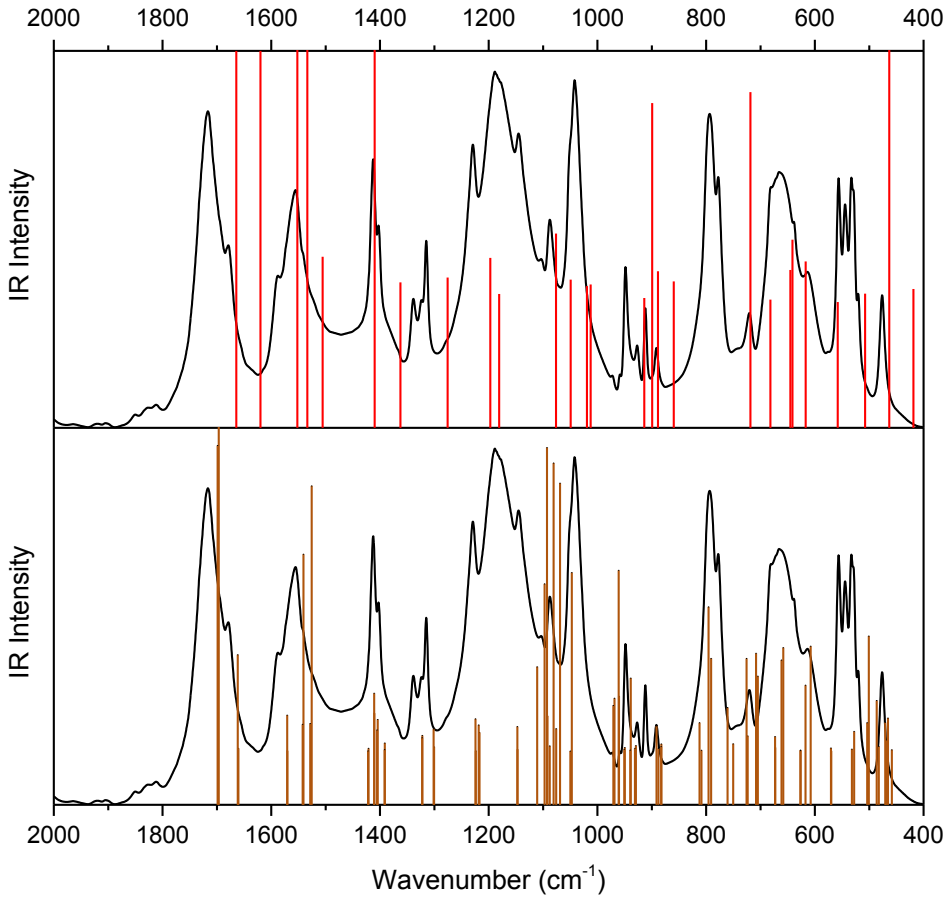

Figure 38: Recorded FTIR spectrum of salt **HpcamCH$_3$SO$_3$** compared with simulated IR spectrum of an isolated **Hpcam^{1+}** cation in vacuum (red lines, upper part) and with solid state simulated IR spectrum (brown lines, lower part).

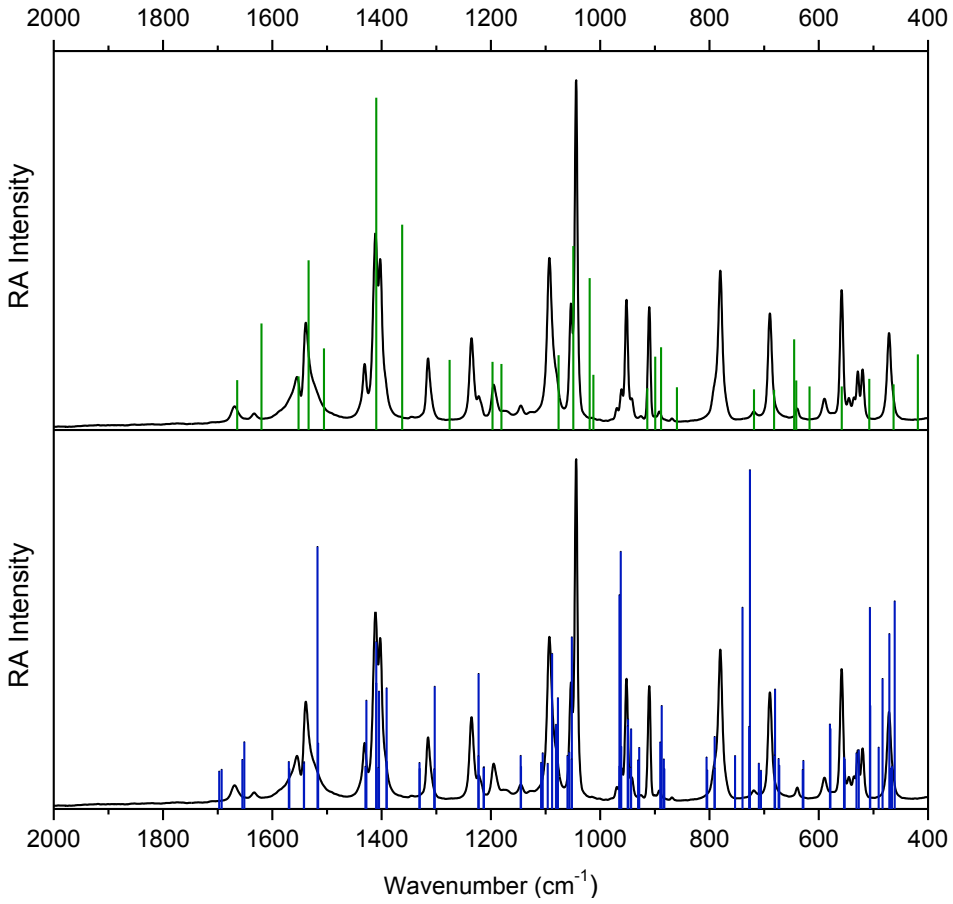

Figure 39: Recorded Raman spectrum of salt **HpcamCH$_3$SO$_3$** compared with simulated Raman spectrum of an isolated **Hpcam**$^{1+}$ cation in vacuum (green lines, upper part) and with solid state simulated Raman spectrum (blue lines, lower part).

4.2.7 1*H*-pyrazole-carboxamidinium sulfamate (HpcamNH$_2$SO$_3$)

Crystal structure

This salt was obtained from water solution of **pcam** with sulfamic acid in molar ratios 1:1, 1:2 and 2:1 (Table 4). Asymmetric unit is shown in Figure 40, crystal packing in Figure 41, hydrogen bonds geometry is listed in Table 19, diffraction maxima and d-spacing obtained by powder X-ray diffraction are listed in Table S16 in Supplement.

Also in this structure centrosymmetric pairs of cations were found but there are not formed any layers, see Figure 41. There are different types of connection between cations and anions. Interesting is that amino group with atom N8 forms H-bonds only with oxygen atoms (O1 and O3) of anion and another one – amino group with atom N7 is involved only in H-bonds with nitrogen atoms (N2 and N9). This structure is also stabilised with weak C-H...O hydrogen bonds.

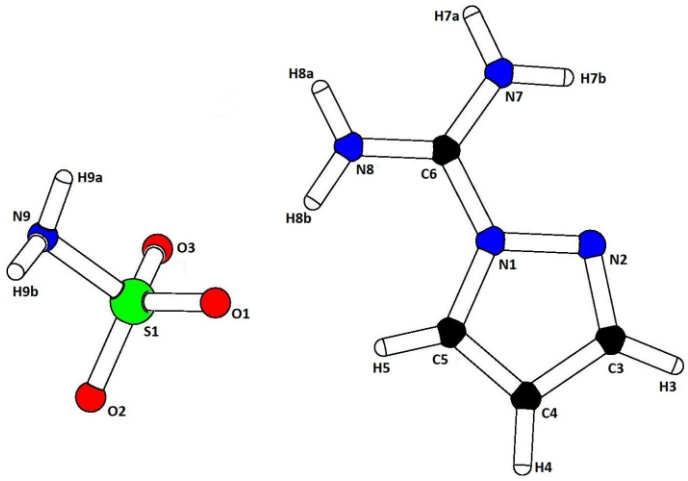

Figure 40: Asymmetric unit of **HpcamNH$_2$SO$_3$**.

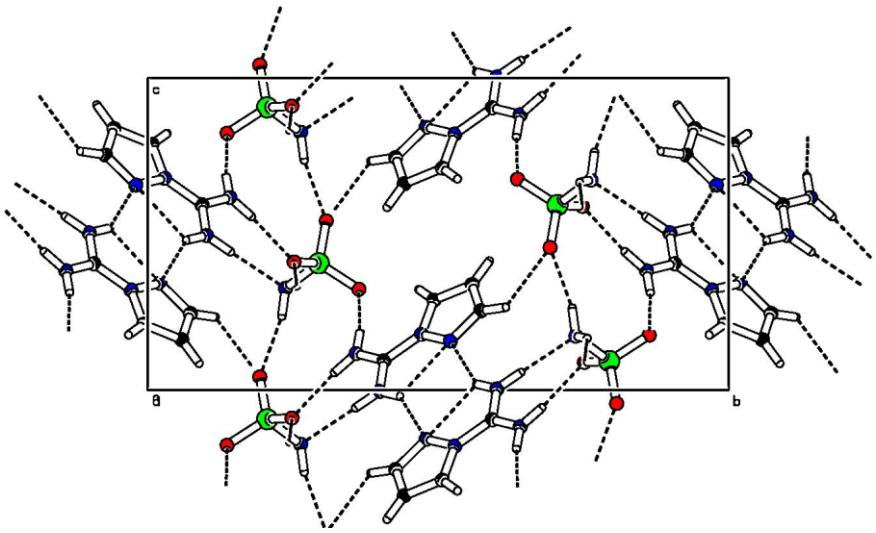

Figure 41: Crystal packing of **HpcamNH$_2$SO$_3$** (projection to plane *bc*). Dashed lines indicate hydrogen bonds.

Table 19: Hydrogen bonds geometry of **HpcamNH$_2$SO$_3$**.

	d(D – H) (Å)	*d*(H···A) (Å)	*d*(D···A) (Å)	∢ D-H···A (°)
N7-H7a...N9[a]	0.89	2.01	2.898(2)	175
N7-H7b...N2	0.89	2.32	2.658(2)	103
N7-H7b...N2[b]	0.89	2.27	3.072(2)	149
N8-H8a...O3[c]	0.89	1.99	2.861(2)	170
N8-H8b...O1	0.90	1.94	2.826(2)	170
N9-H9a...O2[c]	0.89	2.02	2.892(2)	168
N9-H9b...O3[d]	0.92	2.00	2.837(2)	151
C3-H3...O2[e]	0.95	2.54	3.326(2)	141
C5-H5...O1	0.95	2.38	3.250(2)	152

Symmetry codes: a) 1+x, 1/2-y, -1/2+z; b) 2-x, 1-y, -z; c) x, 1/2-y, -1/2+z; d) -1+x, y, z; e) 1-x, 1-y, 1-z

Vibrational spectra

FTIR and Raman spectra of salt **HpcamNH$_2$SO$_3$** are depicted in Figure 44. Vibrational bands of sulfamate anion were assigned using the literature[40]. The rest of the vibrational bands were assigned using quantum-chemical calculations. The comparison of the calculated spectra with the measured ones is shown below, see Figures 42 and 43. The band assignment is listed in Table 20. The overall character of vibrational spectra is in agreement with crystal structure solution – i.e. crystal formed by **Hpcam**$^{1+}$ cations and $NH_2SO_3^-$ anions connected by H-bonds.

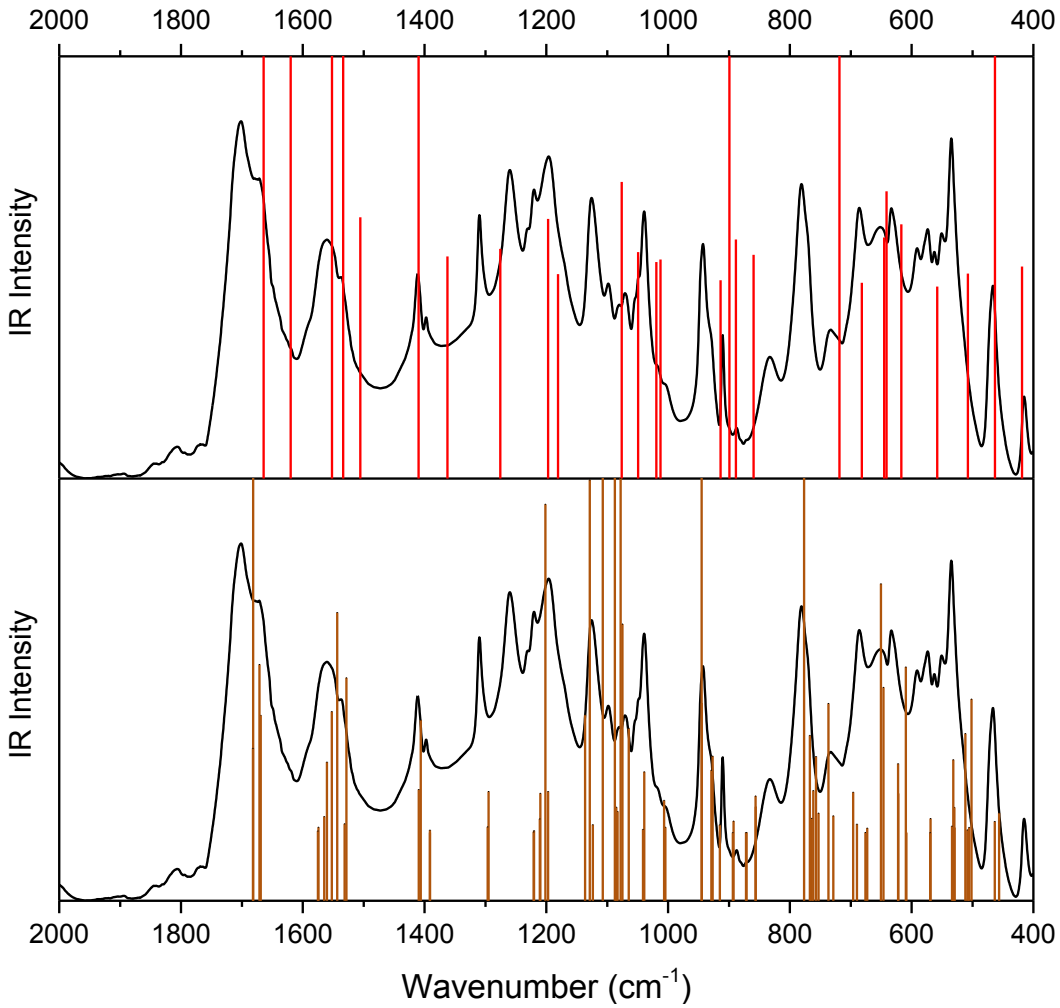

Figure 42: Recorded FTIR spectrum of salt **HpcamNH$_2$SO$_3$** compared with simulated IR spectrum of an isolated **Hpcam**$^{1+}$ cation in vacuum (red lines, upper part) and with solid state simulated IR spectrum (brown lines, lower part).

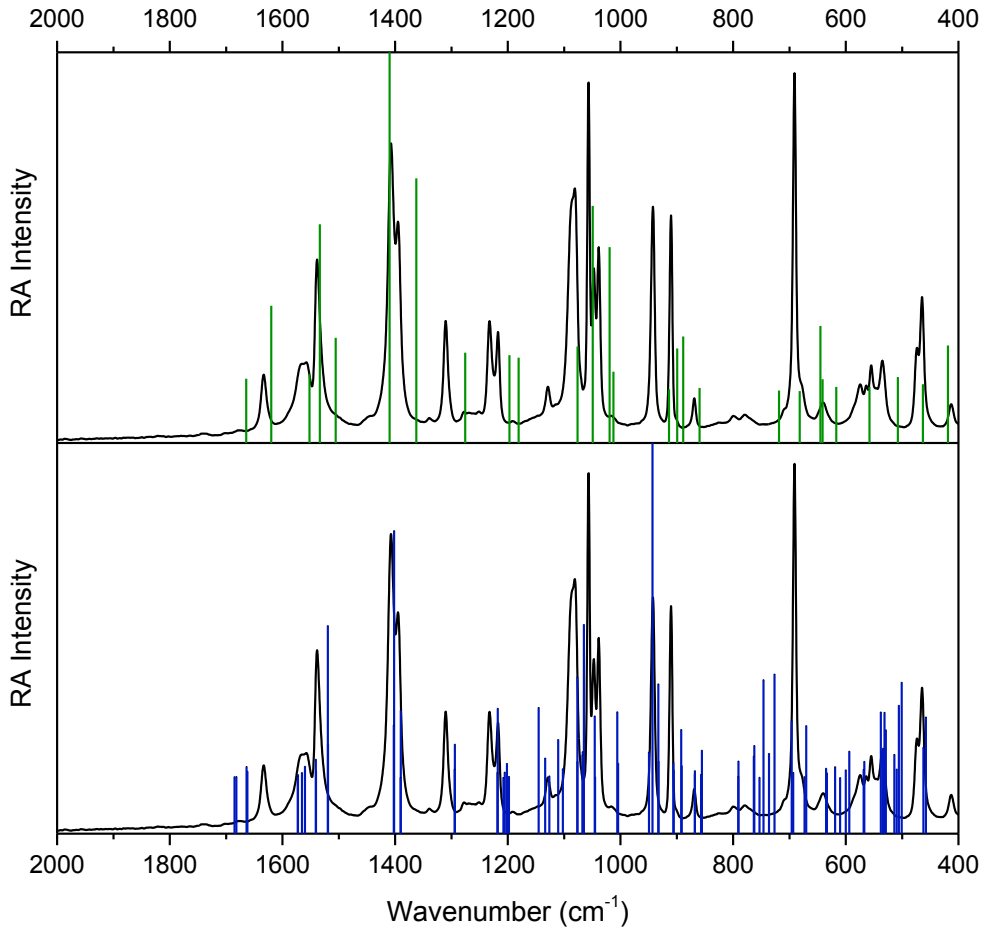

Figure 43: Recorded Raman spectrum of salt **HpcamNH$_2$SO$_3$** compared with simulated Raman spectrum of an isolated **Hpcam^{1+}** cation in vacuum (green lines, upper part) and with solid state simulated Raman spectrum (blue lines, lower part).

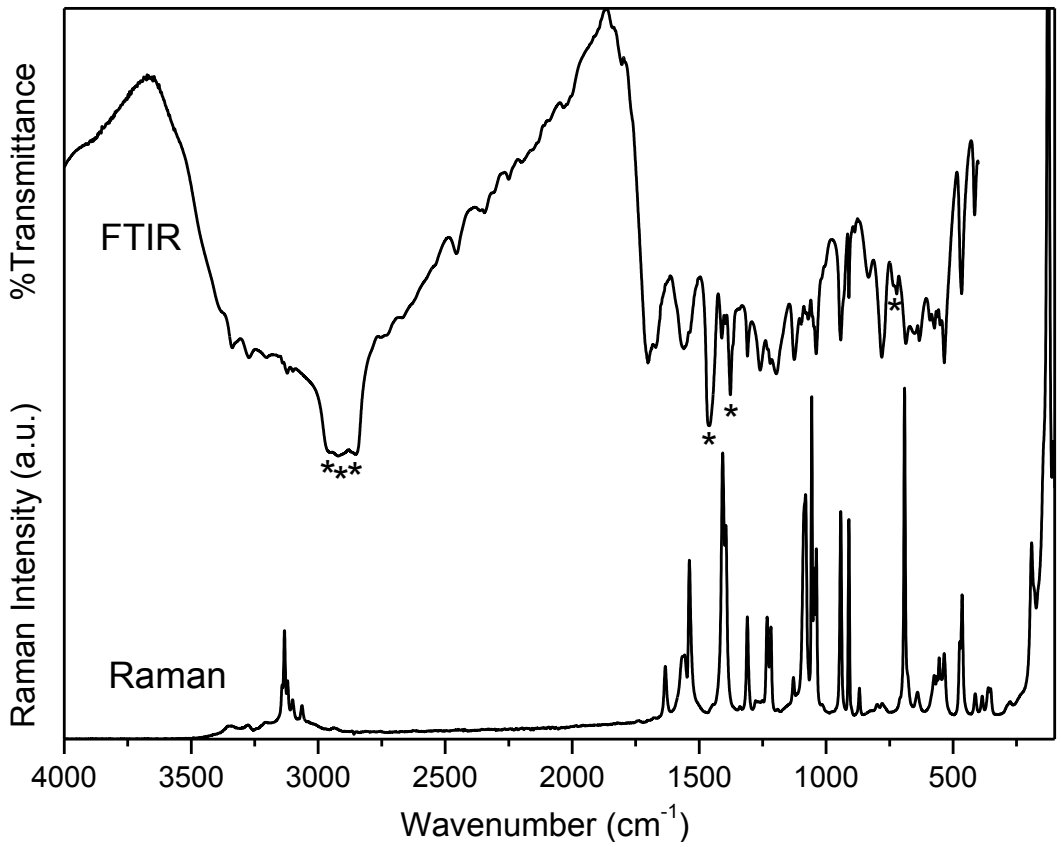

Figure 44: FTIR (nujol mull) and Raman spectra of **HpcamNH$_2$SO$_3$**. Nujol bands are labelled by asterisk.

Table 20: The band assignment of FTIR and Raman spectra of **HpcamNH$_2$SO$_3$**.

FTIR (cm^{-1})	Raman (cm^{-1})	Assignment	FTIR (cm^{-1})	Raman (cm^{-1})	Assignment
	105 m	External modes		1050 m	ρ NH$_2$, δ CH
	124 vs			1056 m	ρ NH$_2$, ν CC, δ CH
	165 m		1071 w		?
	191 m		1098 w	1084 m	ρ NH$_2$, δ CH
	288 wb		1126 m	1117 w	ν rg, ρ NH$_2$, δ CH
	362 w		1196 m		ν_3 SO$_3$
	386 vw		1220 m	1217 sh	ν NN, δ rg, δ NCN, δ CH
415 w	413 vw	?	1231 sh	1232 mb	ρ CH, ν rg, ω NH$_2$, ν CN
466 m	467 m	δ NCN	1260 s	1252 vw	ν_3 SO$_3$
535 m	535 w	ρ rg-C(NH$_2$)$_2$	1310 m	1308 m	ν rg, ν CN$_3$, δ CN$_3$, δ CH
551 w	549 w	ν_2 SO$_3$		1339 vw	?
563 vw	564 m	ν_4 SO$_3$	1397 w	1395 m	ν rg, δ CH, δ CN$_3$
574 m	584 w	γ rg, γ CN$_3$	1411 m	1407 s	ν rg, δ rg, δ CH, ν C-rg
591 w		ν_4 SO$_3$		1539 m	δ NH$_2$
633 m	639 vw	γ rg, γ CN$_3$	1560 m	1558 wb	ν NCN, ν rg, δ NH$_2$,
652 m		τ NH$_2$, γ NH			δ CH
686 m		δ NCN, ν C-rg, δ rg	1671 m	1633 w	δ NH$_2$, δ CN$_3$
	691 s		1702 s		ν CN$_3$, δ NH$_2$, δ CN$_3$
781 m	775 wb	?		3064 vw	ν NH…X
	798 wb	?	3100 m	3101 vw	
833 w		?	3122 m	3121 w	ν CH
887 vw	873 vw	γ CH		3133 w	
910 w	911 m	δ rg, ω NH$_2$		3142 m	
				3207 wb	
942 m	945 m	δ rg, ν CN$_3$, ν CN, ν NN	3273 m	3276 wb	ν NH…X
1039 m	1039 s	ν_1 SO$_3$	3339 m	3342 wb	

Note: Symbol X – atom N or O.

4.2.8 Summary for inorganic salts with 1*H*-pyrazole-carboxamidine

Inorganic anions with different geometry and level of protonation were used as alternative crystallisation partners for target molecule to supress natural tendency to form centrosymmetric pairs.

The target cation is planar in all of these inorganic salts. Even anions forming strong hydrogen bonds with its amino groups did not deform its rigid conformation. Angles and distances between the atoms of cations are similar in all of the previously discussed structures, see Electronic Supplement ES1 – ES8. There are only small differences in bond lengths and angles from the calculated values of the target cation (Table S4, Supplement).

Despite the formation of H-bonds and usage of anions derived from strong acids, centrosymmetric pairs of base were formed in chloride salt, both of the nitrate crystals, methanesulfonate and sulfamate salt. All of these pairs were connected by intramolecular and intermolecular interaction N7-H7b...N2.

Unfortunately, none of the remaining structures where these pairs are not present is non-centrosymmetric.

Quantum-chemical calculations were used for interpretation of the vibrational spectra of prepared inorganic salts. Generally, used model of an isolated **Hpcam**$^{1+}$ cation in vacuum and solid state calculations led to definite band assignment for all of the previously discussed salts except **HpcamClO$_4$**. The match of simulated and vibrational spectra of perchlorate salt is not accurate and will be subject of further studies.

4.3 Prepared salts of 1*H*-pyrazole-carboxamidine with organic acids

Six organic crystalline salts of **pcam** were prepared and characterised. Used acids, ratios and prepared products are listed in Table 21. All of the used molar ratios of particular acid led to the same crystalline salt.

Salts with organic acids preferred triclinic space groups *P*-1 (**HpcamCl-form·H$_2$O, Hpcam-Hox, Hpcam-suc·H$_2$suc**) or *P*1 (**Hpcam-Hmalic**). Only two salts crystallise in monoclinic space groups - $P2_1/c$ (**Hpcam-adip·H$_2$adip·H$_2$O**) and $P2_1$ (**Hpcam-Htart·2H$_2$O**).

Crystal structures and vibrational spectra of all of the prepared crystals are described in this chapter individually. Basic crystallographic data and structure refinement details for all these organic salts are listed in Supplement (Tables S7 and S8) and Electronic Supplement (ES9 - ES14).

The phase uniformity of prepared salts was verified by powder X-ray diffraction, results of which are listed in Supplement for each salt individually (Tables S17 and S22). Measured diffraction patterns are consistent with calculated diffraction maxima (Diamond software[36]) from single crystal data.

Table 21: Crystalline salts of 1*H*-pyrazole-carboxamidine with organic acids.

Acid	Ratio (B:A)		
	1:1	1:2	2:1
adipic	**Hpcam-adip·H$_2$adip·H$_2$O**		
formic	**HpcamCl-form·H$_2$O**		
L-malic	**Hpcam-Hmalic**		
oxalic	**Hpcam-Hox**		
succinic	**Hpcam-suc·H$_2$suc**		
L-tartaric	**Hpcam-Htart·2H$_2$O**		

4.3.1 1*H*-pyrazole-carboxamidinium adipate - adipic acid monohydrate (1/1) (Hpcam-adip·H_2adip·H_2O)

Crystal structure

This product was obtained from water solution of **pcam** with adipic acid in molar ratios 1:1, 1:2 and 2:1 (Table 21). Asymmetric unit is shown in Figure 45, crystal packing in Figure 45, hydrogen bonds geometry is listed in Table 22, diffraction maxima and d-spacing obtained by powder X-ray diffraction are listed in Table S17 in Supplement.

As is apparent from Figure 45 also this structure is formed by H-bonded layers of alternating cations, anions and adipic acids with embed molecules of water. Connection between the layers is provided by O1w-H1w...O1 hydrogen bond between the water molecules and adipate anions. This structure is also stabilised by intramolecular N7-H7b...N2 and weak C5-H5a...O1w hydrogen bonds.

The lengths of C-O bonds in all four carboxylic groups confirm their protonation in solved crystal structure – it consists of deprotonated adipate and neutral adipic acid; see ES9 in Electronic Supplement.

Table 22: Hydrogen bonds geometry of **Hpcam-adip·H_2adip·H_2O**.

	d(D – H) (Å)	*d*(H···A) (Å)	*d*(D···A) (Å)	∢ D-H···A (°)
O1w-H1w...O1[a]	0.88	1.97	2.851(2)	179
O1w-H2w...O3	0.88	1.97	2.776(2)	152
O4-H4...O2	0.86	1.76	2.621(2)	174
N7-H7a...O1	0.92	1.83	2.743(2)	173
N7-H7b...N2	0.89	2.25	2.653(2)	107
N7-H7b...O1[b]	0.89	2.12	2.877(2)	143
N8-H8a...O2	0.91	1.95	2.854(2)	169
N8-H8b...O1w	0.87	2.09	2.953(2)	170
C5-H5a...O1w	0.95	2.41	3.284(2)	152

Symmetry codes: a) 1-x, -1/2+y, 3/2-z; b) 1-x, 1-y, 1-z

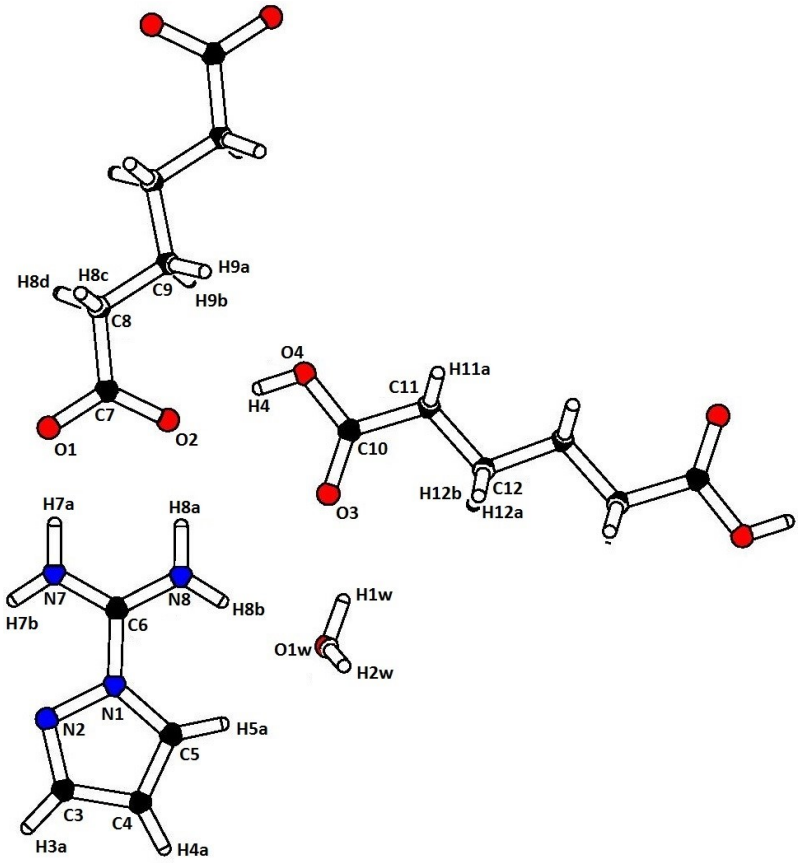

Figure 45: Asymmetric unit of **Hpcam-adip·H$_2$adip·H$_2$O**

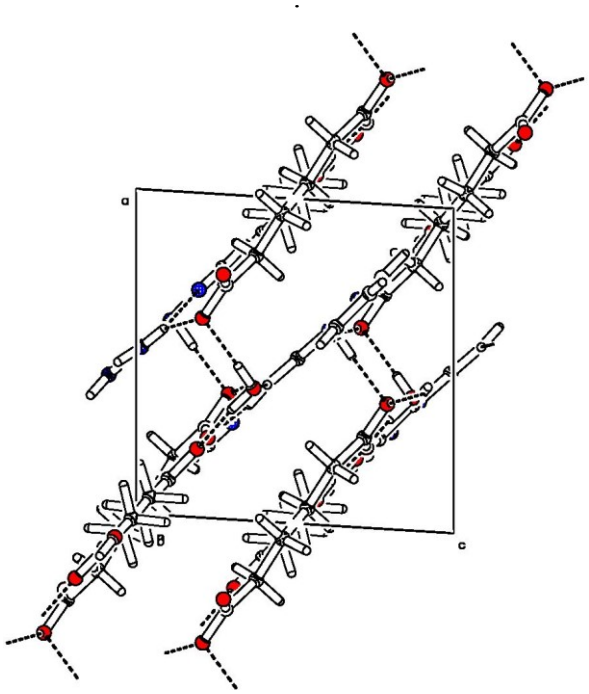

Figure 46: Crystal packing of **Hpcam-adip·H$_2$adip·H$_2$O** (projection to plane *ac*). Dashed lines indicate hydrogen bonds.

Vibrational spectra

FTIR and Raman spectra of **Hpcam-adip·H₂adip·H₂O** are depicted in Figure 47. The overall character of vibrational spectra is in agreement with crystal structure solution.

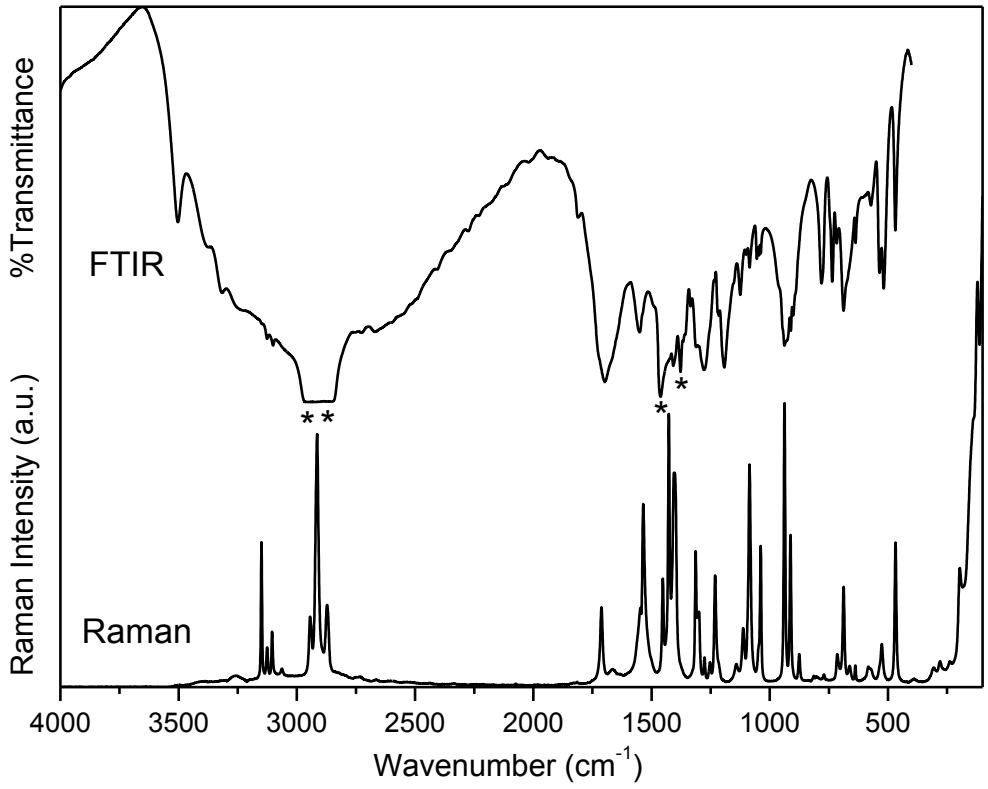

Figure 47: FTIR (nujol mull) and Raman spectra of **Hpcam-adip·H₂adip·H₂O**. Nujol bands are labelled by asterisk.

FTIR (cm^{-1}): ν_{max} 469 w, 518 m, 536 m, 572 wb, 637 w, 688 mb, 717 w, 736 m, 781 m, 901 m, 911 m, 938 mb, 1038 vw, 1045 vw, 1055 vw, 1086 w, 1099 vw, 1125 w, 1192 s, 1215 sh, 1278 sb, 1311 sh, 1335 vw, 1408 m, 1462 s, 1550 m, 1698 vs, 2876 wb, 2930 mb, 2949 m, 2961 m, 3101 m, 3126 m, 3316 w, 3503 vw.

Raman (cm^{-1}): ν_{max} 121 vs, 196 m, 280 w, 306 w, 391 wb, 468 m, 526 m, 583 wb, 638 w, 662 w, 688 m, 715 w, 771 vw, 875 w, 912 m, 938 vs, 1038 m, 1086 s, 1112 m, 1142 w, 1231 m, 1253 w, 1276 w, 1299 m, 1305 m, 1313 m, 1405 s, 1427 vs, 1452 m, 1535 s, 1547 m, 1665 wb, 1712 m, 2872 m, 2914 vs, 2944 m, 3063 vw, 3105 m, 3126 w, 3150 m, 3254 wb.

4.3.2 1*H*-pyrazole-carboxamidinium chloride formate monohydrate (HpcamCl-form·H_2O)

This salt was obtained from water solution of **pcam** with formic acid in molar ratios 1:1, 1:2 and 2:1 (Table 21). Asymmetric unit is shown in Figure 48, crystal packing in Figure 49, hydrogen bonds geometry is listed in Table 23, diffraction maxima and d-spacing obtained by powder X-ray diffraction are listed in Table S18 in Supplement.

As it is seen from crystal packing in Figure 49 also in this structure centrosymmetric pairs of cations were found. These pairs are stabilised by intramolecular and intermolecular N17-H17b...N12 and N27-H27b...N22 hydrogen bonds – same as the ones formed in the previously discussed structures. Pairs of cations are planar (Figure 49) and together with chloride and formate anions and water molecules form layers. Connection between the layers is provided by O1w-H2w...Cl1 and O1w-H1w...O1w hydrogen bonds. The similar lengths of C-O bonds confirm deprotonation of formate anion in solved crystal structure, see ES10 in Electronic Supplement.

Chloride atoms in this structure most likely originate from initial commercial product (they did not precipitate by silver carbonate).

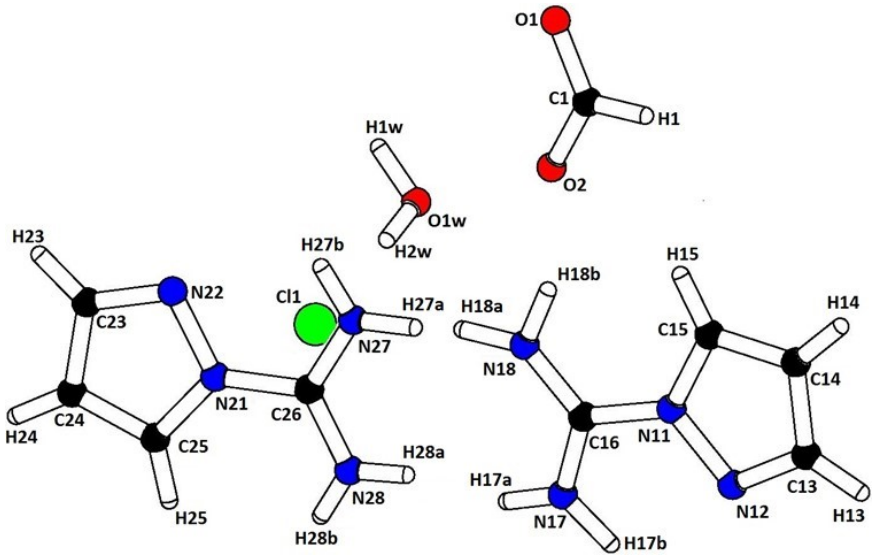

Figure 48: Asymmetric unit of **HpcamCl-form·H_2O**.

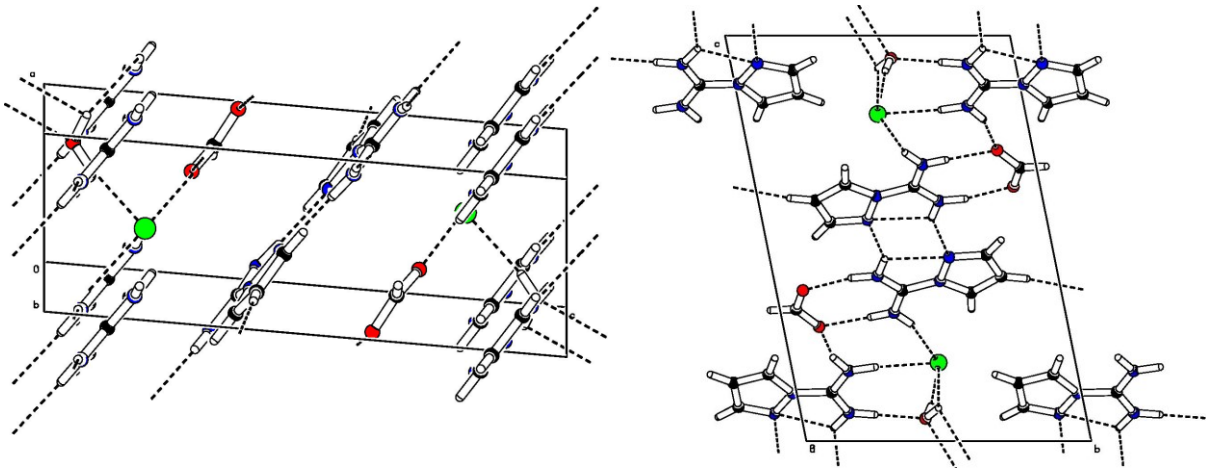

Figure 49: Crystal packing of **HpcamCl-form·H₂O** (projection to plane *ac* - left and projection to plane *bc* - right). Dashed lines indicate hydrogen bonds.

Table 23: Hydrogen bonds geometry of **HpcamCl-form·H₂O**.

	d(D – H) (Å)	*d*(H···A) (Å)	*d*(D···A) (Å)	∢ D-H···A (°)
O1w-H1w...Cl1[a]	0.94	2.42	3.252(2)	147
O1w-H1w...O1w[b]	0.94	2.56	2.956(3)	105
O1w-H2w...Cl1	0.83	2.32	3.139(2)	169
N17-H17a...O1w[c]	0.92	1.83	2.744(4)	171
N17-H17b...N12	0.98	2.26	2.677(4)	104
N17-H17b...N12[d]	0.98	2.16	2.987(3)	142
N18-H18a...Cl1	0.98	2.28	3.251(2)	169
N18-H18b...O2	0.95	1.89	2.803(3)	160
N27-H27a...O1[c]	0.95	1.82	2.763(3)	170
N27-H27b...N22	0.90	2.31	2.679(4)	104
N27-H27b...N22[e]	0.90	2.16	2.954(3)	147
N28-H28a...O2[c]	0.84	1.91	2.753(4)	174
N28-H28b...Cl1[c]	0.89	2.31	3.168(3)	161
C15-H15...O2	0.95	2.39	3.257(4)	152
C24-H24...O1[f]	0.95	2.42	3.364(4)	170

Symmetry codes: a) 1+x, y, z; b) 2-x, 1-y, -z; c) -1+x, y, z; d) -1-x, -y, -z; e) 1-x, 1-y, 1-z; f) -1+x, 1+y, z

Vibrational spectra

FTIR and Raman spectra of **HpcamCl-form·H_2O** are depicted in Figure 50. The overall character of vibrational spectra is in agreement with crystal structure solution.

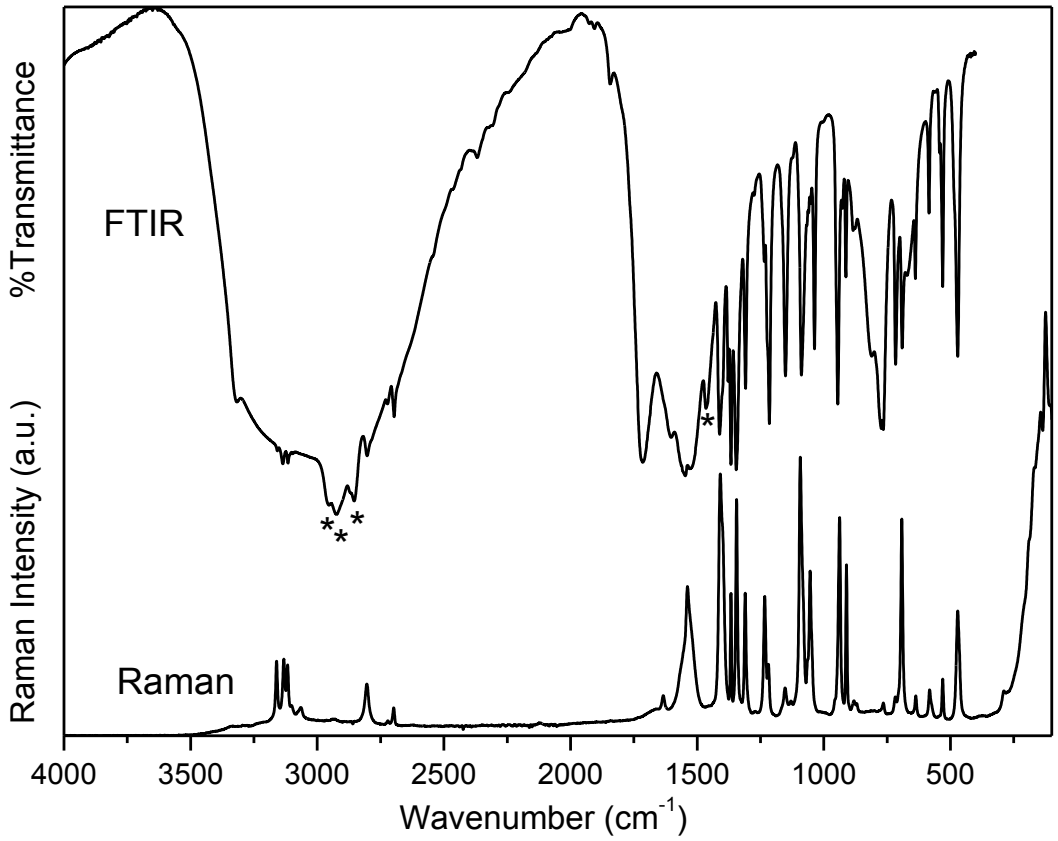

Figure 50: FTIR (nujol mull) and Raman spectra of **HpcamCl-form·H_2O**. Nujol bands are labelled by asterisk.

FTIR (cm^{-1}): ν_{max} 471 m, 531 w, 543 vw, 585 vw, 639 w, 691 m, 716 m, 765 m, 773 m, 811 mb, 884 vw, 913 w, 926 vw, 945 m, 1037 m, 1088 m, 1151 m, 1215 m, 1235 w, 1309 m, 1346 s, 1367 s, 1378 m, 1411 s, 1531 vs, 1547 vs, 1602 mb, 1717 s, 2696 m, 2722 m, 2803 m, 3116 s, 3136 s, 3158 s, 3316 m.

Raman (cm^{-1}): ν_{max} 124 vs, 144 vs, 289 sh, 471 m, 531 w, 582 w, 637 w, 692 m, 718 w, 765 vw, 870 vw, 881 vw, 911 m, 938 m, 1054 m, 1093 s, 1130 vw, 1153 w, 1219 m, 1233 m, 1310 m, 1344 m, 1366 m, 1409 s, 1538 m, 1634 w, 2698 w, 2721 vw, 2804 m, 3065 vw, 3117 m, 3132 m, 3161 m.

4.3.3 1*H*-pyrazole-carboxamidinium hydrogen L-malate (Hpcam-Hmalic)

Crystal structure

This salt was obtained from water solution of **pcam** with L-malic acid in molar ratios 1:1, 1:2 and 2:1 (Table 21). Asymmetric unit is shown in Figure 51, crystal packing in Figure 52, hydrogen bonds geometry is listed in Table 24, diffraction maxima and d-spacing obtained by powder X-ray diffraction are listed in Table S19 in Supplement. Prepared crystals were sticky and therefore needed to be washed with ethanol.

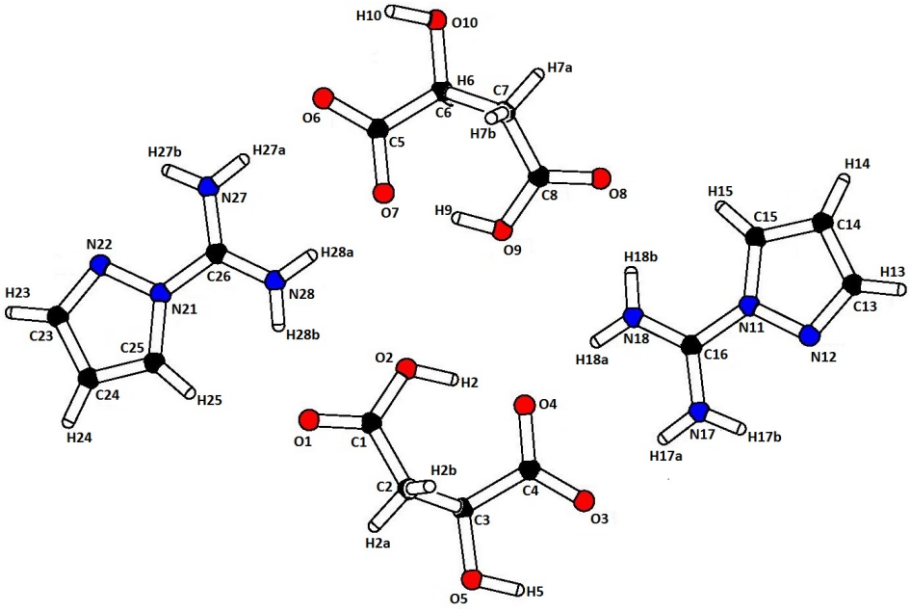

Figure 51: Asymmetric unit of **Hpcam-Hmalic**.

As seen in Figure 52 asymmetric unit contains two cations and two hydrogen L-malate anions. Acidic protons of anions are involved in complicated hydrogen-bonded structure. Also this structure is stabilised with intramolecular H-bond interaction (N17-H17b...N12 and N27-H27b...N22 bonds) and weak H-bonds involving carbon atoms. The lengths of C-O bonds confirm protonation of hydrogen L-malate in solved crystal structure, see ES11 in Electronic Supplement. This complicated structure provides non-centrosymmetric arrangement.

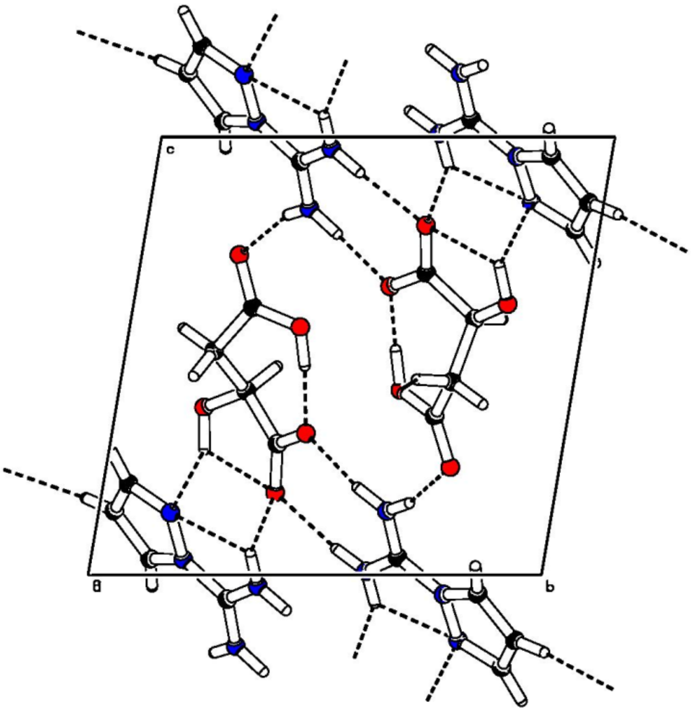

Figure 52: Crystal packing of **Hpcam-Hmalic** (projection to plane *bc*). Dashed lines indicate hydrogen bonds.

Table 24: Hydrogen bonds geometry of **Hpcam-Hmalic**.

	d(D – H) (Å)	*d*(H···A) (Å)	*d*(D···A) (Å)	∢ D-H···A (°)
O2-H2...O4	0.94	1.53	2.458(3)	172
O5-H5...O3	0.93	2.19	2.700(3)	113
O5-H5...N22[a]	0.93	2.16	2.914(3)	138
O9-H9...O7	0.91	1.58	2.483(3)	175
O10-H10...O6	0.96	2.18	2.726(3)	115
O10-H10...N12[b]	0.96	2.15	2.905(3)	135
N17-H17a...O3	0.88	2.01	2.894(3)	178
N17-H17b...O6[a]	0.88	2.07	2.866(3)	149
N17-H17b...N12	0.88	2.31	2.666(3)	104
N18-H18a...O4	0.88	1.91	2.780(3)	168
N18-H18b...O8	0.88	1.97	2.816(3)	162
N27-H27a...O6	0.88	2.01	2.880(3)	173
N27-H27b...O3[b]	0.88	2.08	2.875(3)	149
N27-H27b...N22	0.88	2.32	2.673(3)	104
N28-H28a...O7	0.88	1.91	2.770(3)	164
N28-H28b...O1	0.88	1.97	2.829(3)	166
C2-H2b...O2[c]	0.99	2.52	2.293(3)	135
C14-H14...O1[d]	0.95	2.41	3.339(4)	166
C15-H15...O8	0.95	2.49	3.300(4)	144
C24-H24...O8[e]	0.95	2.35	3.297(4)	172
C25-H25...O1	0.95	2.44	3.282(4)	148

Symmetry codes: a) 1+x, y, 1+z; b) -1+x, y, -1+z; c) 1+x, y, z; d) -1+x, -1+y, 1+z; e) 1+x, -1+y, -1+z

Vibrational spectra

FTIR and Raman spectra of **Hpcam-Hmalic** are depicted in Figure 53. The overall character of vibrational spectra is in agreement with crystal structure solution.

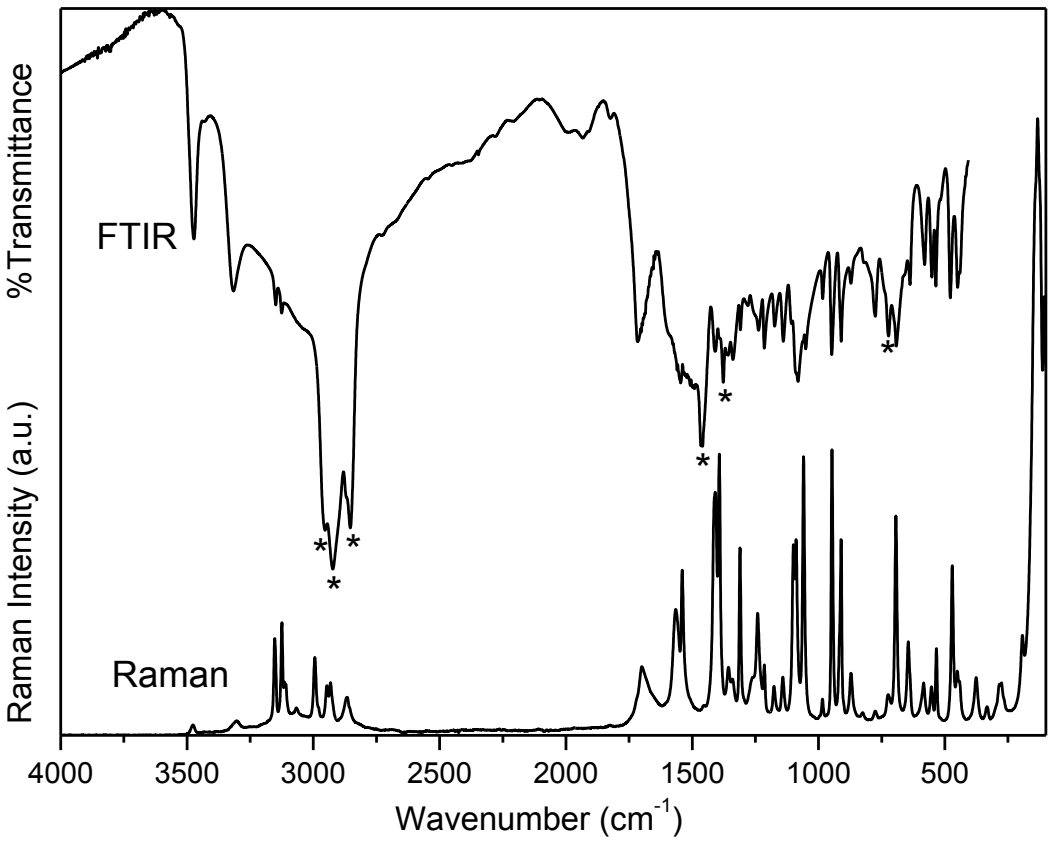

Figure 53: FTIR (nujol mull) and Raman spectra of **Hpcam-Hmalic**. Nujol bands are labelled by asterisk.

FTIR (cm^{-1}): ν_{max} 449 m, 478 m, 536 m, 551 m, 580 w, 638 m, 692 s, 723 s, 775 m, 872 w, 910 s, 948 s, 984 w, 1051 m, 1081 sb, 1140 m, 1174 m, 1215 m, 1238 mb, 1279 w, 1309 m, 1339 m, 1358 m, 1408 m, 1508 s, 1546 s, 1717 m, 3125 m, 3149 m, 3316 m, 3473 w.

Raman (cm^{-1}): ν_{max} 106 vs, 133 vs, 193 m, 276 m, 284 m, 333 vw, 376 m, 451 m, 471 s, 533 m, 553 m, 584 w, 645 m, 694 s, 724 w, 776 vw, 825 vw, 871 w, 911 s, 947 s, 984 vw, 1059 s, 1089 m, 1100 m, 1141 w, 1176 w, 1215 m, 1241 m, 1311 m, 1341 w, 1357 w, 1393 s, 1409 s, 1540 m, 1565 m, 1700 mb, 2866 w, 2932 m, 2947 m, 2994 m, 3067 wb, 3114 sh, 3124 m, 3153 m, 3303 wb, 3477 vw.

4.3.4 1*H*-pyrazole-carboxamidinium hydrogen oxalate (Hpcam-Hox)

Crystal structure

This salt was obtained from water solution of **pcam** with oxalic acid in molar ratios 1:1, 1:2 and 2:1 (Table 21). Asymmetric unit is shown in Figure 54, crystal packing in Figure 55, hydrogen bonds geometry is listed in Table 25, diffraction maxima and d-spacing obtained by powder X-ray diffraction are listed in Table S20 in Supplement.

Asymmetric unit in Figure 54 indicates that only one hydrogen atom from carboxylic anion is removed. Monoprotonated anion together with cation enabled arrangement based on extensive network of hydrogen bonds as shown in Figure 55. There is also possible to see alternating cations and anions forming hydrogen-bonded layers which are connected *via* C4-H4...O2 hydrogen bonds. Also this structure is stabilised with intramolecular N7-H7b...N2 hydrogen bond. The lengths of C-O bonds confirm the formation of hydrogen oxalate anion in solved crystal structure, see ES12 in Electronic Supplement.

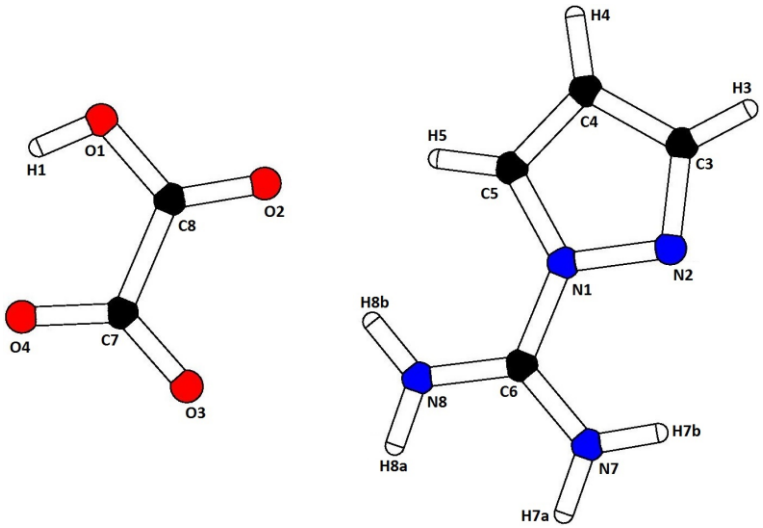

Figure 54: Asymmetric unit of **Hpcam-Hox**.

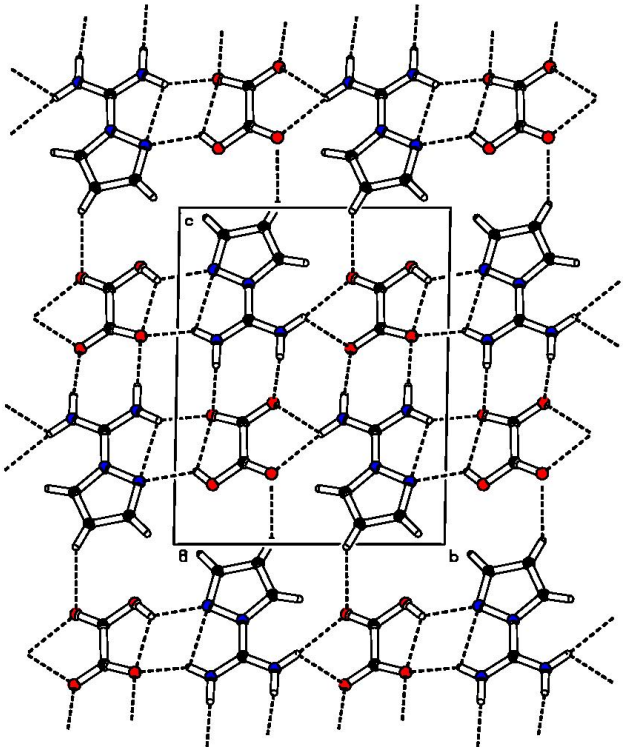

Figure 55: Crystal packing of **Hpcam-Hox** (projection to plane *bc*). Dashed lines indicate hydrogen bonds.

Table 25: Hydrogen bonds geometry of **Hpcam-Hox**.

	d(D – H) (Å)	*d*(H···A) (Å)	*d*(D···A) (Å)	∢ D-H···A (°)
O1-H1...O4	0.86(2)	2.14(2)	2.670(2)	119(2)
O1-H1...N2[a]	0.86(2)	2.13(2)	2.809(2)	135(2)
N7-H7a...O4[b]	0.92	1.91	2.830(2)	178
N7-H7b...O4[c]	0.90	2.01	2.845(2)	153
N7-H7b...N2	0.90	2.33	2.687(2)	103
N8-H8a...O3[b]	0.90	1.89	2.785(2)	173
N8-H8b...O2	0.92	2.21	3.124(2)	173
N8-H8b...O3	0.92	2.48	2.923(2)	110
C4-H4...O2[d]	0.95	2.49	3.349(2)	150
C5-H5...O2	0.95	2.24	3.121(2)	155

Symmetry codes: a) -1+x, -1+y, z; ; b) -x, 1-y, 1-z; c) 1+x, 1+y, z; d) 2-x, 1-y, -z

Vibrational spectra

FTIR and Raman spectra of **Hpcam-Hox** are depicted in Figure 56. The overall character of vibrational spectra is in agreement with crystal structure solution.

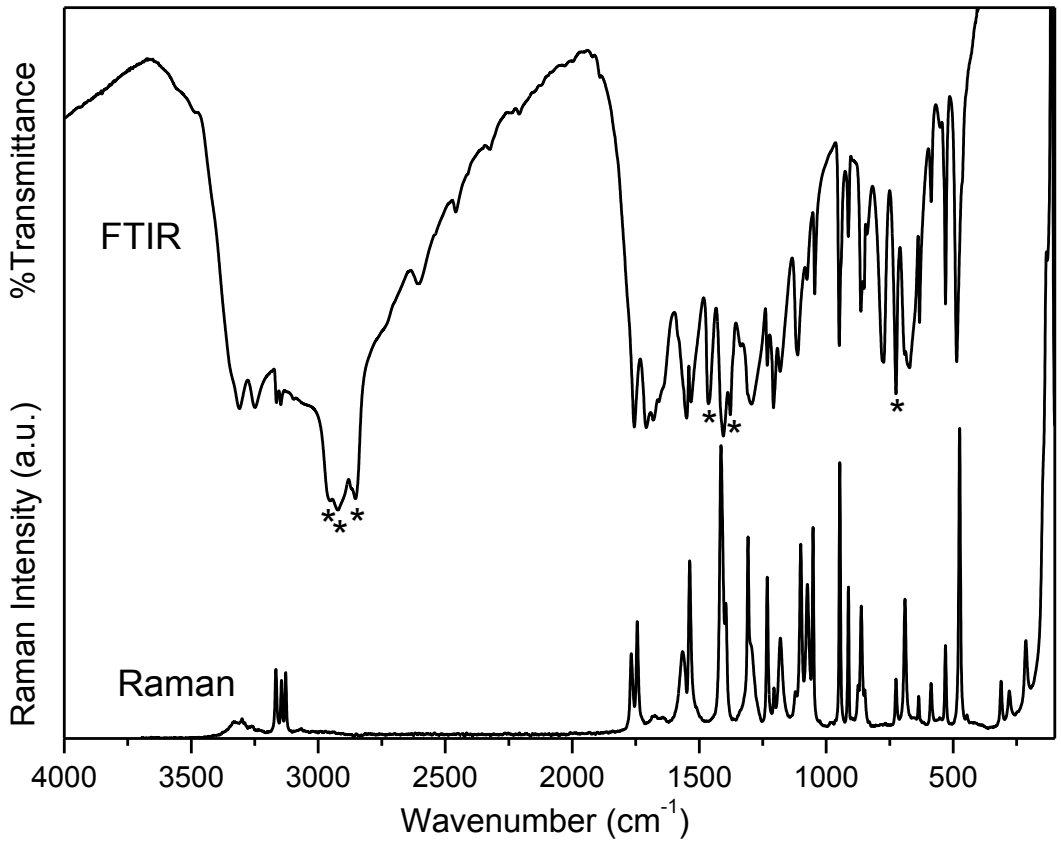

Figure 56: FTIR (nujol mull) and Raman spectra of **Hpcam-Hox**. Nujol bands are labelled by asterisk.

FTIR (cm^{-1}): ν_{max} 486 s, 530 m, 587 w, 633 m, 672 sb, 691 s, 725 s, 774 s, 840 vw, 851 w, 863 m, 913 w, 949 m, 1045 m, 1076 w, 1112 m, 1181 m, 1208 s, 1232 m, 1294 sb, 1337 m, 1405 vs, 1533 s, 1550 s, 1659 sh, 1682 s, 1709 vs, 1756 vs, 3147 s, 3165 s, 3250 s, 3311 s.

Raman (cm^{-1}): ν_{max} 113 vs, 133 s, 214 m, 279 w, 311 w, 446 vw, 475 s, 530 m, 587 w, 636 w, 690 m, 725 w, 848 w, 862 m, 874 w, 912 m, 946 s, 1052 s, 1074 m, 1100 s, 1121 vw, 1181 m, 1206 w, 1232 m, 1308 m, 1395 m, 1414 s, 1538 m, 1565 m, 1677 m, 1744 m, 1768 m, 3128 m, 3145 m, 3167 m, 3300 wb.

4.3.5 1*H*-pyrazole-carboxamidinium succinate - succinic acid (1/1) (Hpcam-suc·H_2suc)

Crystal structure

This product was obtained from water solution of **pcam** with succinic acid in molar ratios 1:1, 1:2 and 2:1 (Table 21). Asymmetric unit is shown in Figure 57, crystal packing in Figure 58, hydrogen bonds geometry is listed in Table 26, diffraction maxima and d-spacing obtained by powder X-ray diffraction are listed in Table S21 in Supplement.

As is apparent from Figure 58 also this structure is formed by hydrogen bonded layers. The connection between them is provided by N7-H7b...O1 hydrogen bonds. This structure is also stabilised with intramolecular N7-H7b...N2 as well as weak C5-H5...O4 hydrogen bonds. Unwanted centrosymmetric pairs of cations were not formed in this structure. The lengths of C-O bonds of succinate anion and succinic acid confirm their presence in solved crystal structure, see ES13 in Electronic Supplement.

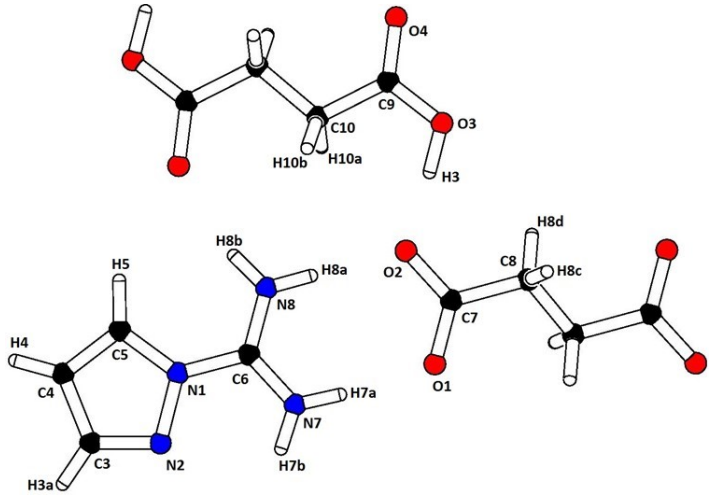

Figure 57: Asymmetric unit of **Hpcam-suc·H_2suc**.

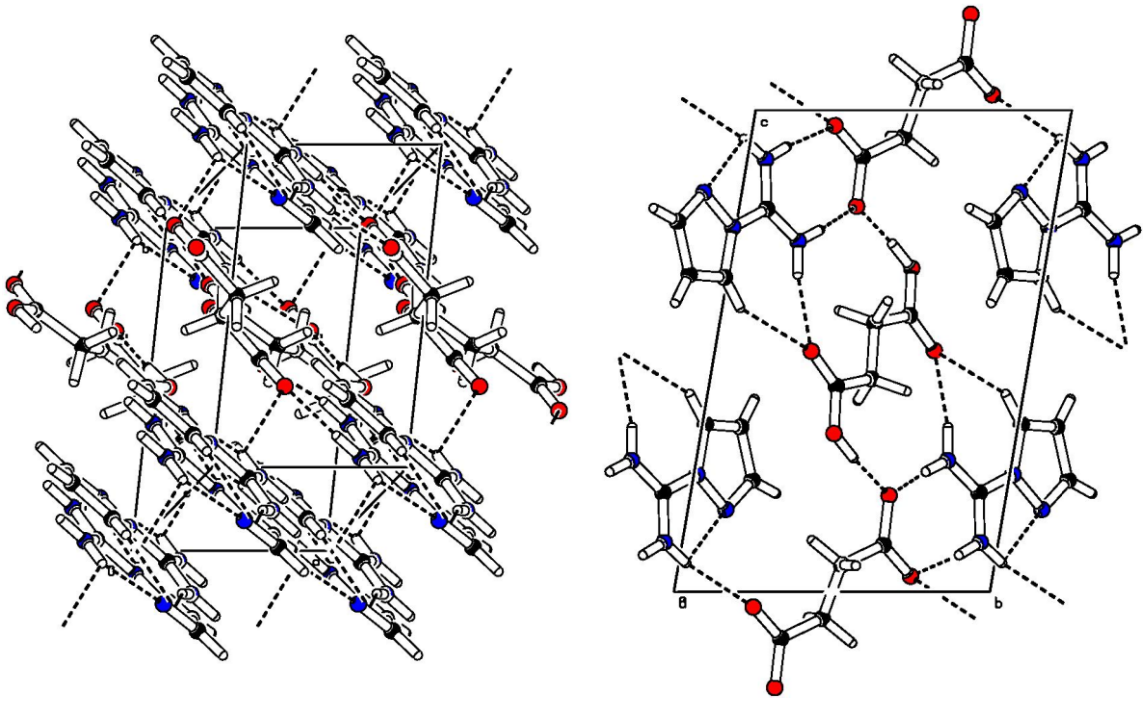

Figure 58: Crystal packing of **Hpcam-suc·H$_2$suc** (projection to plane *ab* - left and projection to plane *bc* - right). Dashed lines indicate hydrogen bonds.

Table 26: Hydrogen bonds geometry of **Hpcam-suc·H$_2$suc**.

	d(D – H) (Å)	*d*(H···A) (Å)	*d*(D···A) (Å)	∢ D-H···A (°)
O3-H3...O2	0.96	1.56	2.521(2)	175
N7-H7a...O1	0.88	1.89	2.762(2)	174
N7-H7b...N2	0.88	2.32	2.673(2)	104
N7-H7b...O1[a]	0.88	2.34	2.910(2)	123
N8-H8a...O2	0.88	1.90	2.773(2)	170
N8-H8b...O4[b]	0.88	2.02	2.881(2)	166
C5-H5...O4[b]	0.95	2.47	3.335(2)	151

Symmetry codes: a) 1-x, -y, 2-z; b) 1-x, 1-y, 1-z

Vibrational spectra

FTIR and Raman spectra of **Hpcam-suc·H₂suc** are depicted in Figure 59. The overall character of vibrational spectra is in agreement with crystal structure solution.

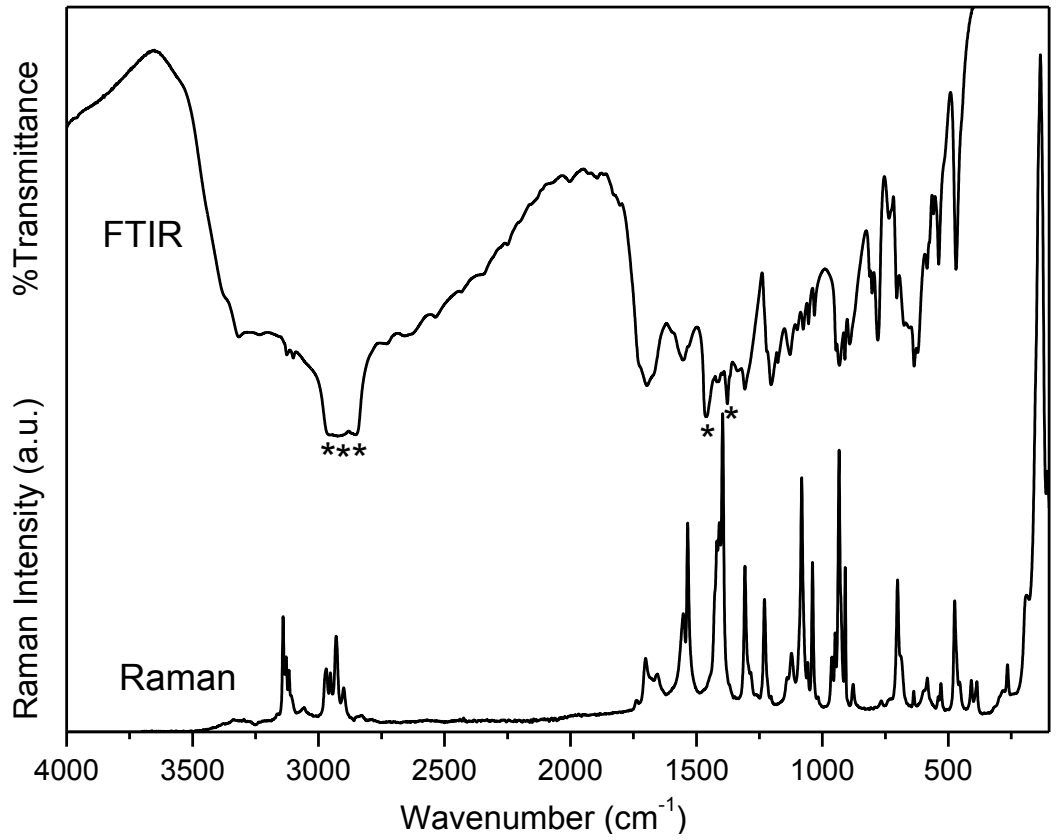

Figure 59: FTIR (nujol mull) and Raman spectra **Hpcam-suc·H₂suc**. Nujol bands are labelled by asterisk.

FTIR (cm^{-1}): ν_{max} 470 m, 538 m, 559 w, 584 m, 621 m, 636 s, 676 m, 705 m, 736 vw, 780 m, 803 m, 812 w, 892 mb, 911 m, 933 s, 946 m, 1032 m, 1055 m, 1076 m, 1100 m, 1129 m, 1177 m, 1204 s, 1308 s, 1337 m, 1419 s, 1552 mb, 1698 sb, 2659 vw, 3100 m, 3128 m, 3234 mb, 3316 mb.

Raman (cm^{-1}): ν_{max} 107 s, 133 vs, 191 m, 265 m, 387 w, 409 w, 475 m, 530 w, 583 w, 638 vw, 692 m, 701 m, 766 vw, 877 vw, 909 m, 934 s, 962 w, 1039 m, 1082 s, 1122 w, 1230 m, 1308 m, 1395 s, 1408 m, 1419 m, 1535 m, 1553 m, 1634 w, 1656 m, 1702 m, 1738 vw, 2834 vw, 2900 w, 2929 m, 2953 m, 2969 m, 3064 vw, 3104 m, 3118 m, 3141 m, 3164 vw.

4.3.6 1*H*-pyrazole-carboxamidinium hydrogen L-tartrate dihydrate (Hpcam-Htart·2H$_2$O)

Crystal structure

This product was obtained from water solution of **pcam** with L-tartaric acid in molar ratios 1:1, 1:2 and 2:1 (Table 21). Asymmetric unit is shown in Figure 60, crystal packing in Figure 61, hydrogen bonds geometry is listed in Table 27, diffraction maxima and d-spacing obtained by powder X-ray diffraction are listed in Table S22 in Supplement. The presence of chiral L-tartrate anions led to non-centrosymmetric arrangement.

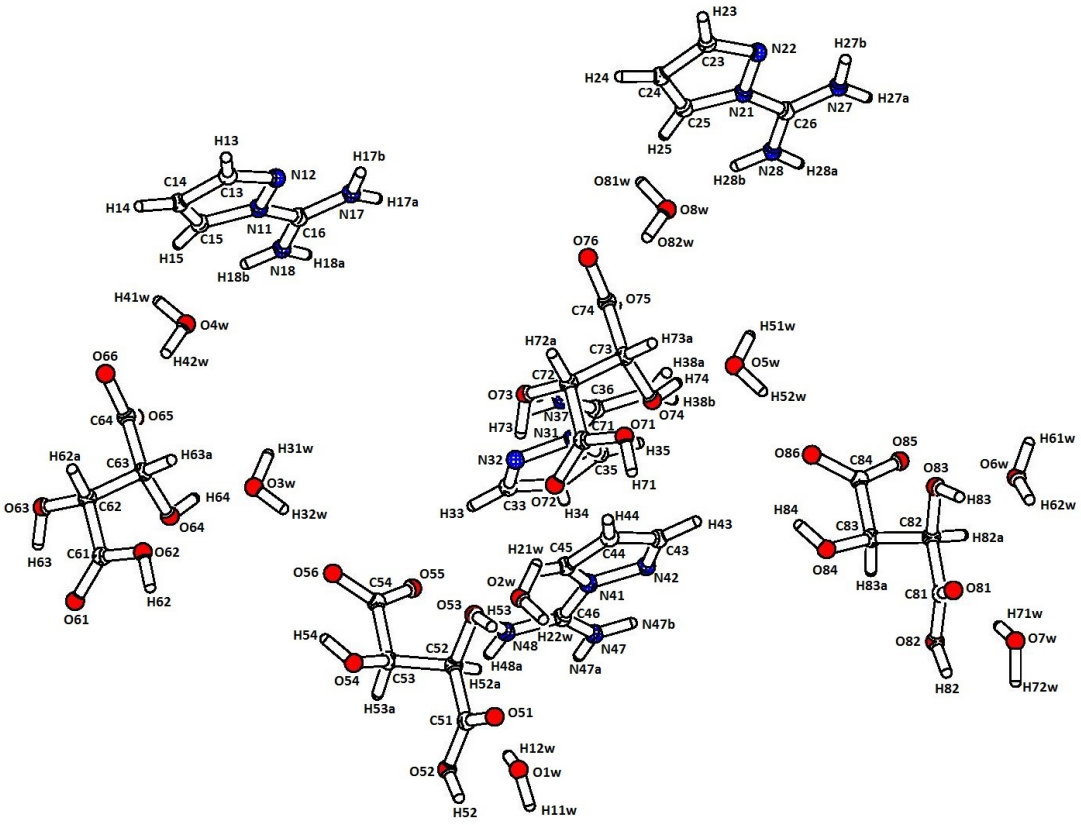

Figure 60: Asymmetric unit of **Hpcam-Htart·2H$_2$O**.

The existence of four formula units in asymmetric unit (see Figure 60) leads to complicated H-bonded crystal packing presented in Figure 61. The lengths of C-O bonds confirm the formation of hydrogen L-tartrate anions in the crystal structure, see ES14 in Electronic Supplement.

Table 27: Hydrogen bonds geometry of **Hpcam-Htart·2H$_2$O**.

	d(D – H) (Å)	*d*(H···A) (Å)	*d*(D···A) (Å)	∢ D-H···A (°)
O1w-H11w...O53[a]	0.85	1.87	2.713(2)	168
O1w-H12w...O51	0.85	1.84	2.685(2)	171
N17-H17b...N12	0.88	2.34	2.690(3)	104
N18-H18b...O4w	0.88	1.98	2.804(3)	154
O2w-H21w...O72	0.84	1.9	2.721(2)	164
O2w-H22w...O73[a]	0.91	1.85	2.759(2)	174
N27-H27b...N22	0.88	2.31	2.672(3)	104
N28-H28b...O8w	0.88	1.98	2.818(2)	157
O3w-H31w...O54[b]	0.9	1.84	2.738(2)	173
O3w-H32w...O56	0.83	1.9	2.705(2)	164
N37-H37a...O75	0.88	2.11	2.904(3)	150
N37-H37b...O51[b]	0.88	2.29	3.152(3)	166
N37-H37b...N32	0.88	2.31	2.671(3)	104
N38-H38a...O5w	0.88	2.06	2.843(2)	148
O4w-H41w...O64[b]	0.86	1.96	2.813(2)	172
O4w-H42w...O65	0.89	1.83	2.718(2)	173
N47-H47b...N42	0.88	2.33	2.681(3)	104
N48-H48b...O55	0.88	2	2.807(3)	152
O52-H52 ...O55[a]	0.82(4)	1.70(4)	2.520(2)	173(2)
O5w-H52w...O86	0.85	1.85	2.695(2)	170
O53-H53 ...O2w	0.9	1.87	2.648(2)	142
O53-H53 ...O51	0.9	2.08	2.642(2)	119
O54-H54 ...O4w[a]	0.84(3)	2.12(3)	2.872(2)	149(3)
O54-H54 ...O56	0.84(3)	2.13(3)	2.610(2)	116(2)
O62-H62 ...O66[a]	0.88(3)	1.66(3)	2.526(2)	169.4(7)
O63-H63 ...O7w[c]	0.86(2)	2.00(2)	2.762(2)	148(2)
O63-H63 ...O61	0.86(2)	2.14(2)	2.627(2)	116(2)
O64-H64 ...O3w	0.90(3)	1.88(3)	2.752(2)	161(2)
O64-H64 ...O65	0.90(3)	2.36(2)	2.669(2)	100(2)
O71-H71 ...O76[a]	0.88(3)	1.64(3)	2.510(2)	169.5(5)
O7w-H71w...O81	0.82	1.89	2.701(3)	173
O73-H73 ...O1w[b]	0.89	2.11	2.855(2)	141
O73-H73 ...O72	0.89	2.07	2.600(2)	118
O74-H74 ...O5w	0.87(3)	1.90(3)	2.758(2)	166(3)
O8w-H82w...O75	0.84	1.92	2.763(2)	173
O83-H83 ...O6w	0.88	1.86	2.662(2)	151
O83-H83 ...O81	0.88	2.17	2.644(3)	113
O84-H84 ...O8w[a]	0.82	2.15	2.852(2)	144
O84-H84 ...O86	0.82	2.15	2.600(2)	114
C15-H15 ...O62[b]	0.95	2.39	3.096(3)	131
C45-H45 ...O53	0.95	2.39	3.191(3)	142

Symmetry codes: a) x, -1+y, z; b) x, 1+y, z; c) 1+x, 1+y, 1+z

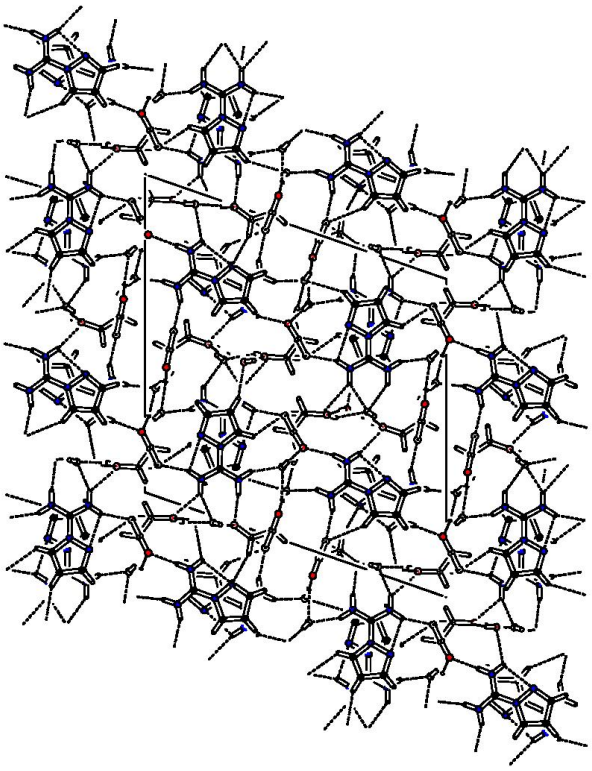

Figure 61: Crystal packing of **Hpcam-Htart·2H$_2$O** (projection to plane *ac*). Dashed lines indicate hydrogen bonds.

Vibrational spectra

FTIR and Raman spectra are depicted in Figure 62. The overall character of vibrational spectra is in agreement with crystal structure solution.

FTIR (cm^{-1}): ν_{max} 454 w, 501 m, 553 m, 600 m, 637 m, 688 sb, 708 s, 771 m, 785 m, 829 vw, 843 w, 875 vw, 893 w, 911 m, 937 m, 992 w, 1040 m, 1084 vs, 1136 vs, 1207 s, 1225 m, 1254 m, 1304 s, 1338 m, 1403 m, 1560 s, 1702 vs, 3150 s, 3331 sb, 3400 mb, 3454 mb.

Raman (cm^{-1}): ν_{max} 106 vs, 123 vs, 149 vs, 249 m, 276 m, 362 wb, 376 wb, 456 m, 469 m, 528 m, 595 wb, 640 w, 676 m, 696 m, 736 w, 763 m, 783 m, 845 vw, 885 m, 912 m, 937 s, 973 w, 991 w, 1037 m, 1084 s, 1120 m, 1208 m, 1228 m, 1266 w, 1308 s, 1331 m, 1394 s, 1404 s, 1532 s, 1546 m, 1706 m, 2916 m, 2967 vw, 3101 vw, 3126 m, 3147 m, 3313 wb.

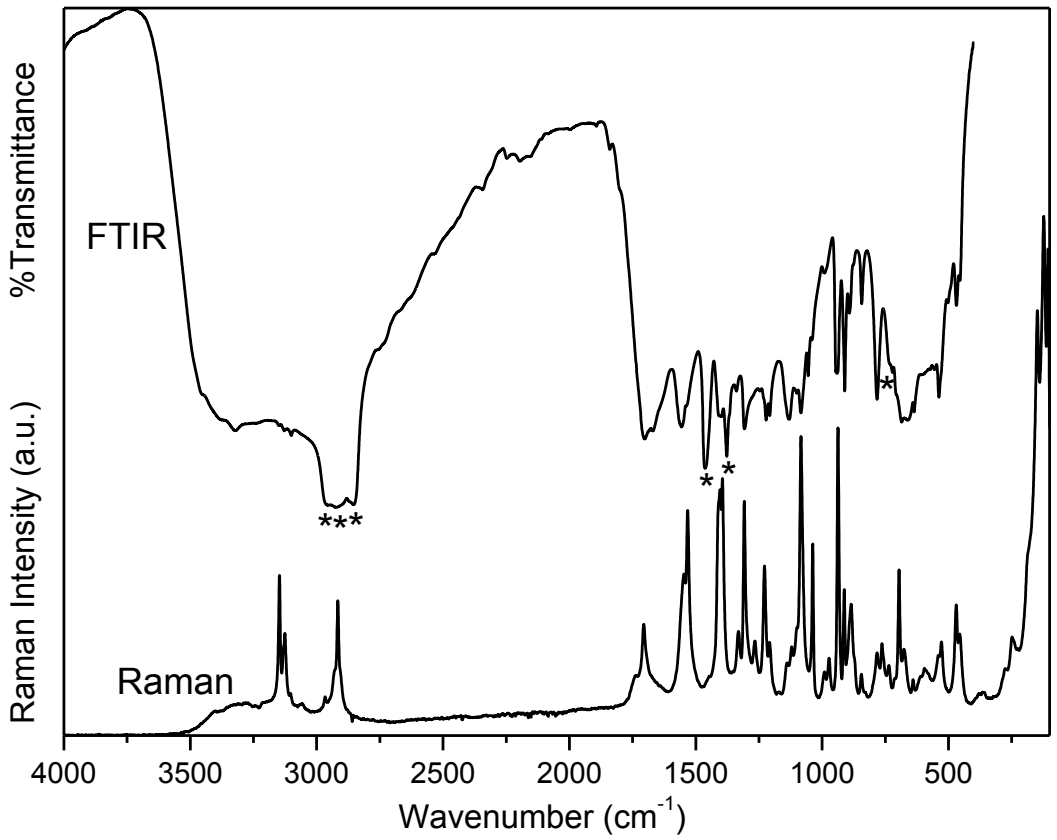

Figure 62: FTIR (nujol mull) and Raman spectra of **Hpcam-Htart·2H$_2$O**. Nujol bands are labelled by asterisk. Nujol bands are labelled by asterisk.

4.3.7 Summary for organic salts of 1*H*-pyrazole-carboxamidine

Carboxylic acids with different size, number of carboxyl groups and geometry were used as alternative crystallisation partners for target molecule.

The level of deprotonation of anions corresponds to the lengths of their CO bonds. Unfortunately, because of overlapping of the manifestations of carboxyl groups (ν (C=O) at ~1700 cm^{-1}) and carboxylate anions (ν_{as} (COO$^-$) at ~1600 cm^{-1} and ν_s (COO$^-$) at ~1400 cm^{-1}) with the vibrational modes of cations, vibrational spectra does not confirm presence of carboxylate or carboxyl group in solved crystal structures.[41]

The rigid planar conformation of target cation was not deformed in any of the prepared crystals. Bond angles and distances of cations are almost similar in all of these salts and adducts (Electronic Supplement ES9 – ES14) and they differ only slightly from the calculated values of **Hpcam^{1+}** cation (Table S5, Supplement).

Centrosymmetric pairs of cations were formed only in **HpcamCl-form·H_2O** crystal with the smallest anions out of all of these organic salts and adducts.

In total, six organic salts of target molecule were described and two of them utilising chiral anions – **Hpcam malic** and **Hpcam-Htart·$2H_2O$**, crystallise in non-centrosymmetric space groups.

4.4 Second harmonic generation

Second harmonic generation efficiency was measured for two prepared salts which crystallise in non-centrosymmetric space groups – **Hpcam-Hmalic** and **Hpcam-Htart·$2H_2O$**. Powder samples of both of these salts were separated according to the size of their particles and their averaged intensity of SHG efficiency were compared to KDP standard. Fraction with 100 – 125 μm particle size of **Hpcam-Htart·$2H_2O$** salt has not been successfully prepared. Results for all of the fractions for both salts are listed in Table 28. Unfortunately, no significant conclusions concerning phase matching conditions could be done with this limited set of results.

Table 28: Relative SHG efficiency for **Hpcam-Hmalic** and **Hpcam-Htart·$2H_2O$** powder samples with different size of particles.

	Relative SHG efficiency	
Size of particles (μm)	**Hpcam-Hmalic**	**Hpcam-Htart·$2H_2O$**
100 - 125	0.05 KDP	-
125 - 150	0.07 KDP	0.01 KDP
150 -	0.06 KDP	0.07 KDP

5 Conclusions

This diploma thesis was focused on preparation and characterisation of novel compounds of 1*H*-pyrazole-carboxamidine as a potential molecule for application in nonlinear optics. Especially, ability of second harmonic generation was a target property.

For a prediction of nonlinear properties and for calculation of vibrational frequencies of the target molecule quantum-chemical calculations were used. Band assignment according to the calculated spectra was optimised using four different approaches to the quantum-chemical calculation. The comparison of measured spectra of inorganic salts with all four results of calculated vibrational spectra indicates that the best matching results are gained by model of an isolated molecule **Hpcam**$^{1+}$ in vacuum using Gaussian09W[23] software (B3LYP/6-311++G(d,p) and by using solid state calculation using CRYSTAL software[25-26].

In total, fourteen crystalline salts of target molecule were prepared and described. They were characterised mainly by X-ray diffraction methods and by vibrational spectroscopy. The protonation status of ions in a set of inorganic salts was confirmed also by the methods of vibrational spectroscopy.

The alternative crystallisation partners should avoid formation of centrosymmetric pairs of cations. Nevertheless, in the **HpcamCl·H$_2$O**, **HpcamNO$_3$ (I)** and **(II)**, **HpcamCH$_3$SO$_3$**, **HpcamNH$_2$SO$_3$** and **HpcamCl-form·H$_2$O** salts these pairs were formed. Prepared salts crystallised in non-centrosymmetric space groups only when chiral dicarboxylic acids were used.

Two of the prepared salts exhibiting non-centrosymmetric arrangement (**Hpcam-Hmalic**, **Hpcam-Htart·2H$_2$O**) were examined for second harmonic generation efficiency. Their maximal SHG efficiency compared to the standard KDP (7 %) indicates only limited application in the field of second order nonlinear optics.

6 List of abbreviations

B3LYP	Becke, three parameter, Lee-Yang-Parr method
CCD	Charge-coupled device
CSD	The Cambridge Structural Database
DFG	Difference frequency generation
DFT	Density functional theory
DRIFTS	Diffuse reflectance infrared Fourier transform spectroscopy
FTIR	Fourier transform infrared spectroscopy
IR	Infrared
KDP	Potassium dihydrogen phosphate
KTP	Potassium titanyl phosphate
NLO	Nonlinear optics
pcam	1*H*-Pyrazole-carboxamidine
RA	Raman
SFG	Sum frequency generation
SHG	Second harmonic generation
UV	Ultraviolet

7 Supplement

Quantum-chemical calculations

Table S1: Calculated values of dipole moment, polarizability and the first hyperpolarizability components for uncharged molecule **pcam** (B3LYP/6-311++G(d,p)).

Dipole moment	μ_x (a.u.) 0.5370	μ_y (a.u.) 1.2831	μ_z (a.u.) 0.2771	**μ (Debye)** **3.6050**
Polarizability (esu)	α_{xx} $1.48\cdot10^{-23}$	α_{xy} $5.85\cdot10^{-25}$	α_{yy} $1.23\cdot10^{-23}$	α_{xz} $1.11\cdot10^{-25}$
	α_{yz} $-1.48\cdot10^{-26}$	α_{zz} $7.17\cdot10^{-24}$		
Hyperpolarizability (esu)	β_{xxx} $-1.65\cdot10^{-30}$	β_{xxy} $-7.02\cdot10^{-34}$	β_{xyy} $6.35\cdot10^{-31}$	β_{yyy} $1.93\cdot10^{-31}$
	β_{xxz} $-4.81\cdot10^{-32}$	β_{xyz} $6.93\cdot10^{-32}$	β_{yyz} $4.61\cdot10^{-32}$	β_{xzz} $3.40\cdot10^{-31}$
	β_{yzz} $3.10\cdot10^{-31}$	β_{zzz} $9.06\cdot10^{-33}$	**$\beta_{tot} = 8.38\cdot10^{-31}$**	

Note: $\beta_{tot} = [(\beta_{xxx} + \beta_{xyy} + \beta_{xzz})^2 + (\beta_{yyy} + \beta_{yzz} + \beta_{yxx})^2 + (\beta_{zzz} + \beta_{zxx} + \beta_{zyy})^2]^{1/2}$
(998.30 a.u. = $8.62\cdot10^{-30}$ esu).

Table S2: Calculated values of dipole moment, polarizability and the first hyperpolarizability components for **Hpcam^{1+}** (B3LYP/6-311++G(d.p)).

Dipole moment	μ_x (a.u.) -1.7757	μ_y (a.u.) 0.7466	μ_z (a.u.) 0.0092	**μ (Debye)** **4.8961**
Polarizability (esu)	α_{xx} $1.48\cdot10^{-23}$	α_{xy} $-1.14\cdot10^{-25}$	α_{yy} $1.11\cdot10^{-23}$	α_{xz} $7.57\cdot10^{-27}$
	α_{yz} $-7.60\cdot10^{-27}$	α_{zz} $5.90\cdot10^{-24}$		
Hyperpolarizability (esu)	β_{xxx} $-3.05\cdot10^{-30}$	β_{xxy} $-1.02\cdot10^{-32}$	β_{xyy} $1.02\cdot10^{-30}$	β_{yyy} $5.58\cdot10^{-32}$
	β_{xxz} $-1.56\cdot10^{-32}$	β_{xyz} $3.05\cdot10^{-32}$	β_{yyz} $1.12\cdot10^{-32}$	β_{xzz} $1.21\cdot10^{-31}$
	β_{yzz} $1.22\cdot10^{-31}$	β_{zzz} $-1.11\cdot10^{-33}$	**$\beta_{tot} = 1.91\cdot10^{-30}$**	

Table S3: Calculated values of dipole moment, polarizability and the first hyperpolarizability components for **H_2pcam^{2+}** (B3LYP/6-311++G(d.p)).

Dipole moment	μ_x (a.u.) -1.24062	μ_y (a.u.) -0.389256	μ_z (a.u.) 0.160994	**μ (Debye)** **3.3301**
Polarizability (esu)	α_{xx} $1.32\cdot10^{-23}$	α_{xy} $-2.96\cdot10^{-25}$	α_{yy} $1.04\cdot10^{-23}$	α_{xz} $-2.73\cdot10^{-26}$
	α_{yz} $-5.57\cdot10^{-26}$	α_{zz} $6.18\cdot10^{-24}$		
Hyperpolarizability (esu)	β_{xxx} $-2.50\cdot10^{-30}$	β_{xxy} $1.84\cdot10^{-31}$	β_{xyy} $6.01\cdot10^{-31}$	β_{yyy} $-2.34\cdot10^{-31}$
	β_{xxz} $-1.45\cdot10^{-31}$	β_{xyz} $1.64\cdot10^{-31}$	β_{yyz} $1.47\cdot10^{-31}$	β_{xzz} $1.43\cdot10^{-31}$
	β_{yzz} $-8.41\cdot10^{-33}$	β_{zzz} $-9.23\cdot10^{-33}$	**$\beta_{tot} = 1.75\cdot10^{-30}$**	

Table S4: Bond lenghts *d* and angles in optimised **Hpcam**$^{1+}$ cation (B3LYP/6-311++G(d.p)).

Bond	*d* (Å)	Angle	Value (°)
N(1)-N(2)	1.379	N(1)-N(2)-C(3)	104.7
N(1)-C(5)	1.392	N(2)- N(1)-C(5)	111.4
N(1)-C(6)	1.370	N(2)- N(1)-C(6)	117.7
N(2)-C(3)	1.310	C(5)- N(1)-C(6)	130.9
C(3)-C(4)	1.431	N(1)-C(5)-C(4)	106.3
C(4)-C(5)	1.359	C(3)-C(4)- C(5)	105.4
C(6)-N(7)	1.320	N(2)-C(3)-C(4)	112.2
C(6)-N(8)	1.330	N(1)-C(6)-N(8)	120.1
		N(1)-C(6)-N(7)	117.3
		N(7)-C(6)-N(8)	122.6

Single crystal X-Ray analysis data

Table S5: Basic crystallographic data and structure refinement details for inorganic salts of **pcam** (diffractometer Bruker D8 VENTURE Kappa Duo PHOTON100, MoKα radiation, λ = 0.71073 Å; T = 150.(2) K).

Identification code	**HpcamCl·H_2O**	**HpcamClO_4**	**HpcamH_2PO_4**	**HpcamHSO_4**
Empirical formula	$C_4H_9ClN_4O$	$C_4H_7ClN_4O_4$	$C_4H_9N_4O_4P$	$C_4H_8N_4O_4S$
Formula weight	164.60	210.59	208.12	208.20
Crystal system	triclinic	monoclinic	monoclinic	monoclinic
Space group	*P*-1	$P2_1/c$	$P2_1/c$	$P2_1/c$
a (Å)	4.8570(3)	5.2966(4)	11.5165(10)	10.6099(4)
b (Å)	8.9691(5)	10.3591(7)	10.1394(10)	9.6426(4)
c (Å)	9.3193(5)	14.2107(9)	7.9577(9)	8.0594(4)
α (°)	68.994(3)	90	90	90
β (°)	88.271(3)	94.725(3)	108.697(4)	95.334(2)
γ (°)	82.112(3)	90	90	90
U (Å^3)	375.33(4)	777.06(9)	880.19(15)	820.96(6)
Z	2	4	4	4
Calculated density (g/cm^3)	1.457	1.800	1.571	1.684
Absorption coefficient (mm^{-1})	0.448	0.482	0.304	0.386
F(000)	172	432	432	432
Crystal size (mm)	0.12 x 0.20 x 0.65	0.11 x 0.16 x 0.28	0.09 x 0.12 x 0.29	0.07 x 0.15 x 0.16
Completeness to θ	99.3 %	99.8 %	99.9 %	99.8 %
Range of *h*, *k*, *l*	-6→5; -11→11; -12→10	-6→6; -12→13; -17→18	-14→14; -11→13; -10→10	-13→13; -12→12; -10→10
θ range for data collection (°)	2.34 - 27.50	2.44 - 27.53	2.74 - 27.51	2.86 - 27.52
Reflection collected/unique (R_{int})	5219/1723 (0.027)	8930/1783 (0.039)	10186/2023 (0.041)	19929/1891 (0.029)
No. of observed reflection	1407	1637	1708	1720
Criterion for observed reflection	$I > 2\sigma(I)$			
Absorption correction	multi-scan			
Funcion minimised	$\sum w(F_0^2 - F_c^2)^2$			
Parameters refined	91	118	134	118
R, wR ($I > 2\sigma(I)$)	0.0338; 0.0696	0.0506; 0.1125	0.0342; 0.0847	0.0283; 0.0734
R', *wR*'(all data)	0.0468; 0.0729	0.0550; 0.1138	0.0447; 0.0900	0.0322; 0.0757
Value of *S*	1.065	1.254	1.074	1.078
Max. and min. heights in final $\Delta\rho$ map (e/Å^3)	-0.275; 0.232	-0.751; 0.304	-0.498; 0.239	-0.507; 0.182
Weighting scheme	$w = 1/[\sigma^2(F_0^2) + (aP)^2 + bP]; P = (F_0^2 + 2F_c^2)/3$			
	a = 0.0295	*a* = 0.0002	*a* = 0.0416	*a* = 0.0340
	b = 0.0636	*b* = 1.8920	*b* = 0.4771	*b* = 0.7134
Programs used	SAINT[29], SHELX[32], PLATON[30]			

Table S6: Basic crystallographic data and structure refinement details for inorganic salts of **pcam** (diffractometer Bruker D8 VENTURE Kappa Duo PHOTON100, MoKα radiation, λ = 0.71073 Å).

Identification code	**HpcamCH$_3$SO$_3$**	**HpcamNH$_2$SO$_3$**	**HpcamNO$_3$ (I)**	**HpcamNO$_3$ (II)**
Empirical formula	$C_5H_{10}N_4O_3S$	$C_4H_9N_5O_3S$	$C_4H_7N_5O_3$	$C_4H_7N_5O_3$
Formula weight	206.23	207.22	173.15	173.15
Crystal system	monoclinic	monoclinic	monoclinic	monoclinic
Space group	$P2_1/n$	$P2_1/c$	$P2_1/n$	$P2_1/c$
a (Å)	11.6938(2)	5.0121(2)	3.6250(2)	5.1311(3)
b (Å)	5.09170(10)	17.6984(8)	12.1660(6)	10.2457(5)
c (Å)	15.1524(3)	9.5198(4)	16.3005(8)	13.8846(8)
α (°)	90	90	90	90
β (°)	103.4630(10)	92.537(2)	92.119(2)	99.681
γ (°)	90	90	90	90
U (Å^3)	877.40(3)	843.64(6)	718.39(6)	719.54(7)
Z	4	4	4	4
Temperature (K)	150.(2)	150.(2)	150.(2)	220.(2)
Calculated density (g/cm^3)	1.561	1.632	1.601	1.598
Absorption coefficient (mm^{-1})	0.352	0.369	0.121	0.137
F(000)	432	432	360	360
Crystal size (mm)	0.09 x 0.25 x 0.83	0.13 x 0.18 x 0.85	0.06 x 0.09 x 0.37	0.50 x 1.09 x 2.10
Completeness to θ	99.5 %	100.0 %	99.6 %	94.8 %
Range of h, k, l	-15→9; -5→6; -18→19	-6→6; -23→23; -12→12	-4→4; -14→15; -21→20	-6→5; -12→9; -15→17
θ range for data collection (°)	1.99 - 27.48	2.30 - 27.52	2.50 - 27.53	2.48 - 26.97
Reflection collected/unique (R_{int})	6683/2010 (0.020)	6953/1953 (0.020)	8480/1651 (0.033)	4233/1484 (0.014)
No. of observed reflection	1805	1794	1386	1344
Criterion for observed reflection	$I > 2\sigma(I)$			
Absorption correction	multi-scan			
Funcion minimised	$\sum w(F_0^2 - F_c^2)^2$			
Parameters refined	119	118	125	109
R, wR ($I > 2\sigma(I)$)	0.0289; 0.0749	0.0282; 0.0733	0.0366; 0.1194	0.0333; 0.0927
R', wR'(all data)	0.0330; 0.0778	0.0310; 0.0751	0.0480; 0.1296	0.0364; 0.0952
Value of S	1.066	1.055	1.042	1.121
Max. and min. heights in final $\Delta\rho$ map (e/Å^3)	-0.423; 0.320	-0.484; 0.283	-0.274; 0.291	-0.210; 0.162
Weighting scheme	$w = 1/[\sigma^2(F_0^2) + (aP)^2 + bP]$; $P = (F_0^2 + 2F_c^2)/3$			
	a = 0.0347 b = 0.5908	a = 0.0371 b = 0.5165	a = 0.1000 b = 0	a = 0.0497 b = 0.1388
Programs used	SAINT[29], SHELX[32], PLATON[30]			

Table S7: Basic crystallographic data and structure refinement details for salts of **pcam** with carboxylic acids (diffractometer Bruker D8 VENTURE Kappa Duo PHOTON100).

Identification code	**Hpcam-adip·H$_2$adip·H$_2$O**	**Hpcam-Hmalic**	**Hpcam-Htart·2H$_2$O**
Empirical formula	$C_{10}H_{18}N_4O_5$	$C_8H_{12}N_4O_5$	$C_8H_{16}N_4O_8$
Formula weight	274.28	244.22	296.25
Crystal system	monoclinic	triclinic	monoclinic
Space group	$P2_1/c$	$P1$	$P2_1$
a (Å)	9.1911(6)	5.1987(2)	19.3749(5)
b (Å)	15.6981(10)	10.2941(5)	7.2897(2)
c (Å)	9.0070(6)	10.3072(5)	19.4231(5)
α (°)	90	79.799(2)	90
β (°)	93.548(3)	77.200(2)	109.1840(10)
γ (°)	90	85.916(2)	90
U (Å^3)	1297.06(15)	529.10(4)	2590.93(12)
Z	4	2	8
Temperature (K)	150.(2)	150.(2)	120.(2)
Radiation λ (Å)	0.71073	0.71073	1.54178
Calculated density (g/cm^3)	1.405	1.533	1.519
Absorption coefficient (mm^{-1})	0.113	0.129	1.190
F(000)	584	256	1248
Crystal size (mm)	0.18 x 0.42 x 0.47	0.17 x 0.30 x 0.52	0.18 x 0.19 x 0.27
Completeness to θ	99.8 %	99.5 %	99.6 %
Range of h, k, l	-11→11; -20→14; -11→11	-6→6; -13→0; -13→12	-23→23; -8→9; -20→ 23
θ range for data collection (°)	2.22 - 27.50	2.01 - 27.71	2.41 - 72.46
Reflection collected/unique (R_{int})	10710/2966 (0.030)	2482/2482 (0.000)	34401/9957 (0.036)
No. of observed reflection	2342	2375	9302
Criterion for observed reflection	$I > 2\sigma(I)$		
Absorption correction	multi-scan		
Funcion minimised	$\sum w(F_0^2 - F_c^2)^2$		
Parameters refined	172	308	738
R, wR ($I > 2\sigma(I)$)	0.0393; 0.0946	0.0355; 0.0986	0.0305; 0.0756
R', wR'(all data)	0.0566; 0.1038	0.0378; 0.1009	0.0339; 0.0775
Value of S	1.046	1.007	1.047
Max. and min. heights in final $\Delta\rho$ map (e/Å^3)	-0.334 and 0.232	-0.280; 0.884	-0.245; 0.228
Weighting scheme	$w = 1/[\sigma^2(F_0^2) + (aP)^2 + bP]$; $P = (F_0^2 + 2F_c^2)/3$		
	a = 0.0471 b = 0.5250	a = 0.0664 b = 0.1921	a = 0.0378 b = 0.5006
Programs used	SAINT[29], SHELX[32], PLATON[30]		

Table S8: Basic crystallographic data and structure refinement details for organic salts of **pcam** (diffractometer Bruker D8 VENTURE Kappa Duo PHOTON100).

Identification code	**HpcamCl-form·H_2O**	**Hpcam-Hox**	**Hpcam-suc ·H_2suc**
Empirical formula	$C_9H_{17}ClN_8O_3$	$C_6H_8N_4O_4$	$C_{16}H_{24}N_8O_8$
Formula weight	320.76	200.16	456.43
Crystal system	triclinic	triclinic	triclinic
Space group	*P*-1	*P*-1	*P*-1
a (Å)	4.9172(5)	3.7237(2)	4.9078(2)
b (Å)	10.2475(14)	9.3312(4)	8.1789(4)
c (Å)	14.7737(17)	11.7149(5)	12.7533(6)
α (°)	100.540(6)	88.763(2)	79.563(2)
β (°)	94.883(7)	81.767(2)	80.811(2)
γ (°)	97.723(6)	88.381(2)	83.888(2)
U (Å^3)	720.62(15)	402.63(3)	495.40(4)
Z	2	2	1
Temperature	120.(2)	150.(2)	120.(2)
Radiation λ (Å)	0.71073	0.71073	1.54178
Calculated density (g/cm^3)	1.478	1.651	1.530
Absorption coefficient (mm^{-1})	0.290	0.140	1.064
F(000)	336	208	240
Crystal size (mm)	0.06 x 0.17 x 0.41	0.04 x 0.13 x 0.34	0.03 x 0.09 x 0.52
Completeness to *θ*	99.5 %	99.7 %	98.6 %
Range of *h*, *k*, *l*	-5→6; -12→12; -18→18	-4→4; -12→12; -15→15	-6→5 ; -10→10; -15→15
θ range for data collection (°)	1.41 - 26.05	2.18 - 27.52	3.56 - 72.19
	2814	1843	1916
Reflection collected/unique (R_{int})	7830/2814 (0.063)	9824/1843 (0.026)	8228/1916 (0.028)
No. of observed reflection	1893	1592	1753
Criterion for observed reflection	$I > 2\sigma(I)$		
Absorption correction	multi-scan		
Funcion minimised	$\sum w(F_0^2 - F_c^2)^2$		
Parameters refined	190	131	145
R, wR ($I > 2\sigma(I)$)	0.0520; 0.1063	0.0345; 0.0902	0.0338; 0.0854
R', *wR*'(all data)	0.0923; 0.1212	0.0415; 0.0950	0.0373; 0.0881
Value of *S*	1.006	1.048	1.056
Max. and min. heights in final $\Delta\rho$ map (e/Å^3)	-0.358; 0.342	-0.305; 0.340	-0.337; 0.300
Weighting scheme	$w = 1/[\sigma^2(F_0^2) + (aP)^2 + bP]; P = (F_0^2 + 2F_c^2)/3$		
	a = 0.0514	*a* = 0.0497	*a* = 0.0414
	b = 0.1627	*b* = 0.1732	*b* = 0.2466
Programs used	SAINT[29], SHELX[32], PLATON[30]		

Powder X-Ray diffraction data

Table S9: Diffraction maxima and d-spacing for **HpcamCl·H_2O**.

2θ (°)	d-spacing (Å)	Rel. Int. (%)	2θ (°)	d-spacing (Å)	Rel. Int. (%)
10.1525	8.71298	22.78	26.1671	3.40562	4.17
17.2224	5.14889	4.16	26.8608	3.31923	13.78
18.3875	4.82519	2.58	27.5695	3.23549	7.37
19.2030	4.62207	2.82	28.1029	3.17528	100.00
20.3088	4.37283	39.03	30.2495	2.95467	6.27
20.9245	4.24553	3.47	30.6431	2.91761	20.42
22.5291	3.94665	3.95	31.1645	2.86998	3.87
23.4552	3.79288	11.37	31.7068	2.82212	2.80
25.1179	3.54544	11.62	36.1130	2.48726	12.69
25.7205	3.46374	3.32	42.1116	2.14580	2.39

Table S10: Diffraction maxima and d-spacing for **HpcamClO_4**.

2θ (°)	d-spacing (Å)	Rel. Int. (%)	2θ (°)	d-spacing (Å)	Rel. Int. (%)
18.1763	4.88077	26.82	26.4767	3.36650	9.41
18.6531	4.75708	4.97	27.1337	3.28646	99.60
19.3232	4.59360	45.15	28.6059	3.12059	20.82
20.4612	4.34062	5.78	29.0045	3.07860	2.78
21.3191	4.16783	15.33	29.6731	3.01073	8.06
21.7774	4.08116	13.07	30.2493	2.95469	6.14
22.9994	3.86701	40.65	30.8267	2.90065	47.61
23.7303	3.74953	2.65	39.1339	2.30194	4.17
24.7783	3.59327	100.00	42.2516	2.13901	2.45
25.2751	3.52376	8.37	49.2480	1.85027	4.16

Table S11: Diffraction maxima and d-spacing for **HpcamNO_3 (I)**.

2θ (°)	d-spacing (Å)	Rel. Int. (%)	2θ (°)	d-spacing (Å)	Rel. Int. (%)
10.8074	8.18640	13.74	26.8938	3.31522	6.83
17.3418	5.11372	6.61	27.2451	3.27327	35.61
17.5738	5.04672	20.65	28.5495	3.12662	100.00
18.5014	4.79575	35.49	29.1963	3.05881	3.82
19.5926	4.53104	94.19	29.4865	3.02937	5.94
21.6123	4.11196	29.77	31.6040	2.83106	9.71
24.7638	3.59534	5.68	32.6202	2.74515	7.12
25.2356	3.52919	13.64	33.5475	2.67137	5.05
25.8062	3.45242	19.93	38.3435	2.34755	4.58
26.3817	3.37841	8.60	39.7059	2.27008	3.96

Table S12: Diffraction maxima and d-spacing for **HpcamNO_3 (II)**.

2θ (°)	d-spacing (Å)	Rel. Int. (%)	2θ (°)	d-spacing (Å)	Rel. Int. (%)
10.8009	8.19133	8.81	26.8871	3.31604	5.97
17.3397	5.11433	4.59	27.2482	3.27291	33.05
17.5712	5.04748	13.81	28.5502	3.12655	100.00
18.5009	4.79587	25.49	29.4675	3.03127	5.59
19.6019	4.52890	64.15	31.6097	2.83056	8.11
21.6133	4.11176	21.75	32.6346	2.74397	6.61
24.7532	3.59686	4.23	33.5702	2.66961	4.42
25.2046	3.53345	11.52	35.4811	2.53009	3.16
25.8049	3.45259	18.18	38.3916	2.34472	4.18
26.3917	3.37715	6.96	39.7008	2.27036	3.54

Table S13: Diffraction maxima and d-spacing for **HpcamH$_2$PO$_4$**.

2θ (°)	d-spacing (Å)	Rel. Int. (%)	2θ (°)	d-spacing (Å)	Rel. Int. (%)
8.0604	10.96914	12.01	25.1437	3.54187	12.20
10.1477	8.71708	10.39	25.4013	3.50654	29.41
16.1065	5.50303	52.29	26.8316	3.32278	12.71
17.5780	5.04553	35.08	27.7296	3.21717	8.43
18.4203	4.81666	37.60	28.0949	3.17617	100.00
18.7536	4.73182	9.79	29.2438	3.05395	14.53
20.3459	4.36495	29.61	30.6654	2.91554	19.39
23.4401	3.79530	10.30	32.5767	2.74872	9.44
24.2407	3.66868	34.13	36.1259	2.48434	44.77
24.3206	3.65984	48.32	36.2229	2.48407	25.99

Table S14: Diffraction maxima and d-spacing for **HpcamHSO$_4$**.

2θ (°)	d-spacing (Å)	Rel. Int. (%)	2θ (°)	d-spacing (Å)	Rel. Int. (%)
8.3831	10.54756	30.81	25.8061	3.45244	78.44
16.7168	5.30345	100.00	26.6193	3.34879	9.85
18.4426	4.81090	93.48	26.7662	3.33075	14.56
19.0892	4.64936	45.82	27.7662	3.21302	14.74
21.4755	4.13783	17.03	28.6211	3.11896	27.24
23.3453	3.81049	37.91	29.7027	3.00780	30.63
24.0810	3.69571	31.82	32.5562	2.75040	7.38
24.7151	3.60231	13.75	33.6624	2.66251	12.97
24.9167	3.57363	19.40	34.2637	2.61715	7.86
25.1193	3.54525	39.70	34.7947	2.57841	9.40

Table S15: Diffraction maxima and d-spacing for **HpcamCH$_3$SO$_3$**.

2θ (°)	d-spacing (Å)	Rel. Int. (%)	2θ (°)	d-spacing (Å)	Rel. Int. (%)
8.6974	10.16720	12.74	24.0172	3.70539	27.25
15.5281	5.70668	15.37	25.0496	3.55497	32.32
17.3569	5.10929	100.00	25.4243	3.50342	10.46
18.3364	4.83853	15.14	26.1136	3.41248	22.61
19.3878	4.57843	8.08	27.4619	3.24793	20.09
21.0889	4.21281	6.64	29.5102	3.02699	15.39
21.5485	4.12399	10.55	29.7611	3.00203	6.18
21.7249	4.09089	5.22	33.8395	2.64898	4.68
22.7854	3.90283	5.85	39.3135	2.29183	7.53
23.4641	3.79146	4.80	42.6150	2.12161	4.94

Table S16: Diffraction maxima and d-spacing for **HpcamNH$_2$SO$_3$**.

2θ (°)	d-spacing (Å)	Rel. Int. (%)	2θ (°)	d-spacing (Å)	Rel. Int. (%)
10.1584	8.70795	23.67	24.6476	3.61203	23.97
17.6827	5.01589	22.01	25.3043	3.51976	50.36
19.2985	4.59942	46.32	26.4976	3.36389	63.39
20.3568	4.36263	96.08	26.8086	3.32557	87.27
21.1614	4.19855	56.36	28.1077	3.17475	100.00
22.0604	4.02943	28.56	28.3898	3.14385	30.93
22.2449	3.99642	31.33	30.3078	2.94912	24.22
23.4543	3.79303	24.30	30.6314	2.91870	22.09
23.9728	3.71215	77.35	32.8362	2.72759	24.58
24.1604	3.68375	26.28	36.1303	2.48611	28.27

Table S17: Diffraction maxima and d-spacing for **Hpcam-adip·H$_2$adip·H$_2$O**.

2θ (°)	d-spacing (Å)	Rel. Int. (%)	2θ (°)	d-spacing (Å)	Rel. Int. (%)
9.6460	9.16931	1.26	22.1787	4.00490	1.05
11.2771	7.84649	1.64	23.0909	3.84870	0.98
14.2853	6.20022	3.09	23.8855	3.72244	3.38
14.8691	5.95809	1.59	25.2426	3.52530	1.96
19.5403	4.54305	4.21	25.8036	3.44992	1.72
20.1628	4.40051	4.36	26.3584	3.37854	100.00
20.2445	4.39384	4.19	26.9746	3.30274	2.86
20.9954	4.22786	1.40	28.7345	3.10434	2.78
21.4783	4.13388	2.03	33.8827	2.64351	1.25
21.6788	4.09610	2.03	54.1912	1.69119	0.99

Table S18: Diffraction maxima and d-spacing for **HpcamCl-form·H$_2$O**.

2θ (°)	d-spacing (Å)	Rel. Int. (%)	2θ (°)	d-spacing (Å)	Rel. Int. (%)
9.7240	9.09592	30.24	25.9523	3.43333	17.89
17.6455	5.02637	8.02	26.7900	3.32784	9.15
18.2744	4.85481	20.57	26.9773	3.30515	18.87
19.4629	4.56093	18.39	27.5104	3.24231	5.23
20.1298	4.41130	7.45	28.4678	3.13541	100.00
20.5325	4.32569	8.20	29.3337	3.04479	8.71
21.4462	4.14343	3.26	29.9716	2.98143	4.49
21.7389	4.08830	3.66	31.7029	2.82245	3.54
23.2616	3.82400	3.74	32.5777	2.74864	3.23
24.2577	3.66920	9.99	37.0529	2.42630	4.33

Table S19: Diffraction maxima and d-spacing for **Hpcam-Hmalic**.

2θ (°)	d-spacing (Å)	Rel. Int. (%)	2θ (°)	d-spacing (Å)	Rel. Int. (%)
8.7152	10.14637	5.29	24.7923	3.59128	3.55
13.5654	6.52759	6.50	25.4494	3.50002	3.10
17.3449	5.11282	14.51	26.0578	3.41967	7.67
17.7781	4.98505	12.43	26.5695	3.35496	100.00
17.8525	4.96855	12.33	28.0083	3.18579	2.46
19.3074	4.59733	4.90	29.4227	3.03579	5.91
20.9414	4.24215	6.52	29.8635	2.99197	2.65
21.1638	4.19806	8.95	31.0041	2.88446	6.10
22.2866	3.98904	7.83	34.9015	2.57077	3.99
22.6141	3.93201	9.54	37.8392	2.37767	1.92

Table S20: Diffraction maxima and d-spacing for **Hpcam-Hox**.

2θ (°)	d-spacing (Å)	Rel. Int. (%)	2θ (°)	d-spacing (Å)	Rel. Int. (%)
7.6752	11.51882	22.26	25.4322	3.50234	3.31
15.3623	5.76789	100.00	27.6283	3.22875	6.48
17.8607	4.96631	4.42	28.1817	3.16658	37.27
18.3023	4.84746	3.84	29.0590	3.07295	3.30
18.7628	4.72951	2.73	30.9478	2.88958	20.87
19.0387	4.66158	12.55	32.1693	2.78259	2.91
23.1010	3.85023	1.87	32.6562	2.74221	3.80
24.2208	3.67471	2.54	37.0672	2.42539	2.45
24.7845	3.59238	2.99	38.9470	2.31064	20.66
25.2814	3.52289	3.67	39.0396	2.31110	14.16

Table S21: Diffraction maxima and d-spacing for **Hpcam-suc·H_2suc**.

2θ (°)	d-spacing (Å)	Rel. Int. (%)	2θ (°)	d-spacing (Å)	Rel. Int. (%)
10.1665	8.70104	14.35	25.1328	3.54338	6.77
12.1424	7.28921	3.95	25.6056	3.47901	5.99
19.2709	4.60594	12.88	26.3145	3.38688	88.23
20.0959	4.41869	100.00	26.8164	3.32462	24.14
20.3182	4.37083	18.23	27.1885	3.27996	12.89
22.0203	4.03668	10.58	27.7464	3.21527	32.63
22.3343	3.98064	7.21	28.1063	3.17491	27.16
22.5500	3.94304	4.14	30.6149	2.92023	5.31
23.4526	3.79329	5.60	31.5752	2.83358	20.46
24.3651	3.65326	3.82	36.1416	2.48536	5.12

Table S22: Diffraction maxima and d-spacing for **Hpcam-Htart·2H_2O**.

2θ (°)	d-spacing (Å)	Rel. Int. (%)	2θ (°)	d-spacing (Å)	Rel. Int. (%)
13.8122	6.41150	29.63	24.2176	3.67518	30.89
15.6663	5.65665	30.47	24.4272	3.64411	46.83
16.6294	5.33116	60.44	26.3048	3.38811	52.80
18.6433	4.75957	89.48	26.9506	3.30837	37.82
19.3042	4.59426	45.51	27.5269	3.24041	21.62
19.3868	4.57866	40.34	28.9322	3.08613	33.41
20.8125	4.26812	23.55	32.7296	2.73623	27.81
22.6337	3.92865	32.75	32.9564	2.71792	32.00
23.0516	3.85837	100.00	33.8768	2.64615	23.14
23.2195	3.83084	76.63	35.9415	2.49873	17.50

8 References

1. Maiman, T. H., Optical maser action in ruby. *British Communications and Electronics* **1960,** *7*, 674-675.
2. Träger, F., *Springer Handbook of Lasers and Optics*. Springer-Verlag Berlin and Heidelberg GmbH & Co. KG: 2007.
3. Boyd, R. W., *Nonlinear optics*. 2 ed.; Academic press: 2003.
4. Matulková, I.; Němec, I.; Němec, P., Materiály pro generování druhé harmonické frekvence. *Československý časopis pro fyziku* **2011,** *61* (2), 76-84.
5. Kaiser Optical Systems, I. Raman Spectroscopy - A Tutorial. http://www.kosi.com/na_en/products/raman-spectroscopy/raman-technical-resources/raman-tutorial.php (accessed 1.5.2018).
6. Le Ru, E.; Etchegoin, P., *Principles of Surface-Enhanced Raman Spectroscopy: and Related Plasmonic Effects*. Elsevier Science: 2008; p 688.
7. Franken, P. A.; Hill, A. E.; Peters, C. W.; Weinreich, G., Generation of optical harmonics. *Phys. Rev. Letters* **1961,** *7* (4), 118-120.
8. Prasad, P. N.; Williams, D. J., *Introduction to Nonlinear Optical Effects in Molecules and Polymers*. John Wiley & Sons, Inc.: New York, USA, 1991.
9. Frequency Doubling. https://www.rp-photonics.com/frequency_doubling.html (accessed 1.5.2018).
10. Campagnola, P. J.; Clark, H. A.; Mohler, W. A.; Lewis, A.; Loew, L. M., Second-harmonic imaging microscopy of living cells. *J. Biomed. Opt.* **2001,** *6* (3), 277-286.
11. Tilbury, K.; Campagnola, P. J., Applications of Second-Harmonic Generation Imaging Microscopy in Ovarian and Breast Cancer. *Perspect. Med. Chem.* **2015,** *7*, 21–32.
12. Freund, I.; Deutsch, M.; Sprecher, A., Connective tissue polarity. Optical second-harmonic microscopy, crossed-beam summation, and small-angle scattering in rat-tail tendon. *Biophys. J.* **1986,** *50* (4), 693-712.
13. Aakeroy, C. B.; Hitchcock, P. B.; Moyle, B. D.; Seddon, K. R., A novel class of salts for second harmonic generation. *J. Chem. Soc., Chem. Commun.* **1989,** (23), 1856-9.
14. Xue, D.; Zhang, S., Chemical Bond Analysis of Nonlinearity of Urea Crystal. *J. Phys. Chem. A* **1997,** *101* (30), 5547-5550.
15. Groom, C. R.; Bruno, I. J.; Lightfoot, M. P.; Ward, S. C., The Cambridge Structural Database. *Acta Cryst.* **2016,** *B72*, 171-179.
16. Zhang, Y.; Fu, Z.; Luo, M.; Li, J.; Chen, S. Preparation of 1,2,5-oxadiazole-3-carboximidamide compounds useful as IDO1 inhibitors. WO 2018024208 (A1) — 2018-02-08, 2018.
17. Purohit, A.; Benites, P.; Cheesman, E. H.; Lazewatsky, J.; Lee, V.; Cesati, R. R. I.; Looby, R.; Radeke, H. S. Preparation of guanidinomethylphenoxypropylsulfonate derivatives and analogs for use as imaging agents and precursors. WO2011143360 (A2) 2011-11-17 2011.
18. Hagras, M.; Mohammad, H.; Mandour, M. S.; Hegazy, Y. A.; Ghiaty, A.; Seleem, M. N.; Mayhoub, A. S., Investigating the Antibacterial Activity of Biphenylthiazoles against Methicillin- and Vancomycin-Resistant Staphylococcus aureus (MRSA and VRSA). *J. Med. Chem.* **2017,** *60* (9), 4074-4085.
19. Bredereck, H.; Effenberger, F.; Hajek, M., Syntheses of s-Triazine and Substituted s-Triazines. *Angew. Chem. Int. Ed. Engl.* **1963,** *2* (11), 655–659.
20. Bernatowicz, M. S.; Wu, Y.; Matsueda, G. R., 1H-Pyrazole-1-carboxamidine hydrochloride an attractive reagent for guanylation of amines and its application to peptide synthesis. *J. Org. Chem.* **1992,** *57* (8), 2497-2502.

21. Bakka, T. A.; Gautun, O. R., Simple generalized reaction conditions for the conversion of primary aliphatic amines to surfactant-like guanidine salts with 1H-pyrazole carboxamidine hydrochloride. *Synth. Commun.* **2017,** *47* (2), 169-172.
22. Zhao, J.; Jin, B.; Peng, R.; Liu, Q.; Tan, B.; Chu, S., Synthesis and characterization of a new energetic salt 1H-pyrazole-1-carboxamidine dinitramide and its thermal properties. *J. Therm. Anal. Calorim.* **2016,** *124* (3), 1431-1439.
23. Frisch, M. J.; Trucks, G. W.; Schlegel, H. B.; Scuseria, G. E.; Robb, M. A.; Cheeseman, J. R.; Scalmani, G.; Barone, V.; Petersson, G. A.; Nakatsuji, H.; Li, X.; Caricato, M.; Marenich, A.; Bloino, J.; Janesko, B. G.; Gomperts, R.; Mennucci, B.; Hratchian, H. P.; Ortiz, J. V.; Izmaylov, A. F.; Sonnenberg, J. L.; Williams-Young, D.; Ding, F.; Lipparini, F.; Egidi, F.; Goings, J.; Peng, B.; Petrone, A.; Henderson, T.; Ranasinghe, D.; Zakrzewski, V. G.; Gao, J.; Rega, N.; Zheng, G.; Liang, W.; Hada, M.; Ehara, M.; Toyota, K.; Fukuda, R.; Hasegawa, J.; Ishida, M.; Nakajima, T.; Honda, Y.; Kitao, O.; Nakai, H.; Vreven, T.; Throssell, K.; Montgomery Jr., J. A.; Peralta, J. E.; Ogliaro, F.; Bearpark, M.; Heyd, J. J.; Brothers, E.; Kudin, K. N.; Staroverov, V. N.; Keith, T.; Kobayashi, R.; Normand, J.; Raghavachari, K.; Rendell, A.; Burant, J. C.; Iyengar, S. S.; Tomasi, J.; Cossi, M.; Millam, J. M.; Klene, M.; Adamo, C.; Cammi, R.; Ochterski, J. W.; Martin, R. L.; Morokuma, K.; Farkas, O.; Foresman, J. B.; Fox, D. J. *Gaussian 09*, Gaussian, Inc.: Wallingford, CT, 2016.
24. Dennington, R. D.; Keith, T. A.; Milam, J. M. *GaussView*, 5.0.; Shawnee Mission, KS, 2009.
25. Dovesi, R.; Orlando, R.; Erba, A.; Zicovich-Wilson, C. M.; Casassa, S.; Civalleri, B.; Maschio, L.; Ferrabone, M.; De La Pierre, M.; D'Arco, P.; Noel, Y.; Causa, M.; Rérat, M.; Kirtman, B., CRYSTAL14: A program for the ab initio investigation of crystalline solids. *Int. J. Quantum Chem.* **2014,** *114* (19), 1287-1317.
26. Dovesi, R.; Erba, A.; Orlando, R.; Zicovich-Wilson, C. M.; Civalleri, B.; Maschio, L.; Rérat, M.; Casassa, S.; Baima, J.; Salustro, S.; Kirtman, B., Quantum-mechanical condensed matter simulations with CRYSTAL. *WIREs Comput. Mol. Sci.* **2018**, e1360.
27. Ferrero, M.; Rérat, M.; Orlando, R.; Dovesi, R., The calculation of static polarizabilities of 1-3D periodic compounds. the implementation in the crystal code. *J. Comput. Chem.* **2008,** *29* (9), 1450-1459.
28. Precomputed vibrational scaling factors. https://cccbdb.nist.gov/vibscalejust.asp (accessed 11.5.1018).
29. *SAINT*, Bruker Instrument Service2, 2013.
30. Spek, A. L. *PLATON, A Multipurpose Crystallographic Tool*, Utrecht, The Netherlands, 1998-2016.
31. Altomare, A.; Burla, M. C.; Camalli, M.; Cascarano, G. L.; Giacovazzo, C.; Guagliardi, A.; Moliterni, A. G. G.; Spagna, G. P. R., SIR97: a new tool for crystal structure determination and refinement. *J. Appl. Cryst.* **1999,** *32* (1), 115-119.
32. Sheldrick, G. M., A short history of SHELX. *Acta Crystallogr.* **2008,** *A64*, 112-122.
33. *X`Pert HighScore*, 2.2e; PANalytical B.V.: Almelo, The Netherlands, 2009.
34. *OMNIC 9*, Thermo Fisher Scientific Inc., 1992-2012.
35. Nakamoto, K., *Infrared and Raman Spectra of Inorganic and Coordination Compounds*. 5th ed.; Wiley: 2011.
36. Putz, H. B., K. *Diamond - Crystal and Molecular Structure Visualization*, 3.2q; Crystal Impact: Bonn, Germany, 1997-2011.
37. Němec, I.; Matulková, I.; Held, P.; Kroupa, J.; Němec, P.; Li, D.; Bohatý, L.; Becker, P., Crystal growth, crystal structure, vibrational spectroscopy, linear and nonlinear optical properties of guanidinium phosphates. *Optical Materials* **2017,** *69*, 420-431.

38. Matulková, I.; Fridrichová, M.; Císařová, I.; Vaněk, P.; Uhlík, F.; Němec, I., Vibrational spectroscopic and crystallographic study of the novel guanylurea salts with sulphuric and selenic acids. *J. Mol. Struct.* **2017,** *1131*, 294-305.
39. Jesariew, D. I., M. M., Crystal structure, phase transition, and disorder in pyridinium methanesulfonate. *J. Phys. Chem. Solids* **2017,** *104*, 304-314.
40. Ilczyszyn, M. M.; Ilczyszyn, M., Raman, infrared and 13C NMR studies on betaine–sulfamic acid (2 : 1) crystal and its hydrogen bonds. *J. Raman Spectrosc.* **2003,** *34* (9), 693-704.
41. Infrared Spectroscopy. http://www.umsl.edu/~orglab/documents/IR/IR2.html (accessed 11.5.2018).